

Electronic Thesis and Dissertation Repository

12-8-2011 12:00 AM

Bifurcations and Stability in Models of Infectious Diseases

Bernard S. Chan

The University of Western Ontario

Supervisor

Pei Yu

The University of Western Ontario

Graduate Program in Applied Mathematics

A thesis submitted in partial fulfillment of the requirements for the degree in Doctor of Philosophy

© Bernard S. Chan 2011

Follow this and additional works at: <https://ir.lib.uwo.ca/etd>



Part of the [Dynamic Systems Commons](#), and the [Ordinary Differential Equations and Applied Dynamics Commons](#)

Recommended Citation

Chan, Bernard S., "Bifurcations and Stability in Models of Infectious Diseases" (2011). *Electronic Thesis and Dissertation Repository*. 347.

<https://ir.lib.uwo.ca/etd/347>

This Dissertation/Thesis is brought to you for free and open access by Scholarship@Western. It has been accepted for inclusion in Electronic Thesis and Dissertation Repository by an authorized administrator of Scholarship@Western. For more information, please contact wlsadmin@uwo.ca.

BIFURCATIONS AND STABILITY IN MODELS OF INFECTIOUS
DISEASES
(Thesis format: Integrated Article)

by

Bernard Chan

Graduate Program in Applied Mathematics

A thesis submitted in partial fulfillment
of the requirements for the degree of
Doctor of Philosophy

The School of Graduate and Postdoctoral Studies
The University of Western Ontario
London, Ontario, Canada

© Bernard Shang Li Chan 2011

THE UNIVERSITY OF WESTERN ONTARIO
School of Graduate and Postdoctoral Studies

CERTIFICATE OF EXAMINATION

<u>Supervisor:</u>	<u>Examiners:</u>
..... Dr. P. Yu Dr. C. Essex
<u>Supervisory Committee:</u> Dr. X. Zou
..... Dr. L. M. Wahl Dr. S. Yu
..... Dr. G. Reid Dr. Y. Chen

The thesis by

Bernard Shang Li Chan

entitled:

Bifurcations and Stability in Models of Infectious Diseases

is accepted in partial fulfillment of the
requirements for the degree of
Doctor of Philosophy

.....
Date

.....
Chair of the Thesis Examination Board

Abstract

This work is concerned with bifurcations and stability in models related to various aspects of infectious diseases.

First, we study the dynamics of a mathematical model on primary and secondary cytotoxic T-lymphocyte (CTL) responses to viral infections by Wodarz *et al.* This model has three equilibria and the stability criteria of them are discussed. The system transitions from one equilibrium to the next as the basic reproductive number, R_0 , increases. When R_0 increases even further, we analytically show that periodic solutions may arise from the third equilibrium via Hopf bifurcation. Numerical simulations of the model agree with the theoretical results and these dynamical behaviours occur within biologically realistic parameter ranges. Normal form theory is also applied to find amplitude, phase and stability information on the limit cycles. Biological implications of the results are discussed.

After studying the single-strain model, we will analyze the bifurcation dynamics of an *in vivo* multi-strain model of *Plasmodium falciparum*. Main attention of this model is focused on the dynamics of cross-reactivity from antigenic variation. We apply the techniques of coupled cell systems to study this model. It is shown that synchrony-breaking Hopf bifurcation occurs from a nontrivial synchronous equilibrium. In proving the existence of a Hopf bifurcation, we also discover the condition under which possible 2-colour synchrony patterns arise from the bifurcation. Dynamics resulting from the bifurcation are qualitatively similar to known behaviour of antigenic variation.

These results are discussed and illustrated with examples and numerical simulations.

Aside from the bifurcation of an *in vivo* multi-strain model, we also study the clustering behaviour found in numerous multi-strain transmission models. Numerical solutions of these models have shown that steady-state, periodic, or even chaotic solutions can be self-organized into clusters. Such clustering behaviour is not *a priori* expected. It has been proposed that the cross-protection from multiple strains of pathogens is responsible for the clustering phenomenon. We show that the steady-state clusterings in existing models can be analytically predicted. The clusterings occur via semi-simple double zero bifurcations from the quotient network of the models and the patterns which follow can be predicted through the stability analysis of the bifurcation. We calculate the stability criteria for different clustering patterns and show that some patterns are inherently unstable. Finally, the biological implications of these results are discussed.

Keywords: Immune system; cytotoxic T-lymphocyte response; Hopf bifurcation; stability; limit cycles; multi-strain infection model; semi-simple double zero bifurcation; clustering.

Statement of Co-Authorship

The article versions of Chapters 2, 3 and 4 are co-authored with Pei Yu.

To my parents and all my teachers.

Acknowledgements

Many people helped me in writing this work and I am grateful for their help. First and foremost, I would like to thank Dr. Pei Yu, my supervisor, for giving me this wonderful opportunity to study with him at The University of Western Ontario. His demand for academic rigour has made me a better researcher. I thank him for being so patient with me throughout this entire process.

The administration at the Department of Applied Mathematics has provided tremendous support to me over the years. I thank all the professors for their continuous encouragement and their invaluable academic discussions. My gratitude extends to the marvellous support staff of Audrey and Karen. They have provided all the graduate students in the department with an efficient and comfortable learning environment. Financial support received from the Natural Sciences and Engineering Research Council of Canada, The University of Western Ontario and the Ontario Graduate Scholarship in Science and Technology program are much appreciated.

I would like to thank Roger and Maruska for putting up with me for three years. They made all those late nights working in Jeffery fun and at times, educational. Furthermore, Anna has been an inspiration for me over my years here at Western.

A journey of a thousand miles begins with a single step. My personal journey in mathematics began when my parents taught me addition and multiplication over some long train rides. Their unconditional love and support made this work possible.

Contents

Certificate of Examination	ii
Abstract	iii
Statement of Co-Authorship	v
Dedication	v
Acknowledgements	vi
Table of Contents	xi
List of Figures	xi
1 Introduction	1
1.1 Overview of Immune Response	1
1.1.1 Primary and secondary responses	2
1.1.2 Antigenic variation	3
1.1.3 Maintenance of strain structure	4
1.2 Review of Models in Immunology and Infectious Diseases	5
1.3 Methodologies for Model Analysis	10
1.3.1 Stability and bifurcation	10
Equilibrium dynamics	10
Bifurcations of equilibrium points	11
1.3.2 Coupled cell systems	12
Defining the coupled cell system	13
Vector fields of coupled cell network	15
Balanced equivalence relations and balanced colourings	18
Quotient networks	20
1.4 Structure of the Thesis	21

Bibliography **24**

2 Bifurcation Analysis in a Model of Cytotoxic T-Lymphocyte Response to Viral Infections **33**

2.1	Introduction	33
2.2	Well-posedness of the model	36
2.3	Stability of E_0 and E_1	38
2.3.1	Infection-free equilibrium E_0	38
2.3.2	Infectious equilibrium without CTL response E_1	40
2.4	Stability of E_2 and Hopf bifurcation	44
2.4.1	Infectious equilibrium with CTL response E_2	44
2.4.2	Hopf bifurcation analysis	47
2.5	Numerical simulations	52
2.5.1	Infection-free equilibrium E_0	53
2.5.2	Infectious equilibrium without CTL response E_1	53
2.5.3	Infectious equilibrium with CTL response E_2	54
2.5.4	Hopf bifurcation	57
2.6	Biological Implications	61

Bibliography **64**

3 Synchrony-Breaking Hopf Bifurcation in a Model of Antigenic Variation **67**

3.1	The Model	69
3.2	Antigenic Variation Model as a Product Network	71
3.3	Stability and Bifurcation Analysis	76
3.3.1	Local stability near \mathbf{x}_1^*	77
3.3.2	Local stability near \mathbf{x}_2^*	80
3.3.3	Bifurcation analysis	82
3.4	Numerical Simulations	90
3.4.1	System with four strains	90
3.4.2	System with eight strains	93
3.5	Conclusions and Discussions	94

Bibliography **99**

4 Bifurcation, Stability, and Cluster Formation of Multi-Strain Infection Models **101**

4.1	Introduction	101
4.2	General Approach	104
4.2.1	Coupled cell network representation	104
4.2.2	Possible 2-colouring patterns	106
4.2.3	Quotient networks	108
4.2.4	The semi-simple double zero bifurcation	109
4.2.5	Jordan canonical form and center manifold reduction	110
4.2.6	Stability of semi-simple double zero bifurcation	112
4.3	Stability and Bifurcation Analysis	113
4.3.1	The model by Gupta, Ferguson, and Anderson (1998)	113
4.3.2	The model by Recker and Gupta (2005)	117
4.4	Numerical Results	122
4.4.1	Numerical results of the model by Gupta <i>et al.</i> (1998)	123
4.4.2	Numerical results of the model by Recker and Gupta (2005)	124
4.4.3	Periodic and chaotic motions	125
4.5	Concluding Remarks	125
	Bibliography	139
	5 Conclusions and Future Works	142
5.1	Conclusions	142
5.2	Future Work	143
	Bibliography	145
	Curriculum Vitae	146

List of Figures

1.1	Examples of coupled cell networks.	16
	(a) A homogenous bi-directional ring.	16
	(b) A three-node non-homogenous network with mixed arrows and node types.	16
1.2	Examples of coupled cell networks with balanced colourings.	19
	(a) A balance-coloured bi-directional ring.	19
	(b) A balance-coloured four-cell network.	19
1.3	Examples of quotient networks.	22
2.1	Simulations of system (2.3) at $\lambda = 3$	53
2.2	Simulations of system (2.3) at $\lambda = 7.5$	54
2.3	Simulations of system (2.3) at $\lambda = 8$	57
2.4	Simulations of system (2.3) with oscillations at $\lambda = 10$ ($\mu = 53/90$). . .	58
2.5	Limit cycles of system (2.3) at $\lambda = 10$ ($\mu = 53/90$).	59
3.1	An example of forming a new network using Theorem 3.2.1	74
3.2	Two different 2-colouring patterns possible for the $S_2 \times S_2$ system. . . .	85
3.3	General 2-colour quotient network.	86
3.4	Simulated pathogen populations (y_{ij}) for four-strain system at $\phi = 0.5$. .	91
3.5	Simulated pathogen populations (y_{ij}) for four-strain system at $\phi = 1.5$. .	92
3.6	Coupled cell network for the a model of eight strains.	93
3.7	Simulated pathogen populations (y_{ij}) for eight-strain system at $\phi = 1$. .	94
3.8	Simulated pathogen populations (y_{ij}) for eight-strain system at $\phi = 1$. .	95
3.9	Two 2-colourings for the eight-strain system.	96

4.1	The directed graph representing the coupled cell network of the 2 locus-2 allele form of the model by Gupta <i>et al.</i> (1998): Each node represents the differential equations set in system (4.2) and each arrow represents the coupling between strains that shares allele; alleles $\{a, b\}$ are used at the first locus and alleles $\{x, y\}$ are used at the second locus.	105
4.2	The three-dimensional directed graph representing the coupled cell network of the 3 locus-2 allele form of the model by Recker and Gupta (2005): Each node represents the set of differential equations in system (4.3); similarly, dashed arrow represents the coupling between two strains when they only share one allele and solid arrow represents the coupling between two strains when they share more than one allele; allele sets $\{a, b\}$, $\{m, n\}$, and $\{x, y\}$ are used respectively at the first, second, and third locus; double headed arrows, minimizing the number of arrow drawn, are used to indicate that there is an arrow originating from each node of the pair.	106
4.3	Three different possible colouring patterns for the 2 locus-2 allele form of the model by Gupta <i>et al.</i> (1998), where black and white represent the two possible classes in each of the coupled cell network.	107
4.4	The directed graph representing the general quotient network for all balanced 2-colourings of the model by Gupta <i>et al.</i> (1998): The topological parameters, s_i , indicating the number of self-connections for each class, and similarly, the topological parameters, m_i , indicating the number of connections received from the other class.	109
4.5	The directed graph representing the general quotient network for all balanced 2-colourings of the model by Recker and Gupta (2005): The parameters, s_{i1} and s_{i2} , indicating respectively the number of dashed and solid self-connections received for each class, and similarly, the parameter, m_{i1} and m_{i2} indicating respectively the number of dashed and solid connections received from the other class.	110
4.6	Simulation results of the 2 locus-2 allele form of system (4.2) for $\sigma = 10$, $\gamma = 0.85$, $\mu = 0.02$, $\beta = 15$, showing the clustering patterns of z_i for each strain. The patterns in these 4.6(a) and 4.6(b) can be obtained by using different initial conditions.	129

4.7	Results for the 3 locus-2 allele version of the model from Gupta <i>et al.</i> (1998): (a) Simulated time history of z_i for $\sigma = 10, R_0 = 1.1, \gamma = 0.58, \mu = 0.02$ with identical initial conditions for strains <i>any</i> , <i>bnx</i> , <i>bm_x</i> and <i>amy</i> ; and (b) The balanced 2-colour pattern corresponding to the numerical results, with each dark node receiving four inputs from white nodes and two from the other dark nodes; similarly, each white node receiving four inputs from dark nodes and two from the other white nodes, and the corresponding 2-colour quotient network having the parameter values $m_i = 4$ and $s_i = 2$	130
4.8	Results for the 3 locus-2 allele version of the model from Gupta <i>et al.</i> (1998): (a) Simulated time history of z_i for $\sigma = 10, R_0 = 1.1, \gamma = 0.58$, and $\mu = 0.02$ with identical initial conditions for strains <i>any</i> and <i>bm_x</i> ; and (b) The balanced 2-colour pattern corresponding to the numerical results and with each dark node receiving six inputs from white nodes and none from the other dark node; similarly, each white node receiving one input from dark nodes and five from the other white nodes, and the corresponding 2-colour quotient network having the parameter values $m_1 = 2, s_1 = 4, m_2 = 6$ and $s_2 = 0$	131
4.9	Results for 3 locus-2 allele version of the model from Gupta <i>et al.</i> (1998): (a) Simulated time history of z_i for $\sigma = 10, R_0 = 1.1, \gamma = 0.45, \mu = 0.02$ with mixed initial conditions are used. (b) The corresponding coupled cell system showing that all strains being synchronized in identical steady-state.	132
4.10	Results for the 3 locus-2 allele version of the model from Recker and Gupta (2005): (a) Simulated time history of z_i for $\sigma = 10, R_0 = 1.2, \gamma_1 = 0.5, \gamma_2 = 0.8, \mu = 0.09$ with identical initial conditions for strains <i>am_x</i> , <i>any</i> , <i>bn_y</i> , and <i>bm_x</i> ; and (b) The balanced 2-colour pattern corresponding to the numerical results, and the corresponding 2-colour quotient network having the parameter values $m_{ij} = 2$ and $s_{ij} = 1$, for $i, j \in \{1, 2\}$	133

4.11	Results for the 3 locus-2 allele version of the model from Recker and Gupta (2005): (a) Simulated time history of z_i for $\sigma = 10, R_0 = 1.2, \gamma_1 = 0.5, \gamma_2 = 0.8, \mu = 0.09$ with identical initial conditions for strains amx and bny ; and (b) The balanced 2-colour pattern corresponding to the numerical results and the corresponding 2-colour quotient network having the parameter values $m_{1i} = 1, m_{2i} = 3, s_{1i} = 2$ and $s_{2i} = 0$, for $i \in \{1, 2\}$	134
4.12	Results for the 3 locus-2 allele version of the model from Recker and Gupta (2005): (a) Simulated time history of z_i for $\sigma = 10, R_0 = 1.2, \gamma_1 = 0.45, \gamma_2 = 0.48, \mu = 0.09$; and (b) The corresponding coupled cell system showing that all strains being synchronized in identical steady-state.	135
4.13	Simulated time history of z_i for $\sigma = 10, R_0 = 2, \gamma_1 = 0.65, \gamma_2 = 0.76, \mu = 0.09$ with identical initial conditions for strains amx, any, bny , and $bm x$, converging to two classes (amx, any, bny , and $bm x$; bnx, bmy, amy , and anx) of periodic solutions with the same amplitude but a phase difference of half-period.	136
4.14	Simulated time history of z_i for $\sigma = 10, R_0 = 2, \gamma_1 = 0.65, \gamma_2 = 0.76, \mu = 0.09$ with identical initial conditions for strains amx and bny , converging to two classes (amx and bny ; $any, bnx, bmy, bm x, amy$, and anx) of periodic solutions with different amplitudes and phase difference of half-period.	137
4.15	Results for the 3 locus-2 allele version of the model from Recker and Gupta (2005): (a) Simulated time history of z_i for $\sigma = 10, R_0 = 2, \gamma_1 = 0.65, \gamma_2 = 0.76, \mu = 0.09$ with mixed initial conditions, showing three classes (anx and bmy ; amy and bnx ; any, amx, bny , and $bm x$) of chaotically synchronized motions; (b) The corresponding coupled cell system with a balanced 3-colouring pattern; and (c) Quotient network of the 3-colouring pattern.	138

Chapter 1

Introduction

Pathogens, such as viruses, bacteria, and parasites, are constantly acting to infect other organisms to take advantage of the hosts. In response to these threats, many organisms have evolved defences against the pathogens. Understanding the complicated dynamics of infectious diseases is crucial to enhance the health of the general population. Researchers have built mathematical models to supplement clinical research in hope to understand the dynamics. In this work, we apply dynamical system techniques to models of infectious diseases to better understand their behaviour. We provide the basics of immunology in this chapter and then review the models which are relevant to this study.

1.1 Overview of Immune Response

Broadly speaking, innate and adaptive immunity are the two different ways the body defends itself against invading pathogens (Abbas and Lichtman, 2004; Coico and Sunshine, 2009). Innate immunity is always present for people with healthy immune systems and its primary function is to defend against pathogens before they can establish infections within the host.

When innate immunity fails to prevent pathogens from establishing an infection and the population of pathogens increases, adaptive immunity will take over in eliminating the pathogens. The two types of adaptive immunity are humoral and cell-mediated responses. Humoral responses are established by antibodies released by B-lymphocytes. These antibodies are responsible for helping with potentially harmful pathogens in the bloodstream and the mucosal organs and thus preventing them from getting into other tissues in the body and establishing an infection. Cell-mediated response is detailed below.

1.1.1 Primary and secondary responses

Once the microbes have successfully invaded cells and tissues, the humoral response is no longer effective against them. At this point, cell-mediated response becomes activated and cytotoxic T-lymphocytes (CTLs) will try to eliminate the threat. When threats are detected, some T-cells activate phagocytes to ingest and digest the infected cells in order to eliminate them, though other T-lymphocytes become target-specific through the activation process. Upon encountering a particular pathogen for the first time, naive T-cells differentiate into effector lymphocytes and they become responsible for eliminating the specific pathogen. This first response to the pathogen is called the primary response. Upon elimination of the specific threat, many of these effectors will die via apoptosis. Surviving effectors may become long-lived memory cells. As their name suggests, these cells can live in the body for a long time and they provide continual protection against the specific microbe. Future encounters with the same microbe will be met with responses from these memory cells. Responses from the memory cells are called secondary responses and they are quicker and more efficient than the primary response.

1.1.2 Antigenic variation

T-cells recognize different pathogens by the surface chemicals, called antigens. Given that secondary responses are more effective, pathogens have difficulties in establishing infection if the host has been exposed to the pathogen before. To circumvent this immune mechanism, the pathogens may disguise themselves with many different antigen variants on their surfaces. Receptors on the T-cells are specific to the protein structure, also known as the epitopes, of the antigen. By having variations of the epitopes, these antigens can avoid detection from the immune system. Aside from being more effective in establishing infection on exposed hosts, this type of systemic variation will also allow the pathogen to stay inside the host longer and thus increase its chances of infecting another host.

Variations of the same pathogen can arise by different ways. Viruses are prone to mutation due to imperfection during the replication process (Craig and Scherf, 2003). These mutations can lead to genotypic as well as phenotypic differences between generations. If the phenotypic differences include changes to the epitopes, the immune system would not recognize this new protein on the surface. This type of antigenic variation may be observed in the human immunodeficiency virus (HIV) and the influenza virus. Alternatively, the genotype of the pathogen need not change for antigenic variations to occur. Research by Recker *et al.* (2011) suggests that pathogens, such as the malaria causing *Plasmodium falciparum*, varies its epitopes systematically while keeping the same DNA structure. All strains of the pathogen express different phenotypic properties using the same genomic information.

As an immune escape strategy, the pathogens using antigenic variation must meet several prerequisites in order to be successful (Turner, 2002). Many parasites that employ this strategy stay within one host for an extended period of time. Given the adaptive nature of the immune system, a large repertoire of variants is necessary for

continual evasion and survival in the host. These pathogens must also not present their entire arsenal of variants all at once to maximize their advantage against the immune system. Many scientists hypothesize that there must be a management system for the appearance of the variations, but the precise mechanism controlling such sequence is still an open question (Craig and Scherf, 2003)

Shared epitopes are commonly found between antigenic variants of the same pathogen. Since the acquired immune system identifies each pathogen type by its protein structure, the specific immune cells for one subtype may be cross-reactive for another subtype of pathogen. Given that the protein structures between subtypes are not identical, the binding sites for detection will not match perfectly for immune detection. Thus, this cross-protection is usually only partially effective.

1.1.3 Maintenance of strain structure

Given that the strategy of antigenic variation requires many repertoires of the pathogen to be successful, one might expect that pathogens would evolve to have ever increasing number of variants and increase the number of variants at an increasing rate. Examples from clinical observations suggest that these notions are not necessary for the strategy to succeed and strain structures are often maintained with the host population (Gupta *et al.*, 1996). For example, switching of dominant strains of influenza occurs seasonally instead of the timescale which takes to mutate and reproduce clonally many times over. Furthermore, theoretical and clinical data both support that there is a controlled and hierarchical expressions of phenotypic variations for *P. falciparum* (Recker *et al.*, 2011; Turner, 2002). The organized switching of variations suggest that switching rate and the number of strains may not be the most important factors for the strategy to succeed.

A number of limiting factors have been suggested for the limited appearance of new strains. In order to reproduce, pathogens can only take advantage of specific cells of the

host and there are only limited number of protein combinations that would work for the binding sites on these target cells. For the pathogens that do not change their genome, there are limited number of variations that are useful. As for other pathogens that derive new variations from mutations, many new strains may be produced quickly. The sheer number of new strains imply that there should be more combinations that are suitable for binding sites. However, this process may also introduce undesired effects and thus limit the strains that are actually viable. Aside from these factors, cross-protective immunity may also contribute to the observed strain structure for pathogens. A host may have gained partial immunity from a previous infection. While this protection is not fully effective, it is enough to give strains that do not share epitopes in the cross-protection an advantage and establish themselves as the dominant strains within the host. Having one population dominating will limit the exchange of genetic information between strains and thus maintain the discrete strain structure.

1.2 Review of Models in Immunology and Infectious Diseases

There exists a vast literature of mathematical models studying the immunological phenomena described in the previous section. Selected literatures relevant to our work are reviewed here.

Differential equation models of immunology and infectious diseases are similar to the Lotka-Volterra predator-prey models in population dynamics. In the basic in-host immunological models, the effector class, acting as predator, is responsible for culling of the pathogens as prey. Similarly, the basic epidemiological model has an infected class that act as predators and infect the population in the susceptible class. Anderson and May (1991) provided an overview on the historical development and the biological

basis of these models.

Many models studying *in vivo* single strain dynamics of the immune system are based on the work established by Nowak and Bangham (1996). The authors established three minimal models to study different aspects of viral population dynamics: viral replication, immune responses, and variations in immune responses to different viral strains. Extending on established models of viral dynamics, Bonhoeffer *et al.* (1997) added drug treatment to the basic model. By incorporating two classes of virus and correspondingly, two types of susceptible cells, the authors were able to demonstrate the dynamics of drug resistance and understand the difficulty in eradicating some viral population completely.

As mentioned in Section 1.1, the adaptive immune response has effector cells that are responsible for killing pathogens and memory cells that are responsible for long term protection against the same pathogen. Instead of having one general CTL class in the model, Wodarz *et al.* (1998) added a class of memory cells to study both primary and secondary responses. This model established criteria that would lead to the exhausting CTL cells and defeating the immune system by viral infection.

The roles of effectors and precursor cells were further studied in terms of HIV infections in (Wodarz and Nowak, 1999) . Counterintuitively, the authors found that a deliberate break from drug therapy may stimulate in the immune system and boost the production level of immune cells. Thus, intentional therapy interruption may enhance the innate protection. Given that HIV targets cells of the immune system to replicate, Korthals *et al.* (2002) improved upon the previous models by adding the dynamics of CD4⁺ helper cells and found that precursors and helper cells do not generally change the outcome of infection. To study hepatitis C infections, Wodarz (2003) replaced the precursor class with antibody responses. This model showed that strong antibody response is necessary to stimulate the CTL response in order to avoid chronic

infection.

Instead of having only one strain, many pathogens are successful in establishing infection because they present themselves within-host with many different variants. Models by Nowak *et al.* (1990) and Nowak *et al.* (1991) studied many quasispecies of HIV-1 in the human immune system. Their results suggested that the antigenic diversity of the HIV populations contributed to the development of AIDS. In 1994, Sasaki (1994) studied co-evolution of host and pathogen. Instead of focusing on the immune dynamics of effector cells killing pathogens, the author focused on the genetic drift of the pathogens caused by interactions with the immune system.

Improving upon previous multi-strain models, Nowak and May (1992) incorporated strain specific parameter values for individual strains into their model. Coexistence and competitions between strains were more accurately reflected in this model and this improvement led to more general condition for threshold condition in establishing infection. To describe the genetic variations between strains more precisely, epitopes sharing between strains were explicitly incorporated in models by Nowak *et al.* (1995a,b) and Bittner *et al.* (1997). These models showed that the dynamics induced from shared epitopes and cross-protective immune responses could cause chaotic oscillations.

Multiple strains of pathogen may also affect functions of the immune system. Taking into account of multiple antigenic variants, Wodarz (2001) studied the effects of multi-strain infections on memory cells. In this work, the author specifically studied the immune system to control multiple infections and establishing memory cells. An assumption in many multi-strain viral models is that a cell can only be infected with one strain of virus at a time, but it has been shown experimentally that a cell may be simultaneously infected by multiple strains of viruses. Wodarz and Levy (2009) created a model to study coinfection of target cells by HIV-1 to understand these dynamical contribution to viral escape.

Other than viruses, parasites may also employ antigenic variations as a strategy. An-tia *et al.* (1996) proposed a model specifically for studying parasitemia antigenic vari-ation. For specific parasites, Lythgoe *et al.* (2007) and Gjini *et al.* (2010) studied anti-genic variation of the protozoan organism *Typanosome brunei*. These differential equa-tion models showed that variant-specific host immunity and density-dependent differ-entiation rate are key factors in studying antigenic variation of this pathogen. Multi-strain antigenic variation model of *P. falciparum*, another protozoan parasite, was also studied by Recker and Gupta (2006).

Alternative to predator-prey interpretations of pathogen-immune dynamics, emer-gence of multiple strains within-host may be considered as an evolutionary phenomenon. As such, Iwasa *et al.* (2004) considered the pressure of strain specific immunity on the evolutionary dynamics of pathogens. Other researchers have considered the multi-strain within-host system dynamics in lights of coevolution of the pathogens and the immune system. Sardanyés and Solé (2007) and Dercole *et al.* (2010) have studied the dynamics between the hosts and parasitic pathogens under the Red Queen hypothesis.

Not only do multiple strains affect the within-host dynamics, these additional vari-ants may also affect the transmission dynamics. Multi-strain epidemiological mod-els have been used to study the transmission of various common diseases, such as in-fluenza (Lin *et al.*, 1999; Gog and Grenfell, 2002; Casagrandi *et al.*, 2006; Recker *et al.*, 2007; Gog, 2008; Minayev and Ferguson, 2009; Omori *et al.*, 2010), malaria (Mitchell and Carr, 2010; Childs and Boots, 2010), and dengue fever (Ferguson *et al.*, 1999; Recker *et al.*, 2009; Lourenço and Recker, 2010; Wikramaratna *et al.*, 2010). Oscil-lating solutions are often the result of the additional pathogen variants and they may explain seasonal fluctuations observed for some of the diseases.

Unlike many of the aforementioned multi-strain transmission models, the epidemi-ological models by Gupta *et al.* (1996) and Gupta and Galvani (1999) explicitly account

for the effects of shared epitopes between strains and cross-protection at the epidemiological level. These models showed that the discrete strain structure was maintained in the host population due to cross-protection caused by shared epitopes. Dawes and Gog (2002) compared several transmission models that included cross-immunity, and concluded that oscillatory dynamics can occur through a Takens-Bogdanov bifurcation. Instead of classifying the population based on the history of infection, one could classify the population based on the status of the infection (Gog and Swinton, 2002). This status based approach provided results that are qualitatively different from that obtained using traditional history based approach.

Given that contact is necessary for transmission, geographical information is an important consideration for transmission of diseases. Buckee *et al.* (2007) combined techniques used in studying complex networks to investigate multi-strain infections. Another approach to infectious diseases is to combine the kinetics at the cellular level with epidemiological consequences in one model. Volkov *et al.* (2010) used a differential equation system to represent within-host dynamics and then generalized the results to the transmission level. In a similar vein, Lange and Ferguson (2009) also incorporated within-host and intra-host dynamics in one model. With the pathogen reproductive number as a gauge for fitness, their work showed tradeoffs between transmissibility and antigenic diversity.

Complexity of many immunological models has grown over the years and authors of these models often only explored the dynamics numerically. Details of the models' analytic properties are often explored by other mathematicians. For example, Korobeinikov and his collaborators investigated asymptotic behaviour of various within-host (Korobeinikov, 2004, 2009a,c) and intra-host models (Korobeinikov and Wake, 2002; Korobeinikov, 2006, 2007; Iwami *et al.*, 2008; Korobeinikov, 2009b; O'Regan *et al.*, 2010). Global stability of general pathogen-infection model with the loss of

pathogen was explored by Kajiwara and Sasaki (2010). Similarly, Elaiw (2010) analyzed the global stability properties of a class of HIV infection models. These methods have been extended by De Leenheer and Pilyugin (2008) and Souza and Zubelli (2011) to study global stability in immune response models that include the effects of antigenic variation.

Beside global asymptotic properties, sustained oscillations through Hopf bifurcation are also analyzed. In 1997, Liu (1997) presented his work on oscillations of immune responses to a single strain of virus. Various authors, such as de Leenheer and Smith (2003); Murase *et al.* (2005); Wang *et al.* (2006); Song and Neumann (2007); Jiang *et al.* (2009); Egami (2009) as well as Yang and Xiao (2010), showed that the infection free equilibria of viral models are generally globally stable and sustained oscillations may occur from the infected state through a Hopf bifurcation.

1.3 Methodologies for Model Analysis

In this work, we analyze models of infectious diseases using various techniques and we describe them in this section.

1.3.1 Stability and bifurcation

Equilibrium dynamics

Homeostasis is the regulation of biological functions, such as internal temperature and glucose level, at an optimal operating point. Even slight deviations (e.g. human body temperature from normal of 37°C to 35°C) from these points can be lethal. For biological dynamics, equilibrium points of dynamical systems are analogous to these operating points. Given their importance, we first analyze the properties of stability of the equilibria for these systems.

For a given equilibrium point, one finds its local stability by analyzing the eigenvalues of its Jacobian matrix. If all the eigenvalues at the equilibrium point have negative real-part, then the equilibrium is locally asymptotically stable. Otherwise, it is unstable. Equivalently, the roots of the characteristic polynomial provide the same information.

The linear analysis of the Jacobian can only provide local information, so we must use other methods, such as Lyapunov functions, in order to obtain information on the global stability of an equilibrium. A suitable Lyapunov function candidate $V(x)$ must be an unbounded positive definite function and the first derivative of this function, with respect to time along the system trajectories, must be negative definite, except at the equilibrium point. If such a function exists for an equilibrium point, then the point is globally asymptotically stable.

Bifurcations of equilibrium points

Parameters of the system describe the biological considerations for a given model. Eigenvalues that determine the stability of an equilibrium point are functions of these parameters. As the parameters change to reflect changes in biological conditions, the eigenvalues change along with them. Some of eigenvalues may move from the left to right half of the complex plane. The point at which at least one eigenvalue has zero real-part is called the bifurcation point. After the eigenvalues completely cross into the right half plane, the equilibrium point loses its stability and changes to another state. This process is called bifurcation.

Of the parameters in a system, researchers usually only consider changing of one or two parameters at a time to understand the effects of specific parameters. Bifurcations that only involve one parameter are called codimension-one bifurcations. Generically, codimension one bifurcations involve the crossing of one specific eigenvalue or a pair of complex conjugate eigenvalues. One can find the bifurcation points by explicitly

calculating the eigenvalues.

The task of finding the expressions of eigenvalues is often difficult for high dimensional systems. Instead of using eigenvalues, Liu (1994) developed a criterion for finding simple Hopf bifurcation based on only the Hurwitz determinants calculated from the characteristic polynomial. Furthermore, Yu (2005) extended the use of Hurwitz determinants to find k -Hopf bifurcations, the crossing of multiple pairs of eigenvalues at the same time. The advantage in these two methods is that one does not need to solve the nonlinear characteristic equation to find the bifurcations. These methods only describe finding bifurcating solutions. We need to apply more advanced techniques, such as expansion and the center manifold theorem in order to know the stability of these bifurcation solutions.

Beyond center manifold reduction, we could further simplify bifurcating dynamical systems using normal form theory. While useful, normal forms are often tedious and difficult to calculate analytically. Yu (1998, 2002) developed techniques using computer algebra systems, such as Maple, to calculate the normal forms for bifurcations of vector fields efficiently. Normal forms of dynamical systems often contain higher order terms that may be further reduced using computationally intensive techniques. The further reduced forms are called the simplest normal forms and Yu and Leung (2003) and Yu and Yuan (2003) developed the theory and computer algorithms for these simplifications.

1.3.2 Coupled cell systems

In Chapters 3 and 4, we analyze immunological models with multiple strains. The dynamics of each individual strain is compartmentalized into systems of differential equations. These subsystems are coupled to reflect that the dynamics of different strains affects each other. While the principles of the techniques mentioned in the previous section still apply, they can be difficult to use in practice due to the high number of

dimensions involved. Instead of attacking the problem directly, we take advantage of the compartmentalized structure of the multi-strain system. We apply the coupled cell systems based on the groupoid formalism first established by Stewart *et al.* (2003) and then refined later by Golubitsky *et al.* (2005) to analyze the coupled systems of differential equations. In this subsection, we will summarize the necessary parts of the formalism for our analysis in the upcoming chapters.

Defining the coupled cell system

The groupoid formalism is a systematic way to represent systems of coupled differential equations and analyze synchronization patterns. A directed graph, or digraph, is a convenient way to represent the connections between the subsystems. Each node in the directed graph is labelled to represent a sets of differential equations. Labels, or the shapes, of the nodes of the digraph denote specific set of differential equations. Identical sets of differential equations are represented in the graph with nodes of the same shape. Similarly, each directed edge, or arrow, in the graph represents the coupling between different sets of differential equations. Different arrows are used to denote different kinds of coupling terms between systems. Based on these considerations, we can define a coupled cell network as follows (Golubitsky *et al.*, 2005) :

Definition 1.3.1. *A coupled cell network \mathcal{G} consists of:*

- a. *A finite set $\mathcal{C} = \{1, \dots, N\}$ of nodes.*
- b. *An equivalence relation $\sim_{\mathcal{C}}$ on nodes in \mathcal{C} . The type of node c is the $\sim_{\mathcal{C}}$ -equivalence class $[c]_{\mathcal{C}}$ of c .*
- c. *A finite set \mathcal{E} of edges or arrows.*
- d. *An equivalence relation $\sim_{\mathcal{E}}$ on edges in \mathcal{E} . The type or coupling label of edge e is the $\sim_{\mathcal{E}}$ -equivalence class $[e]_{\mathcal{E}}$ of e .*

- e. Two maps $\mathcal{H} : \mathcal{E} \rightarrow \mathcal{C}$ and $\mathcal{T} : \mathcal{E} \rightarrow \mathcal{C}$; for $e \in \mathcal{E}$ $\mathcal{H}(e)$ is called the head of e and $\mathcal{T}(e)$ is called the tail of e .
- f. Equivalent arrows have equivalent tails and heads. That is, if $e_1, e_2 \in \mathcal{E}$ and $e_1 \sim_E e_2$, then

$$\mathcal{H}(e_1) \sim_C \mathcal{H}(e_2) \quad \text{and} \quad \mathcal{T}(e_1) \sim_C \mathcal{T}(e_2).$$

The terms cell and node are used interchangeably in the mathematical literature to describe the vertexes in these directed graphs or the differential equation systems that represent the network. Aside from the phrases “coupled cell network” or “coupled cell system”, the term *cell* will be used exclusively for its biological meaning to avoid confusion.

This definition of coupled cell network by Golubitsky *et al.* (2005) permits self-couplings as $\mathcal{H}(e) = \mathcal{T}(e)$ for a given e . Multiple arrows from one node to another are also allowed because $\mathcal{H}(e_1) = \mathcal{H}(e_2)$ and $\mathcal{T}(e_1) = \mathcal{T}(e_2)$ are both permitted for $e_1 \neq e_2$.

The following definitions allow us to speak of inputs of a node as a set and a way to compare inputs of different nodes.

Definition 1.3.2. *If $c \in \mathcal{C}$, then the input set of c is*

$$I(c) = \{e \in \mathcal{E} : \mathcal{H}(e) = c\}.$$

An element of $I(c)$ is called an input edge or input arrow of c .

Definition 1.3.3. *The relation \sim_I of input equivalence on \mathcal{C} is defined by $c \sim_I d$ if and*

only if there exists an arrow type preserving bijection

$$\beta : I(c) \rightarrow I(d).$$

That is, for every input arrow $i \in I(c)$

$$i \sim_E \beta(i).$$

Any such bijection β is called an input isomorphism from node c to node d . The set $B(c, d)$ denotes the collection of all input isomorphisms from node c to node d . The set $\mathcal{B}_G = \bigcup_{c,d \in \mathcal{C}} B(c, d)$ is the (symmetry) groupoid of the network. The set $B(c, c)$ is a permutation group acting on the input set $I(c)$, which we call the vertex group of node c .

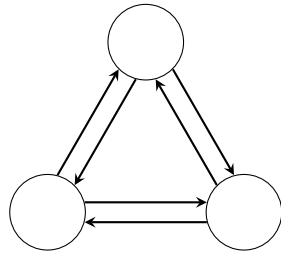
Formed by the input isomorphisms, the groupoid structure underpins the couple cell systems much like the way symmetry groups are the keys to equivariant bifurcation theory.

Definition 1.3.4. *A homogeneous network is a coupled cell network such that $B(c, d) \neq \emptyset$ for every pair of nodes c, d . A homogeneous network that has one equivalence class of edges is said to have identical coupling. The valence of an identical coupling network is the number of arrows in any (and hence every) input set.*

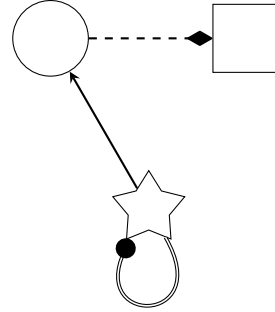
Examples of homogenous and non-homogenous coupled cell networks are provided in Figure 1.1.

Vector fields of coupled cell network

Now that we have described the topological component, we need to describe the suitable, or *admissible*, dynamics for a given network. Let \mathcal{F}_G^P denote the class of vector



(a) A homogenous bi-directional ring.



(b) A three-node non-homogenous network with mixed arrows and node types.

Figure 1.1: Examples of coupled cell networks.

fields compatible with a given coupled cell network \mathcal{G} . Each node of \mathcal{G} may represent a system of differential equations, so we associate a phase space P_c and state variables $x_c(t)$ at time t for each $c \in \mathcal{C}$. For this work, the phase space will be a nonzero finite-dimensional real-vector space. Two equivalent nodes over $\sim_{\mathcal{C}}$ must satisfy

$$c \sim_{\mathcal{C}} d \Rightarrow P_c = P_d$$

and we require the same coordinate systems on P_c and P_d .

For the coupled cell network \mathcal{G} as a whole, we define the *total phase space* to be

$$P = \prod_{c \in \mathcal{C}} P_c$$

and the corresponding coordinate system on P to be

$$x = (x_c)_{c \in \mathcal{C}}.$$

Let $\mathcal{D} = \{d_1, \dots, d_s\}$ be any ordered subset of s nodes in \mathcal{C} . The same node can appear in the set more than once. The phase space of this subset of nodes can be defined

as

$$P_{\mathcal{D}} = P_{d_1} \times \cdots \times P_{d_s}$$

and for $x_{d_j} \in P_{d_j}$, the corresponding coordinate system is

$$x_{\mathcal{D}} = (x_{d_1}, \dots, x_{d_s}).$$

For a given node c , we define the *internal phase space* to be P_c and the *coupling phase space* to be

$$P_{\mathcal{T}(I(c))} = P_{\mathcal{T}(i_1)} \times \cdots \times P_{\mathcal{T}(i_s)},$$

where $\mathcal{T}(I(c))$ denotes the ordered sets of nodes $(P_{\mathcal{T}(i_1)} \times \cdots \times P_{\mathcal{T}(i_s)})$ with the edges $i_k \in I(c)$. Suppose $c, d \in \mathcal{C}$ and $c \sim_I d$. For any $\beta \in B(c, d)$, define the pullback map

$$\beta^* : P_{\mathcal{T}(I(d))} \rightarrow P_{\mathcal{T}(I(c))}$$

by

$$(\beta^* z)\mathcal{T}(i) = z\mathcal{T}(\beta(i))$$

for all $i \in I(c)$ and $z \in P_{\mathcal{T}(I(d))}$. Now, we are ready to define the class of vector fields that is suitable for a coupled cell network.

Definition 1.3.5. A vector field $f : P \rightarrow P$ is \mathcal{G} -admissible if

- a. (domain condition) For all $c \in \mathcal{C}$ the component $f_c(x)$ depends only on the internal phase space variables x_c and the coupling phase space variables $x_{\mathcal{T}(I(c))}$; that is, there exists $\hat{f}_c : P_c \times P_{\mathcal{T}(I(c))} \rightarrow P_c$ such that

$$f_c(x) = \hat{f}_c(x_c, x_{\mathcal{T}(I(c))}),$$

b. (pullback condition) For all $c, d \in \mathcal{C}$ and $\beta \in B(c, d)$,

$$\hat{f}_d(x_d, x_{\mathcal{T}(I(d))}) = \hat{f}_c(x_d, \beta^* x_{\mathcal{T}(I(d))}),$$

for all $x \in P$.

These two conditions are combined to ensure that a vector field is suitable for a given network. An admissible vector field along with its coupled cell network is a *coupled cell system*.

Balanced equivalence relations and balanced colourings

To study the possible synchrony clusters in a network, the concepts of balanced equivalence relation and balanced colouring in a coupled cell networks are needed. Many synchronization patterns may occur for a given network paired with a specific vector field. However, these patterns may not persist under another vector field for the same network. We are interested in patterns of synchrony that are invariant under all admissible vector fields and such subspaces are said to be *robust*.

To speak of these patterns of synchrony mathematically, we can use equivalence relations \bowtie on the set of nodes \mathcal{C} . Such equivalence relation \bowtie partitions the nodes in \mathcal{C} into different classes. Obviously, any partition of the nodes will also form an equivalence relation. The corresponding *polysynchronous subspace* is given by

$$\Delta_{\bowtie} = \{x \in P : c \bowtie d \Rightarrow x_c = x_d\}.$$

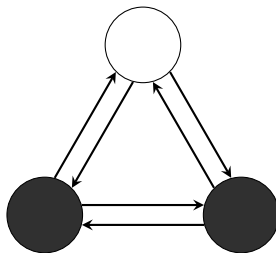
Whenever $c \bowtie d$, we can identify variables x_c and x_d using equivalence relations \bowtie . This restriction is the same as restricting vector field f to Δ_{\bowtie} . Hence, for

$$c \bowtie d \Rightarrow f_c = f_d \quad \text{on} \quad \Delta_{\bowtie}$$

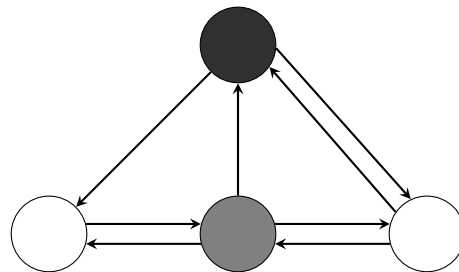
is a sufficient condition for $f \in \mathcal{F}_G^P$ to be flow-invariant on Δ_{\bowtie} . Reformulating these ideas using input isomorphisms, we can now state the idea of balanced equivalence relations.

Definition 1.3.6. *An equivalence relation \bowtie on \mathcal{C} is balanced if for every $c, d \in \mathcal{C}$ with $c \bowtie d$, there exists an input isomorphism $\beta \in B(c, d)$ such that $\mathcal{T}(i) \bowtie \mathcal{T}(\beta(i))$ for all $i \in I(c)$.*

This abstract idea of balanced equivalence relations on the node set \mathcal{C} of network \mathcal{G} may be made concrete graphically. We can colour the nodes in \mathcal{C} using the same colour whenever two nodes are in the same equivalence class. Furthermore, we colour the tail of each input arrow for each node the same colour of the equivalence class. Then, input isomorphism β is *colour preserving* if $\mathcal{T}(i)$ and $\mathcal{T}(\beta(i))$ share the same colour for all $i \in I(c)$. Then, a pattern of synchrony is balanced if and only if there exists a colour-preserving input isomorphism $\beta : I(c) \rightarrow I(d)$ between any two nodes of the same colour. Figure 1.2 shows examples of networks with balanced colouring patterns.



(a) A balance-coloured bi-directional ring with a 2-colour pattern, with various classes of nodes being represented by black and white.



(b) A balanced four-cell network with a 3-colour pattern, with various classes of nodes being represented by white, grey, and black.

Figure 1.2: Examples of coupled cell networks with balanced colourings.

We now connect the idea between balanced colouring and robust pattern of syn-

chrony with the following theorem.

Theorem 1.3.7. *Let \bowtie be an equivalence relation on a coupled cell network. Then \bowtie is robustly polysynchronous if and only if \bowtie is balanced.*

Proof. The proof may be found in the works by Stewart *et al.* (2003) and Golubitsky *et al.* (2005). □

Quotient networks

For a coupled cell network, each balanced equivalence relation \bowtie , induces a unique canonical quotient network. It can be shown that every vector field on the canonical network \mathcal{G}_{\bowtie} can be lifted to a corresponding vector field on \mathcal{G} . Given a \bowtie -equivalence over the nodes of network \mathcal{G} , we can define its quotient network using the following steps:

1. Let \bar{c} denote the \bowtie -equivalence class of $c \in \mathcal{C}$. The nodes in c_{\bowtie} are the \bowtie -equivalence classes in \mathcal{C} ; that is,

$$c_{\bowtie} = \{c : c \in \mathcal{C}\}.$$

Thus we obtain \mathcal{C}_{\bowtie} by forming the quotient of \mathcal{C} by \bowtie , that is, $\mathcal{C}_{\bowtie} = \mathcal{C} / \bowtie$.

2. Define

$$\bar{c} \sim_{c_{\bowtie}} \bar{d} \Leftrightarrow c \sim_C d.$$

The relation $\sim_{c_{\bowtie}}$ is well defined since \bowtie refines \sim_C .

3. Let $\mathcal{S} \subset \mathcal{C}$ be a set of nodes consisting of precisely one node c from each \bowtie -equivalence class. The input arrows for a quotient node \bar{c} are identified with the input arrows in node c , where $c \in \mathcal{S}$, that is, $I(\bar{c}) = I(c)$. When viewing the arrow $i \in I(c)$ as an arrow in $I(\bar{c})$, we denote that arrow by i . Thus, the arrows in

the quotient network are the projection of arrows in the original network formed by the disjoint union

$$\mathcal{E}_{\bowtie} = \dot{\bigcup}_{c \in \mathcal{S}} I(c).$$

The definition of the quotient network structure is independent of the choice of the representative nodes $c \in \mathcal{S}$.

4. Two quotient arrows are equivalent when the original arrows are equivalent. That is,

$$\bar{i}_1 \sim_{\mathcal{E}_{\bowtie}} \bar{i}_2 \Leftrightarrow i_1 \sim_{\mathcal{E}} i_2,$$

where $i_1 \in I(c_1)$, $i_2 \in I(c_2)$, and $c_1, c_2 \in \mathcal{S}$.

5. Define the heads and tails of quotient arrows by

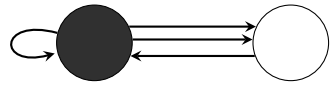
$$\mathcal{H}(\bar{i}) = \overline{\mathcal{H}(i)} \quad \text{and} \quad \mathcal{T}(\bar{i}) = \overline{\mathcal{T}(i)}.$$

6. It is easy to verify that the quotient network satisfies the consistency condition in Definition 1.3.1f. The quotient network is independent of the choice of nodes in \mathcal{S} because \bowtie is balanced.

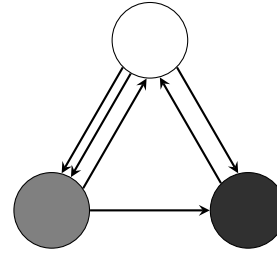
The nodes of the quotient network represent the equivalence classes in a balanced \bowtie -equivalence relations. In this work, we will lump together nodes with synchronized dynamics to simplify the analysis. Examples of quotient networks are shown in Figure 1.3

1.4 Structure of the Thesis

This chapter has outlined the need for better understanding of the process related to infectious diseases and the mathematical models that are associated with them. We



(a) A quotient network corresponding to the balanced colouring shown in Figure 1.2(a).



(b) A quotient network corresponding to the balanced colouring shown in Figure 1.2(b).

Figure 1.3: Examples of quotient networks, based on balanced colourings shown in Figure 1.2.

have also introduced the coupled cell system for analyzing models in later chapters of this thesis. Dynamics at the pathogen level and at the transmission level are intricately linked and they are complicated to model and difficult to analyze. The rest of this thesis is devoted to applying dynamical system techniques to differential equation models of infectious diseases. Our goal is to further our understanding of the model and in turn, the biological processes that inspired them.

We first analyze the dynamics of an *in vivo* single strain immunological model in Chapter 2. Unlike many other immunological models in the literature, this model takes into account and studies the secondary response of the immune system. Applying Lyapunov stability method, we show that the disease free and infectious equilibria can be globally asymptotically stable. For the nontrivial equilibrium of the system, we show that it may be locally stable and a Hopf bifurcation occurs from this equilibrium.

In Chapter 3, instead of having only one strain of pathogen, we analyze a multi-strain *in vivo* immunological model. Specifically, this model studies the antigenic variation of *P. falciparum* within the human immune system by explicitly accounting for the effects of epitopes. Numerical solutions of the model show that sustained oscillations may cluster together. Recasting the model using the theory of coupled cell system, we

show that these oscillations occur through a synchrony-breaking Hopf bifurcation of the proper quotient representation.

Continuing to study the effects of multiple strains of pathogens on infectious diseases, we turn our attention to a family of multi-strain epidemiological models in Chapter 4. These models explore the maintenance of pathogen strain structure at the host level. Again, we investigate the models as coupled cell systems and show that the discrete strain structure observed in these models may be mathematically explained through a synchrony-breaking semi-simple double-zero bifurcation from the trivial equilibrium of the quotient network.

This work is concluded in Chapter 5 with a look at potential future research.

Bibliography

- A. K. Abbas and A. H. Lichtman. *Basic Immunology: Functions and Disorders of The Immune System*. Saunders, 2004.
- R. Anderson and R. May. *Infectious Diseases Of Humans: Dynamics And Control*. Oxford University Press, USA, 1991.
- R. Antia, M. Nowak, and R. Anderson. Antigenic variation and the within-host dynamics of parasites. *Proceedings of the National Academy of Sciences*, 93(3):985, 1996.
- B. Bittner, S. Bonhoeffer, and M. Nowak. Virus load and antigenic diversity. *Bulletin of Mathematical Biology*, 59(5):881–896, 1997.
- S. Bonhoeffer, R. May, G. Shaw, and M. Nowak. Virus dynamics and drug therapy. *Proceedings of the National Academy of Sciences*, 94(13):6971, 1997.
- C. Buckee, L. Danon, and S. Gupta. Host community structure and the maintenance of pathogen diversity. *Proceedings of the Royal Society B: Biological Sciences*, 274(1619):1715, 2007.
- R. Casagrandi, L. Bolzoni, S. Levin, and V. Andreasen. The SIRC model and influenza A. *Mathematical Biosciences*, 200(2):152–169, 2006.

- D. Childs and M. Boots. The interaction of seasonal forcing and immunity and the resonance dynamics of malaria. *Journal of The Royal Society Interface*, 7(43):309, 2010.
- R. Coico and G. Sunshine. *Immunology: A Short Course*. Blackwell Pub, 2009.
- A. Craig and A. Scherf. *Antigenic Variation*. Academic Pr, 2003.
- J. Dawes and J. Gog. The onset of oscillatory dynamics in models of multiple disease strains. *Journal of Mathematical Biology*, 45(6):471–510, 2002.
- P. De Leenheer and S. Pilyugin. Immune response to a malaria infection: properties of a mathematical model. *Journal of Biological Dynamics*, 2(2):102–120, 2008.
- P. de Leenheer and H. Smith. Virus dynamics: a global analysis. *SIAM Journal on Applied Mathematics*, pages 1313–1327, 2003.
- F. Dercole, R. Ferriere, and S. Rinaldi. Chaotic red queen coevolution in three-species food chains. *Proceedings of the Royal Society B: Biological Sciences*, 277(1692):2321, 2010.
- C. Egami. Bifurcation analysis of the Nowak-Bangham model in CTL dynamics. *Mathematical Biosciences*, 221(1):33–42, 2009.
- A. Elaiw. Global properties of a class of HIV models. *Nonlinear Analysis: Real World Applications*, 11(4):2253–2263, 2010.
- N. Ferguson, R. Anderson, and S. Gupta. The effect of antibody-dependent enhancement on the transmission dynamics and persistence of multiple-strain pathogens. *Proceedings of the National Academy of Sciences*, 96(2):790, 1999.

- E. Gjini, D. Haydon, J. Barry, and C. Cobbold. Critical interplay between parasite differentiation, host immunity, and antigenic variation in Trypanosome infections. *The American Naturalist*, 176(4):424–439, 2010.
- J. Gog. The impact of evolutionary constraints on influenza dynamics. *Vaccine*, 26:C15–C24, 2008.
- J. Gog and B. Grenfell. Dynamics and selection of many-strain pathogens. *Proceedings of the National Academy of Sciences*, 99(26):17209, 2002.
- J. Gog and J. Swinton. A status-based approach to multiple strain dynamics. *Journal of Mathematical Biology*, 44(2):169–184, 2002.
- M. Golubitsky, I. Stewart, and A. Török. Patterns of synchrony in coupled cell networks with multiple arrows. *SIAM J. Appl. Dynam. Sys*, 4(1):78–100, 2005.
- S. Gupta and A. Galvani. The effects of host heterogeneity on pathogen population structure. *Philosophical Transactions of the Royal Society of London. Series B: Biological Sciences*, 354(1384):711, 1999.
- S. Gupta, M. Maiden, I. Feavers, S. Nee, R. May, and R. Anderson. The maintenance of strain structure in populations of recombining infectious agents. *Nature Medicine*, 2(4):437–442, 1996.
- S. Iwami, Y. Takeuchi, A. Korobeinikov, and X. Liu. Prevention of avian influenza epidemic: What policy should we choose? *Journal of Theoretical Biology*, 252(4):732–741, 2008.
- Y. Iwasa, F. Michor, and M. Nowak. Some basic properties of immune selection. *Journal of Theoretical Biology*, 229(2):179–188, 2004.

- X. Jiang, P. Yu, Z. Yuan, and X. Zou. Dynamics of an HIV-1 therapy model of fighting a virus with another virus. *Journal of Biological Dynamics*, 3(4):387–409, 2009.
- T. Kajiwara and T. Sasaki. Global stability of pathogen-immune dynamics with absorption. *Journal of Biological Dynamics*, 4(3):258–269, 2010.
- A. Korobeinikov. Global properties of basic virus dynamics models. *Bulletin of Mathematical Biology*, 66(4):879–883, 2004.
- A. Korobeinikov. Lyapunov functions and global stability for SIR and SIRS epidemiological models with non-linear transmission. *Bulletin of Mathematical Biology*, 68(3):615–626, 2006.
- A. Korobeinikov. Global properties of infectious disease models with nonlinear incidence. *Bulletin of Mathematical Biology*, 69(6):1871–1886, 2007.
- A. Korobeinikov. Global asymptotic properties of virus dynamics models with dose-dependent parasite reproduction and virulence and non-linear incidence rate. *Mathematical Medicine and Biology*, 26(3):225, 2009a.
- A. Korobeinikov. Global properties of SIR and SEIR epidemic models with multiple parallel infectious stages. *Bulletin of Mathematical Biology*, 71(1):75–83, 2009b.
- A. Korobeinikov. Stability of ecosystem: Global properties of a general predator–prey model. *Mathematical Medicine and Biology*, 26(4):309, 2009c.
- A. Korobeinikov and G. C. Wake. Lyapunov functions and global stability for SIR, SIRS, and SIS epidemiological models. *Applied Mathematics Letters*, 15(8):955–960, 2002.
- A. Korthals *et al.* The dual role of CD4 T helper cells in the infection dynamics of

- HIV and their importance for vaccination. *Journal of Theoretical Biology*, 214(4): 633–646, 2002.
- A. Lange and N. Ferguson. Antigenic diversity, transmission mechanisms, and the evolution of pathogens. *PLoS Computational Biology*, 5(10):e1000536, 2009.
- J. Lin, V. Andreasen, and S. Levin. Dynamics of influenza A drift: the linear three-strain model. *Mathematical Biosciences*, 162(1-2):33–51, 1999.
- W. Liu. Criterion of Hopf bifurcations without using eigenvalues. *Journal of Mathematical Analysis And Applications*, 182(1):250–256, 1994.
- W. Liu. Nonlinear oscillations in models of immune responses to persistent viruses. *Theoretical Population Biology*, 52(3):224–230, 1997.
- J. Lourenço and M. Recker. Viral and epidemiological determinants of the invasion dynamics of novel dengue genotypes. *PLoS Neglected Tropical Diseases*, 4(11): e894, 2010.
- K. Lythgoe, L. Morrison, A. Read, and J. Barry. Parasite-intrinsic factors can explain ordered progression of trypanosome antigenic variation. *Proceedings of the National Academy of Sciences*, 104(19):8095, 2007.
- P. Minayev and N. Ferguson. Improving the realism of deterministic multi-strain models: implications for modelling influenza A. *Journal of The Royal Society Interface*, 6(35):509, 2009.
- J. Mitchell and T. Carr. Oscillations in an intra-host model of *Plasmodium falciparum* malaria due to cross-reactive immune response. *Bulletin of Mathematical Biology*, 72(3):590–610, 2010.

- A. Murase, T. Sasaki, and T. Kajiwara. Stability analysis of pathogen-immune interaction dynamics. *Journal of Mathematical Biology*, 51(3):247–267, 2005.
- M. Nowak and C. Bangham. Population dynamics of immune responses to persistent viruses. *Science*, 272(5258):74, 1996.
- M. Nowak and R. May. Coexistence and competition in hiv infections. *Journal of Theoretical Biology*, 159(3):329–342, 1992.
- M. Nowak, R. May, and R. Anderson. The evolutionary dynamics of HIV-1 quasispecies and the development of immunodeficiency disease. *AIDS*, 4(11):1095–1103, 1990.
- M. Nowak, R. Anderson, A. McLean, T. Wolfs, J. Goudsmit, and R. May. Antigenic diversity thresholds and the development of AIDS. *Science*, 254(5034):963, 1991.
- M. Nowak, R. May, R. Phillips, S. Rowland-Jones, D. Lalloo, S. McAdam, P. Klenerman, B. Köppe, K. Sigmund, C. Bangham, *et al.* Antigenic oscillations and shifting immunodominance in HIV-1 infections. *Nature*, 1995a.
- M. Nowak, R. May, and K. Sigmund. Immune responses against multiple epitopes. *Journal of Theoretical Biology*, 175(3):325–353, 1995b.
- R. Omori, B. Adams, and A. Sasaki. Coexistence conditions for strains of influenza with immune cross-reaction. *Journal of Theoretical Biology*, 262(1):48–57, 2010.
- S. O'Regan, T. Kelly, A. Korobeinikov, M. O'Callaghan, and A. Pokrovskii. Lyapunov functions for SIR and SIRS epidemic models. *Applied Mathematics Letters*, 23(4):446–448, 2010.
- M. Recker and S. Gupta. Conflicting immune responses can prolong the length of

- infection in *Plasmodium falciparum* malaria. *Bulletin of Mathematical Biology*, 68(4):821–835, 2006.
- M. Recker, O. Pybus, S. Nee, and S. Gupta. The generation of influenza outbreaks by a network of host immune responses against a limited set of antigenic types. *Proceedings of the National Academy of Sciences*, 104(18):7711, 2007.
- M. Recker, K. Blyuss, C. Simmons, T. Hien, B. Wills, J. Farrar, and S. Gupta. Immunological serotype interactions and their effect on the epidemiological pattern of dengue. *Proceedings of the Royal Society B: Biological Sciences*, 276(1667):2541, 2009.
- M. Recker, C. Buckee, A. Serazin, S. Kyes, R. Pinches, Z. Christodoulou, A. Springer, S. Gupta, and C. Newbold. Antigenic variation in *Plasmodium falciparum* malaria involves a highly structured switching pattern. *PLoS Pathogens*, 7(3):e1001306, 2011.
- J. Sardanyés and R. Solé. Red queen strange attractors in host-parasite replicator gene-for-gene coevolution. *Chaos, Solitons & Fractals*, 32(5):1666–1678, 2007.
- A. Sasaki. Evolution of antigen drift/switching: continuously evading pathogens. *Journal of Theoretical Biology*, 168(3):291–308, 1994.
- X. Song and A. Neumann. Global stability and periodic solution of the viral dynamics. *Journal of Mathematical Analysis And Applications*, 329(1):281–297, 2007.
- M. Souza and J. Zubelli. Global stability for a class of virus models with cytotoxic T lymphocyte immune response and antigenic variation. *Bulletin of Mathematical Biology*, 73(3):609–625, 2011.
- I. Stewart, M. Golubitsky, and M. Pivato. Symmetry groupoids and patterns of synchrony in coupled cell networks. *SIAM J. Appl. Dynam. Sys.*, 2(4):609–646, 2003.

- C. Turner. A perspective on clonal phenotypic (antigenic) variation in protozoan parasites. *Parasitology*, 125:17–24, 2002.
- I. Volkov, K. Pepin, J. Lloyd-Smith, J. Banavar, and B. Grenfell. Synthesizing within-host and population-level selective pressures on viral populations: the impact of adaptive immunity on viral immune escape. *Journal of The Royal Society Interface*, 7(50):1311, 2010.
- K. Wang, W. Wang, and X. Liu. Global stability in a viral infection model with lytic and nonlytic immune responses. *Computers & Mathematics with Applications*, 51(9-10):1593–1610, 2006.
- P. Wikramaratna, C. Simmons, S. Gupta, and M. Recker. The effects of tertiary and quaternary infections on the epidemiology of dengue. *PLoS One*, 5(8):e12347, 2010.
- D. Wodarz. Cytotoxic T-lymphocyte memory, virus clearance and antigenic heterogeneity. *Proceedings of the Royal Society of London. Series B: Biological Sciences*, 268(1465):429, 2001.
- D. Wodarz. Hepatitis C virus dynamics and pathology: the role of CTL and antibody responses. *Journal of General Virology*, 84(7):1743, 2003.
- D. Wodarz and D. Levy. Multiple HIV-1 infection of cells and the evolutionary dynamics of cytotoxic t lymphocyte escape mutants. *Evolution*, 63(9):2326–2339, 2009.
- D. Wodarz and M. Nowak. Specific therapy regimes could lead to long-term immunological control of HIV. *Proceedings of the National Academy of Sciences*, 96(25):14464, 1999.
- D. Wodarz, P. Klenerman, and M. Nowak. Dynamics of cytotoxic T-lymphocyte exhaustion. *Proceedings of the Royal Society of London. Series B: Biological Sciences*, 265(1392):191, 1998.

- Y. Yang and Y. Xiao. Threshold dynamics for an HIV model in periodic environments. *Journal of Mathematical Analysis and Applications*, 361(1):59–68, 2010.
- P. Yu. Computation of normal forms via a perturbation technique. *Journal of Sound and Vibration*, 211(1):19–38, 1998.
- P. Yu. Analysis on double Hopf bifurcation using computer algebra with the aid of multiple scales. *Nonlinear Dynamics*, 27(1):19–53, 2002.
- P. Yu. Closed-form conditions of bifurcation points for general differential equations. *International Journal of Bifurcation and Chaos*, 15(4):1467–1483, 2005.
- P. Yu and A. Leung. The simplest normal form of Hopf bifurcation. *Nonlinearity*, 16: 277, 2003.
- P. Yu and Y. Yuan. A matching pursuit technique for computing the simplest normal forms of vector fields. *Journal of Symbolic Computation*, 35(5):591–615, 2003.

Chapter 2

Bifurcation Analysis in a Model of Cytotoxic T-Lymphocyte Response to Viral Infections

2.1 Introduction

From the advances in immunology over the last few decades, we are now able to understand the dynamics of infections at the cellular level. This detailed level of understanding allows researchers to simulate the interactions between pathogens and the host immune system using computer models. Of the many different mechanisms of the immune system, defences against viral infections are of interest because many of the diseases caused by them, e.g. hepatitis B and AIDS, are chronic and incurable (Male *et al.*, 2006; Nowak and May, 2000).

A virus cannot replicate on its own and it must take over host cells and use them in order to replicate. Once invaded by the viruses, these infected cells will cause a cytotoxic T-lymphocyte (CTL) response from the immune system. Cells involved in the

CTL response are also known as killer T-cells because they are responsible for apoptosis, i.e. programmed cell death, of the infected cells. Through the lysis of the infected cells, the viruses are prevented from further replicating (Nowak and May, 2000). The CTL response is also notable because it sometimes damages the body in its attempt to clear the virus. Over half the tissues damaged in hepatitis are actually caused by the CTL response (Male *et al.*, 2006; Wodarz, 2007).

To model the immune response resulting in a viral infection, researchers first consider the basic interactions between the immune system and the virus using the following system of differential equations (Anderson and May, 1991; De Boer and Perelson, 1998):

$$\begin{aligned}\dot{x} &= \lambda - dx - \beta xv, \\ \dot{y} &= \beta xv - ay, \\ \dot{v} &= ky - \mu v,\end{aligned}\tag{2.1}$$

where variables x , y and v represent the density of healthy cells, infected cells, and virus, respectively. Healthy cells are produced at rate λ and they died out naturally at rate dx . These cells may come into contact with the virus and become infected cells at rate βxv . Infected cells would died out naturally at rate ay . From the infected cells, the virus are replicated at rate ky and they are cleared naturally at rate μv .

To recover from a viral infection, cytotoxic T-lymphocytes effectors (CTLe) of the immune system will clear away the infected cells to prevent further viral replications. To model these extra dynamics, researchers modified model (2.1) by assuming that the virus population is at a quasi-steady state, i.e. $v = (k/\mu)y$, and let z represent the CTLe population to get a simple model of viral interaction with CTL response (De Boer and

Perelson, 1998; Nowak and Bangham, 1996):

$$\begin{aligned}
 \dot{x} &= \lambda - dx - \beta xy, \\
 \dot{y} &= \beta xy - ay - pyz, \\
 \dot{z} &= cyz - bz.
 \end{aligned} \tag{2.2}$$

Compared to model (2.1), healthy cells in this model become infected cells at rate βxy and the infected cells are removed by the CTL at pyz . The CTL population increases nonlinearly at rate cyz and they are removed at rate bz .

After a viral infection, the CTL that were responsible for clearing away the infected cells become cytotoxic T-lymphocytes precursors (CTLp) and they have receptors specifically for detecting the virus from the previous infection (Wodarz, 2007). Upon contact with the virus during a subsequent infection, the precursors differentiate and become cytotoxic T-lymphocyte effectors (CTLe) and these cells are again responsible for clearing away the invading virus. Hence, the following model from (Wodarz *et al.*, 2000) more accurately describes the dynamics of CTL response in the immune system:

$$\begin{aligned}
 \dot{x} &= \lambda - dx - \beta xy \\
 \dot{y} &= \beta xy - ay - pyz \\
 \dot{w} &= (1 - q)cyw - bw \\
 \dot{z} &= qcYW - hz.
 \end{aligned} \tag{2.3}$$

For this system, the healthy cells, x , and infected cells, y , are described similarly as in system (2.2). Instead of just one class of CTL response, there are the CTLp represented by w and the CTLe represented by z . These precursors emerge at rate cYW . They may become effectors at rate $qcYW$ or cleared away naturally at rate bw . Similarly, the

effectors are created at rate $cqyw$ and cleared at rate hz .

Dynamics of system (2.3) were analyzed mostly by numerical methods in (Wodarz *et al.*, 2000). In this study, we provide a rigorous analysis of system (2.3) similar to those done in (Jiang *et al.*, 2009; Egami, 2009). To start, we show that the system is a well-posed biological model in Section 2.2. Local stability of equilibria for system (2.3) were partially analyzed in (Wodarz *et al.*, 2000), so we complete the local as well as global stability analysis in Section 2.3. Aside from stability, we will analyze bifurcation dynamics using conditions established by Yu (2005) in Subsection 2.4.2. We provide some numerical illustrations to the system in Section 2.5. Finally, the biological significance of the results are discussed in Section 2.6.

2.2 Well-posedness of the model

For a biological model to be well-posed, only non-negative initial conditions are considered and the solution must not be negative. Let the parameters in (2.3) be positive constants. Directly solving for x , $x(t)$ can be expressed as

$$x(t) = e^{-\int_0^t (d+\beta y(s)) ds} \left(x(0) + \lambda \int_0^t e^{\int_s^t (d+\beta y(u)) du} ds \right).$$

For $t > 0$ and $x(0) \geq 0$, one can see that $x(t) > 0$. In a similar fashion, we can show that the other three variables have solutions as

$$\begin{aligned} y(t) &= y(0) e^{\int_0^t [\beta x(s) - a - pz(s)] ds}, \\ w(t) &= w(0) e^{\int_0^t [cy(s)(1-q) - b] ds}, \\ \text{and } z(t) &= e^{-ht} \left(z(0) + \int_0^t cqy(s)w(s)e^{hs} ds \right). \end{aligned}$$

All solutions are positive for $t > 0$ if $y(0) > 0$, $w(0) > 0$, and $z(0) \geq 0$.

From the first equation in system (2.3), we see that $\dot{x} \leq \lambda - dx$, so $\limsup_{t \rightarrow \infty} x(t) \leq \frac{\lambda}{d}$.

By adding the first two equations in (2.3), we get

$$\begin{aligned} \dot{x} + \dot{y} &= \lambda - dx - ay - pyz \\ &\leq \lambda - \tilde{\mu}_1(x + y), \end{aligned}$$

where $\tilde{\mu}_1 = \min\{a, d\}$. Thus, $\limsup_{t \rightarrow \infty} (x(t) + y(t)) \leq \frac{\lambda}{\tilde{\mu}_1}$.

Having shown that x and y are bounded, we will show by contradiction that w and z are also bounded. Let us assume z is unbounded. Then from the y equation in system (2.3), we have $\lim_{t \rightarrow \infty} y(t) = 0$. It follows from the z equation in system (2.3) that $\lim_{t \rightarrow \infty} z(t) = 0$. This result is a contradiction to the assumption, so z must be bounded. Similarly, assume that w is unbounded. Based on the z equation of system (2.3), we again have $\lim_{t \rightarrow \infty} y(t) = 0$. In this case, we see from the w equation in system (2.3) that $\lim_{t \rightarrow \infty} w(t) = 0$ when $\lim_{t \rightarrow 0} y(t) = 0$ and we have another contradiction. Based on this discussion, we have shown that there exists a bounded positive invariant region for the system. We define this region as $\Gamma \subset \mathbb{R}_+^4$.

For system (2.3), the three equilibria are given by

$$E_0 = \left(\frac{\lambda}{d}, 0, 0, 0 \right), \quad (2.4)$$

$$E_1 = \left(\frac{a}{\beta}, \frac{\lambda\beta - da}{a\beta}, 0, 0 \right), \quad \text{and} \quad (2.5)$$

$$E_2 = \left(\frac{\lambda}{dR_1}, \frac{b}{cQ}, \frac{h}{pqbcd} \left(\frac{R_0}{R_1} - 1 \right), \frac{1}{pcdQ} \left(\frac{R_0}{R_1} - 1 \right) \right), \quad (2.6)$$

where

$$\begin{aligned} Q &= (1 - q), \\ R_0 &= \frac{\lambda\beta}{ad}, \\ \text{and } R_1 &= 1 + \frac{\beta b}{cdQ}. \end{aligned}$$

In the next section, we will discuss the stability of E_2 and Hopf bifurcation. The stability of the equilibria is based on the Jacobian matrix of (2.3):

$$J(x, y, w, z) = \begin{bmatrix} -d - y\beta & -\beta x & 0 & 0 \\ y\beta & -\beta x - a - pz & 0 & -py \\ 0 & cw(1 - q) & cy(1 - q) - b & 0 \\ 0 & cqw & cqy & -h \end{bmatrix}. \quad (2.7)$$

2.3 Stability of E_0 and E_1

2.3.1 Infection-free equilibrium E_0

By the way of (2.7), we obtain the characteristic polynomial at the equilibrium E_0 as follow:

$$\Lambda_{E_0}(s) = \det[\lambda I - J(E_0)] = (s + d)(s + b)(s + h) \left(s + a - \frac{\lambda\beta}{d} \right).$$

For an equilibrium to be locally asymptotically stable, all the roots of the characteristic polynomial must be located in $\mathbb{C}^- = \{z \in \mathbb{C} : \text{Re}(z) < 0\}$. Given that all the parameters of the system are positive, the system is locally asymptotically stable at this equilibrium if

$$\lambda\beta - da < 0 \quad \text{or} \quad R_0 \triangleq \frac{\lambda\beta}{ad} < 1,$$

where R_0 represents the basic reproductive number. To show that this equilibrium is globally stable inside Γ , we will follow the method of fluctuation employed by Hirsch *et al.* (1985) and Jiang *et al.* (2009). To start, we denote

$$f_\infty = \liminf_{t \rightarrow \infty} f(t) \quad \text{and} \quad f^\infty = \limsup_{t \rightarrow \infty} f(t)$$

for any continuous and bounded function $f : [0, \infty) \rightarrow \mathbb{R}$. As shown in Section 2.2, the solutions $x(t)$, $y(t)$, $w(t)$, and $z(t)$ are always non-negative and bounded from above for any well-posed initial conditions. Hence, $\liminf_{t \rightarrow \infty}$ and $\limsup_{t \rightarrow \infty}$ always exist for each component. By the theorems on fluctuations (Thieme, 2003), there exists sequences t_n and s_n such that if $t_n \rightarrow \infty$ whenever $n \rightarrow \infty$, then

$$\begin{aligned} \lim_{n \rightarrow \infty} x(t_n) &= x^\infty, \quad \lim_{n \rightarrow \infty} \dot{x}(t_n) = 0 \\ \lim_{n \rightarrow \infty} x(s_n) &= x_\infty, \quad \lim_{n \rightarrow \infty} \dot{x}(s_n) = 0. \end{aligned} \tag{2.8}$$

Suppose $t = t_n$, then the first equation from system (2.3) gives

$$\dot{x}(t_n) + dx(t_n) + \beta x(t_n)y(t_n) = \lambda.$$

As $n \rightarrow \infty$, one can apply identities in (2.8) and the previous equation becomes

$$dx^\infty \leq (d + \beta y_\infty)x^\infty \leq \lambda. \tag{2.9}$$

By similar arguments on the other equations in system (2.3), we have

$$ay^\infty \leq (a + pz_\infty)y^\infty \leq \beta x^\infty y^\infty, \tag{2.10}$$

$$bw^\infty \leq c(1 - q)y^\infty w^\infty, \tag{2.11}$$

$$\text{and} \quad hz^\infty \leq cqy^\infty w^\infty. \tag{2.12}$$

Now, we can derive from equations (2.9) and (2.10) to get

$$ay^\infty \leq \beta x^\infty y^\infty \leq \frac{\lambda\beta}{d}y^\infty. \quad (2.13)$$

Suppose $y^\infty > 0$, inequality (2.13) implies

$$1 \leq \frac{\lambda\beta}{ad} = R_0,$$

which contradicts $R_0 < 1$, and so $y^\infty = 0$. Given $y^\infty = 0$, Equations (2.11) and (2.12) imply that $w^\infty = 0$ and $z^\infty = 0$. Since the solutions are non-negative and $\liminf \leq \limsup$, we must have $y(t), w(t), z(t) \rightarrow 0$ as $t \rightarrow \infty$. Because $y(t) \rightarrow 0$ asymptotically, the first equation in (2.3) becomes $\dot{x} = \lambda - dx$. Similar to the results in (Castillo-Chavez and Thieme, 1995), the solution $x(t) \rightarrow \lambda/d$ as $t \rightarrow \infty$. By the local stability result established earlier and global attractive property shown here, we have proven the following theorem.

Theorem 2.3.1. *When $R_0 < 1$, the infection-free equilibrium E_0 is globally asymptotically stable in Γ .*

2.3.2 Infectious equilibrium without CTL response E_1

When $R_0 > 1$, E_0 becomes unstable and a new equilibrium E_1 emerges. For this equilibrium solution to be physically meaningful, we must have $R_0 > 1$. Similarly, with the aid of (2.7) the characteristic equation at E_1 can be obtained as

$$\begin{aligned} \Lambda_{E_1}(s) &= \det[\lambda I - J(E_1)] \\ &= \frac{1}{a^2\beta}(s+h)(as^2 + \lambda\beta s + \beta\lambda a - da^2)[a\beta s + cQ(ad - \beta\lambda) + a\beta b]. \end{aligned}$$

There are two first-degree factors and one second degree factor. Given that all the parameters are positive, the first root is obviously stable. For the roots of the second-degree factor to be in \mathbb{C}^- , all its coefficients must have the same sign. Hence, its roots would be stable if and only if $R_0 > 1$. This condition is same as the condition for the equilibrium to be biologically meaningful, so we only need to check the remaining root. This equilibrium is locally stable if and only if

$$\begin{aligned} cQ(ad - \beta\lambda) + a\beta b > 0 &\Leftrightarrow cdQ(R_0 - 1) - \beta b < 0 \\ &\Leftrightarrow R_0 - 1 - \frac{\beta b}{cdQ} < 0, \\ &\Leftrightarrow R_0 < 1 + \frac{\beta b}{cdQ} \triangleq R_1. \end{aligned}$$

Not only that the system is locally stable at this equilibrium, one can show that this equilibrium is globally stable.

Theorem 2.3.2. *When $1 < R_0 < R_1$, the infectious equilibrium without CTL response (i.e. E_1) is globally asymptotically stable in Γ .*

Proof. To prove that the system is globally asymptotically stable, we will use Lyapunov stability theory to show that the system must converge to a region in hyperspace and upon entering such region, the solutions must converge to the equilibrium asymptotically. Based on the Lyapunov function candidates suggested in (Korobeinikov, 2004), we investigate the system using

$$V(x, y, w, z) = m \left(x - x_1 - x_1 \ln \frac{x}{x_1} + y - y_1 - y_1 \ln \frac{y}{y_1} \right) + \tilde{m}(w + z),$$

where m as well as \tilde{m} are positive coefficients yet to be determined, and x_1 as well as y_1 are the equilibrium expressions of x and y at E_1 . Clearly, $V(E_1) = 0$, which is the unique global minimum of the function. Now, we need to show that the equilibrium is globally attractive. The derivative of V with respect to time along the trajectory of the

system is

$$\begin{aligned}
\dot{V} &= m \left(\dot{x} - \frac{x_1}{x} \dot{x} + \dot{y} - \frac{y_1}{y} \dot{y} \right) + \tilde{m} (\dot{w} + \dot{z}) \\
&= m \left(\lambda + \frac{ad}{\beta} - \left(dx + \frac{\lambda a}{\beta x} \right) + \left(\lambda - \frac{ad}{\beta} \right) - \frac{\lambda\beta - ad}{a} x - pyz + \frac{\lambda\beta - ad}{a\beta} pz \right) \\
&\quad + \tilde{m}(cyw - bw - hz) \\
&= -m\lambda \left(\frac{x_1}{x} + \frac{x}{x_1} - 2 \right) - (\tilde{m}h + mp(y - y_1))z + \tilde{m}c \left(y - \frac{b}{c} \right) w \\
&= -\frac{m\lambda}{xx_1} (x - x_1)^2 - (\tilde{m}h + mp(y - y_1))z + \tilde{m}c \left(y - \frac{b}{c} \right) w.
\end{aligned}$$

For different values of y relative to y_1 and $\frac{b}{c}$, we can define the positive constants m and \tilde{m} to scale the different expressions properly to ensure that $\dot{V} < 0$. For most cases, the scaling can be performed directly based on the bounds on the variables. First, assume $y > y_1$. In this case, we only need to consider $y > \frac{b}{c}$ and we need to ensure that $\lim_{t \rightarrow \infty} z(t) = 0$ does not happen before $\lim_{t \rightarrow \infty} w(t) = 0$. As $z \rightarrow 0$ when $t \rightarrow 0$, the equation $\dot{w} + \dot{z} = (cy - b)w - hz$ approaches $\dot{w} = (cy - b)w$. Given that $y - \frac{b}{c} > 0$, w will grow unboundedly, which is contradictory to the result that the system is well-posed. Hence, as z approaches zero, w must also approach zero. Hence, for $w > 0$, we must have $z > 0$. For the terms $-mp(y - y_1)z + \tilde{m}c \left(y - \frac{b}{c} \right) w$, we can choose $m \gg \tilde{m}$, so that $\dot{V} < 0$. This result implies that the trajectory enters the region bounded by $y < y_1 + \epsilon$ at some finite time $T_1 > 0$ and then it will stay in this region for $t \in [T_1, \infty)$. Noticing that

$$\begin{aligned}
\frac{b}{cQ} - y_1 &= \frac{b}{cQ} - \frac{\lambda\beta - ad}{a\beta} \\
&= \frac{d}{\beta} \left(1 + \frac{b\beta}{cdQ} - \frac{\lambda\beta}{ad} \right) \\
&= \frac{d}{\beta} (R_1 - R_0) \\
&> 0 \quad \text{for } 1 < R_0 < R_1,
\end{aligned}$$

we can always select the appropriate m and \tilde{m} to ensure that $b/cQ > y_1 > y - \varepsilon$, i.e., $y < b/cQ + \varepsilon$ for arbitrary small ε . Hence, at some finite time $T > T_1$, the solution must enter $y \leq b/cQ$ and stay in this region for $t \in [T, \infty)$.

Having shown that y must be bounded above by b/cQ in finite time, we now proceed to prove that the solution trajectory will approach E_1 asymptotically. Using the inequality in (2.11), we have

$$bw^\infty \leq c(1-q)y^\infty w^\infty \quad \text{or} \quad \left(\frac{b}{c} - y^\infty\right)w^\infty \leq 0. \quad (2.14)$$

For $t \in [T, \infty)$, (2.14) will only hold if $w^\infty = 0$. Asymptotically, system (2.3) has the same dynamics as

$$\begin{aligned} \dot{x} &= \lambda - dx - \beta xy \\ \dot{y} &= \beta xy - ay \end{aligned} \quad (2.15)$$

and this subsystem has two equilibria at

$$\hat{E}_0 = \left(\frac{\lambda}{d}, 0\right) \quad \text{and} \quad \hat{E}_1(x_1, y_1).$$

It can be easily verified that when $1 < R_0 < R_1$, subsystem (2.15) is unstable at \hat{E}_0 and locally stable at \hat{E}_1 . Applying Lyapunov stability theory to the subsystem, we choose the Lyapunov function as

$$\hat{V}(x, y) = x - x_1 - x_1 \ln \frac{x}{x_1} + y - y_1 - y_1 \ln \frac{y}{y_1}.$$

Then

$$\dot{\hat{V}} = -\frac{\lambda}{xx_1}(x - x_1)^2 \leq 0,$$

for $x \neq x_1$. For $1 < R_0 < R_1$, subsystem (2.15) is globally asymptotically stable at \hat{E}_1

implying that the equilibrium E_1 of system (2.3) is globally asymptotically stable. \square

2.4 Stability of E_2 and Hopf bifurcation

2.4.1 Infectious equilibrium with CTL response E_2

As R_0 increases and passes R_1 , E_1 becomes unstable and the system moves to the third equilibrium E_2 . By equation (2.7), we obtain the characteristic equation at E_2 :

$$\Lambda_{E_2}(s) = \det[\lambda I - J(E_2)] = s^4 + \alpha_1 s^3 + \alpha_2 s^2 + \alpha_3 s + \alpha_4,$$

where

$$\alpha_1 = dR_1 + h,$$

$$\alpha_2 = ad\frac{R_0}{R_1}(R_1 - 1) + h \left[dR_1 + a \left(\frac{R_0}{R_1} - 1 \right) \right],$$

$$\alpha_3 = ah \left[(b + dR_1) \left(\frac{R_0}{R_1} - 1 \right) + d\frac{R_0}{R_1}(R_1 - 1) \right],$$

$$\text{and } \alpha_4 = abdh(R_0 - R_1).$$

It is clear that all $\alpha_i > 0$, $i = 1, 2, 3, 4$ due to $R_0 > R_1 > 1$.

Unlike the previous characteristic polynomials at other equilibria, Λ_{E_2} cannot be easily factored into polynomials of lesser degree. Hence, local stability of this equilibrium cannot be as easily identified. Instead, we will use the Routh-Hurwitz criterion to analyze its local stability. The criterion states that the corresponding equilibrium is locally asymptotically stable if and only if all the Hurwitz determinants of the characteristic polynomial are positive (Pritchard, 2005). For a four dimensional system, the

relevant Hurwitz determinants are

$$\Delta_1 = \alpha_1,$$

$$\Delta_2 = \alpha_1\alpha_2 - \alpha_3,$$

$$\Delta_3 = \alpha_3\Delta_2 - \alpha_1^2\alpha_4,$$

and $\Delta_4 = \alpha_4\Delta_3$.

Moreover, Δ_2 and Δ_3 can be written more explicitly as

$$\Delta_2 = A_2(h - b)^2 + B_2(h - b) + C_2,$$

$$\Delta_3 = ah [A_3(h - b)^2 + B_3(h - b) + C_3],$$

where

$$\begin{aligned} A_2 &= a \left(\frac{R_0}{R_1} - 1 \right) + dR_1, \\ B_2 &= ab \left(\frac{R_0}{R_1} - 1 \right) + d(2b + dR_1)R_1, \\ C_2 &= d [b(b + dR_1)R_1 + adR_0(R_1 - 1)], \\ A_3 &= a(b + dR_1) \left(\frac{R_0}{R_1} - 1 \right)^2 + d^2R_1(R_0 - R_1) + d^2R_0(R_1 - 1) \\ &\quad + ad \frac{R_0}{R_1} (R_1 - 1) \left(\frac{R_0}{R_1} - 1 \right), \\ B_3 &= (b + dR_1) \left[ab \left(\frac{R_0}{R_1} - 1 \right)^2 + d^2R_1(R_0 - R_1) + d^2R_0(R_1 - 1) \right] \\ &\quad + bd \frac{R_0}{R_1} (R_1 - 1) \left[a \left(\frac{R_0}{R_1} - 1 \right) + dR_1 \right], \\ C_3 &= d^2 \frac{R_0}{R_1} (R_1 - 1) [(b + dR_1) [a(R_0 - R_1) + bR_1] + adR_0(R_1 - 1)]. \end{aligned} \tag{2.16}$$

It is easy to see that all the coefficients A_i, B_i and C_i are positive for any parameter values, since $R_0 > R_1 > 1$ for this case. Therefore, $\Delta_2 > 0$, $\Delta_3 > 0$ as long as $h > b$. In other words, the infectious equilibrium with CTL response, E_2 , is always stable if

the death rate of the CTL_e is higher than that of the CTL_p.

In order to obtain more precise stability conditions for the infectious equilibrium with CTL response E_2 , we first prove the following lemma to show that if both Δ_2 and Δ_3 can become zero (requiring $h < b$), then Δ_3 will cross zero before Δ_2 does.

Lemma 2.4.1. *For $R_0 > R_1$, Δ_2 is positive when Δ_3 crosses zero for some change in parameters.*

Proof. Suppose $\Delta_3 = 0$, then we can rewrite the expression as

$$\Delta_2 = \frac{\alpha_1^2 \alpha_4}{\alpha_3}.$$

Since each α_i is positive as long as $R_0 > R_1$, we have $\Delta_2 > 0$. On the other hand, suppose $\Delta_2 = 0$, then we have $\Delta_3 = -\alpha_1^2 \alpha_4 < 0$. The proof is complete. \square

Thus, to consider the stability of E_2 , we only need to consider the possibility of $\Delta_3 = 0$. Now, let

$$\Delta = B_3^2 - 4A_3C_3, \quad h^* = b - \frac{B_3}{2A_3},$$

$$h_1^* = b - \frac{B_3 + \sqrt{\Delta}}{2A_3} \quad (\Delta > 0), \quad \text{and} \quad h_2^* = b - \frac{B_3 - \sqrt{\Delta}}{2A_3} \quad (\Delta > 0).$$

It is easy to see that $h_1^* < h^* < h_2^* < b$. Then, we have the following theorem.

Theorem 2.4.2. *In Γ , the stability of the infectious equilibrium with CTL response E_2 belongs to one of the following cases:*

- (i) when $\Delta < 0$, E_2 is always stable;
- (ii) when $\Delta = 0$, E_2 is always stable if $h^* \leq 0$; or is stable for $h \in (0, h^*) \cup (h^*, \infty)$ if $h^* > 0$;
- (iii) when $\Delta > 0$, E_2 is always stable if $h_2^* \leq 0$, or is stable for $h \in (h_2^*, \infty)$ if $h_2^* > 0 > h_1^*$, or is stable for $h \in (0, h_1^*) \cup (h_2^*, \infty)$ if $h_1^* > 0$.

Proof. The proof is straightforward by considering the sign of the quadratic polynomial $A_3(h - b)^2 + B_3(h - b) + C_3$, and thus the details are omitted here for brevity. \square

2.4.2 Hopf bifurcation analysis

In the previous sections, we showed that, as R_0 increases, E_0 loses its stability and transitions to E_1 . As R_0 further increases, E_1 would too lose its stability and goes to E_2 . In this section, we will show that Hopf bifurcation can occur from E_2 if R_0 increases even further with other conditions on the parameter h . Bifurcations are usually determined by the eigenvalues of the Jacobian matrix, but they are often difficult to determine explicitly for high dimensional systems. The next theorem states necessary and sufficient condition for finding Hopf critical point without finding the eigenvalues and its proof can be found in (Yu, 2005).

Theorem 2.4.3. *For $x \in \mathbb{R}^n$, $\mu \in \mathbb{R}$, and $f : \mathbb{R}^n \times \mathbb{R} \rightarrow \mathbb{R}^n$, assume that the general nonlinear ordinary differential system*

$$\dot{x} = f(x, \mu)$$

has a locally asymptotically stable equilibrium. The necessary and sufficient condition for a Hopf bifurcation to occur from the equilibrium is

$$\Delta_{n-1} = 0,$$

with α_n and $\Delta_i > 0$, where $1 \leq i \leq n - 2$.

For the present study, this theorem implies that a Hopf bifurcation from E_2 would occur when Δ_3 crosses from the positive to the negative and at the same time, $\Delta_1 > 0$ and $\Delta_2 > 0$ hold. From Lemma 2.4.1, we know that the only possible bifurcation which

can occur from the infectious equilibrium with CTL response E_2 is a Hopf bifurcation and it may only occur if $h < b$. In particular, we have the following theorem.

Theorem 2.4.4. *Let R_H denote the Hopf critical point. Then,*

- (i) *when $\Delta < 0$, $R_H = \infty$, that is, there is no Hopf bifurcation;*
- (ii) *when $\Delta = 0$, $R_H = \infty$ if the corresponding $h^* \leq 0$, or R_H is finite if the corresponding $h^* > 0$ (which only gives a single value for E_2 unstable), so there is no Hopf bifurcation;*
- (iii) *when $\Delta > 0$, $R_H = \infty$ if the corresponding $h_2^* \leq 0$, giving no Hopf bifurcation; or there is one finite critical value R_H if the corresponding $h_2^* > 0 > h_1^*$, giving rise to a Hopf bifurcation; or there are two finite critical values R_{H_1} and R_{H_2} if the corresponding $h_1^* > 0$, giving rise to two Hopf bifurcations.*

Proof. $\Delta_3 = 0$ is equivalent to find the roots of the quadratic polynomial equation $A_3(h - b)^2 - B_3(h - b) + C_3 = 0$, where all the three coefficients are positive and do not contain h . It is clear that when $\Delta = B_3^2 - 4A_3C_3 < 0$, the quadratic polynomial is positive for any positive parameter values, and thus E_2 is always stable, implying that there is no Hopf bifurcation and so the Hopf critical point is $R_H = \infty$. When $\Delta = 0$, the quadratic polynomial equation has one root

$$h - b = -\frac{B_3}{2A_3}, \quad \text{or} \quad h = b - \frac{B_3}{2A_3} \equiv h^* \quad \text{for } h > 0.$$

So if $h^* \leq 0$, then E_2 is always stable because $h > 0$ and no Hopf bifurcation can occur. If $0 < h^* < b$, we have a positive solution for h , and E_2 is stable except for the point $h = h^*$. Thus, the corresponding R_H is an isolated point, that is, except for this point, E_2 is always stable. Thus, for $\Delta = 0$, generically there is no Hopf bifurcation. Finally, for $\Delta > 0$, it may have three possibilities. The roots of the quadratic polynomial for

this case is given by

$$h - b = \frac{B_3 \mp \sqrt{\Delta}}{2A_3}, \quad \text{or} \quad h = b - \frac{B_3 \pm \sqrt{\Delta}}{2A_3} \equiv h_{1,2}^* \quad \text{for } h > 0.$$

If $h_1^* < h_2^* \leq 0$, E_2 is always stable (i.e. $R_H = \infty$); if $h_2^* > 0 > h_1^*$, then E_2 is stable for $h > h_2^*$ and there is a Hopf bifurcation emerging from the point $h = h_2^*$ with a finite R_H ; and if $h_1^* > 0$, then E_2 is stable for $h \in (0, h_1^*) \cup (h_2^*, \infty)$, and there are two Hopf bifurcations, which happen at the critical point $h = h_1^*$ and $h = h_2^*$ (the corresponding values in terms of R_0 equal R_{H_1} and R_{H_2}).

To verify if it is possible to have $\Delta = 0$, rewrite Δ as

$$\begin{aligned} \Delta = & \frac{\{R_1(dR_1 + b) - R_0[d(2R_1 - 1) + b]\}^2}{d^2R_1^4} \\ & \times \{b^2d^2R_1^2a^2 - 2dR_1[bd^3R_1^3 + \beta\lambda(-2d(R_1 - 1) + b^2)]a \\ & + d^6R_1^6 + 2\beta\lambda d^3R_1^3[b - 2d(R_1 - 1)] + \beta^2\lambda^2[b^2 - 4d^2(R_1 - 1)R_1]\}. \end{aligned}$$

Since R_1 does not contain a , we can solve the above equation $\Delta = 0$ to find a expressed in terms of other parameters. The first factor gives

$$a = \frac{\lambda\beta[d(2R_1 - 1) + b]}{dR_1(dR_1 + b)},$$

and the second quadratic polynomial of a yields

$$\begin{aligned} a = & dR_1\{bd^3R_1^3 + \beta\lambda[-2d(R_1 - 1) + b^2]\} \\ & \pm 2d^3R_1^2\sqrt{\lambda\beta(R_1 - 1)[\lambda\beta(R_1 - 1) - bR_1(dR_1 - b)]}. \end{aligned}$$

The above expressions show that all the three cases $\Delta < 0$, $\Delta = 0$ and $\Delta > 0$ are possible. \square

The next step is to study the stability of the limit cycles generated from the Hopf

bifurcations. To achieve this, consider general system

$$\dot{\mathbf{X}} = J\mathbf{X} + F(\mathbf{X}), \quad \mathbf{X} \in \mathbb{R}^n,$$

where $J\mathbf{X}$ is the linear part of the system. We must first find the differential equations on its centre manifold and then reduce the system to its normal form. Without loss of generality, we assume that $\mathbf{X} = \mathbf{0}$ is the fixed point of interest for the system.

Suppose J has n_c eigenvalues with zero real-part and n_s eigenvalues with negative real-part and $n = n_c + n_s$. Using the eigenvectors of J to form a transformation matrix, the system can be rewritten in block matrix form as

$$\begin{aligned} \dot{\mathbf{x}}_c &= A\mathbf{x}_c + f(\mathbf{x}_c, \mathbf{x}_s) \\ \dot{\mathbf{x}}_s &= B\mathbf{x}_s + g(\mathbf{x}_c, \mathbf{x}_s) \end{aligned} \quad (\mathbf{x}_c, \mathbf{x}_s) \in \mathbb{R}^{n_c} \times \mathbb{R}^{n_s}, \quad (2.17)$$

where $A \in \mathbb{R}^{n_c \times n_c}$ and $B \in \mathbb{R}^{n_s \times n_s}$. With the eigenvalues of zero real-part, the Centre Manifold Theorem (Guckenheimer and Holmes, 1990) guarantees that there exists a smooth manifold $W_c = \{(\mathbf{x}_c, \mathbf{x}_s) | \mathbf{x}_s = q(\mathbf{x}_c)\}$ near the equilibrium point such that the local behaviour in the centre direction of the system is qualitatively the same as that on the manifold. By differentiating $\mathbf{x}_s = q(\mathbf{x}_c)$, we get $\dot{\mathbf{x}}_s = Dq(\mathbf{x}_c)\dot{\mathbf{x}}_c$. Substituting (2.17) into the previous identity and rearranging the equation, we get

$$Dq(\mathbf{x}_c)[A\mathbf{x}_c + f(\mathbf{x}_c, q(\mathbf{x}_c))] - Bq(\mathbf{x}_c) - g(\mathbf{x}_c, q(\mathbf{x}_c)) = 0. \quad (2.18)$$

By solving for $q(\mathbf{x}_c)$, we get a function describing the center manifold. In general, $q(\mathbf{x}_c)$ cannot be solved explicitly. Instead, substituting a Taylor expansion $q(\mathbf{x}_c) = a\mathbf{x}^2 + b\mathbf{x}^3 + \mathcal{O}(\mathbf{x}^4)$ into (2.18), we can find the coefficients for the expansion by balancing the

lower order terms. Based on $q(\mathbf{x}_c)$, we now have a system in the reduced form:

$$\dot{\mathbf{x}}_c = A\mathbf{x}_c + f(\mathbf{x}_c, q(\mathbf{x}_c)).$$

Now we have the system reduced to the centre manifold, we will find its normal form of the system associated with the Hopf bifurcation. To transform the reduced system, we use nonlinear functions $\mathbf{x}_c = \mathbf{y} + h_i(\mathbf{y})$, where each $h_i(\mathbf{y})$ is an i th-degree homogenous polynomial ($2 \leq i \leq s$). Given that we are interested in Hopf bifurcation in this paper, we assume that $n_c = 2$ and $\mathbf{x}_c, \mathbf{y} \in \mathbb{R}^2$. Then the system can be transformed to

$$\dot{\mathbf{y}} = A\mathbf{y} + f_2(\mathbf{y}) + f_3(\mathbf{y}) + \cdots + f_{n_s}(\mathbf{y}) + DAh_{n_s}(\mathbf{y}) - Dh_{n_s}A(\mathbf{y}) + \mathcal{O}(|\mathbf{y}|^{n_s+1}),$$

where $f_i(\mathbf{y})$ represents the i th order terms in the expansion for the function f . We can choose the functions h_{n_s} such that $f_{n_s}(\mathbf{y}) = Dh_{n_s}A(\mathbf{y}) - DAh_{n_s}(\mathbf{y})$. Essential terms must remain regardless of our choice of h_s (Guckenheimer and Holmes, 1990). Hence, we can simplify the system up to a finite degree of terms by applying the process repeatedly. After a simplification up to third order, the normal form of a system associated with a Hopf bifurcation is

$$\begin{pmatrix} \dot{y}_1 \\ \dot{y}_2 \end{pmatrix} = \begin{pmatrix} (\nu_0\mu + \nu_1(y_1^2 + y_2^2))y_1 - (\omega + \tau_0\mu + \tau_1(y_1^2 + y_2^2))y_2 \\ (\omega + \tau_0\mu + \tau_1(y_1^2 + y_2^2))y_1 + (\nu_0\mu + \nu_1(y_1^2 + y_2^2))y_2 \end{pmatrix} + \mathcal{O}(|\mathbf{y}|^5).$$

We transform these two equations to the polar coordinates as

$$\begin{aligned} \dot{r} &= r(\nu_0\mu + \nu_1r^2) + \mathcal{O}(r^5) \\ \dot{\theta} &= \omega_0 + \tau_0\mu + \tau_1r^2 + \mathcal{O}(r^4), \end{aligned} \tag{2.19}$$

where r describes the amplitude and θ represents the phase of the periodic motion. By constructing a Poincaré map of the polar coordinate system, one can show that the bifurcating limit cycle is asymptotically stable when $\nu_1 < 0$ and unstable when $\nu_1 > 0$.

We have described a classical approach on determining the stability of Hopf bifurcation here. In order to perform the series of transformations to find the relevant coefficients, we must first determine the analytic expressions of the eigenvectors for the Jacobian to diagonalize it. We have not been successful in finding these expressions, thus we will not be able to determine the stability of the Hopf bifurcation found in Theorem 2.4.4 analytically. An alternative numerical method based on perturbation expansion is described in (Yu and Huseyin, 1988) and we use the associated algorithm to investigate stability for our system in the next section.

2.5 Numerical simulations

In this section, we demonstrate the analytic results in the previous sections through numerical simulations. To show that the system undergoes qualitative changes as R_0 increases, we vary R_0 by increasing λ and fix the rest of the parameters. The parameter values are chosen as

$$\beta = \frac{3}{400}, \quad d = c = h = q = \frac{1}{10}, \quad b = \frac{1}{5}, \quad a = \frac{1}{2}, \quad \text{and} \quad p = 1.$$

Their selections are biologically realistic and are based on (Wodarz *et al.*, 2000; Wang *et al.*, 2009) and the references therein. With these parameter values, we have

$$R_0 = \frac{3}{20}\lambda \quad \text{and} \quad R_1 = \frac{7}{6}.$$

2.5.1 Infection-free equilibrium E_0

For $0 < \lambda < \frac{20}{3} \triangleq \lambda_1^c$, $R_0 < 1$. Let $\lambda = 3$, then $R_0 = \frac{9}{20}$. Analytic expression for E_0 is stated in (2.4). As stated in Theorem 2.3.1, E_0 is globally asymptotically stable at these values. At the chosen parameters, the equilibrium values are $(x, y, w, z) = (30, 0, 0, 0)$. Numerical simulation for infection-free equilibrium E_0 is shown in Figure 2.1 and it shows that the healthy cells settle to the expected equilibrium value and all other populations die out after a brief period of time.

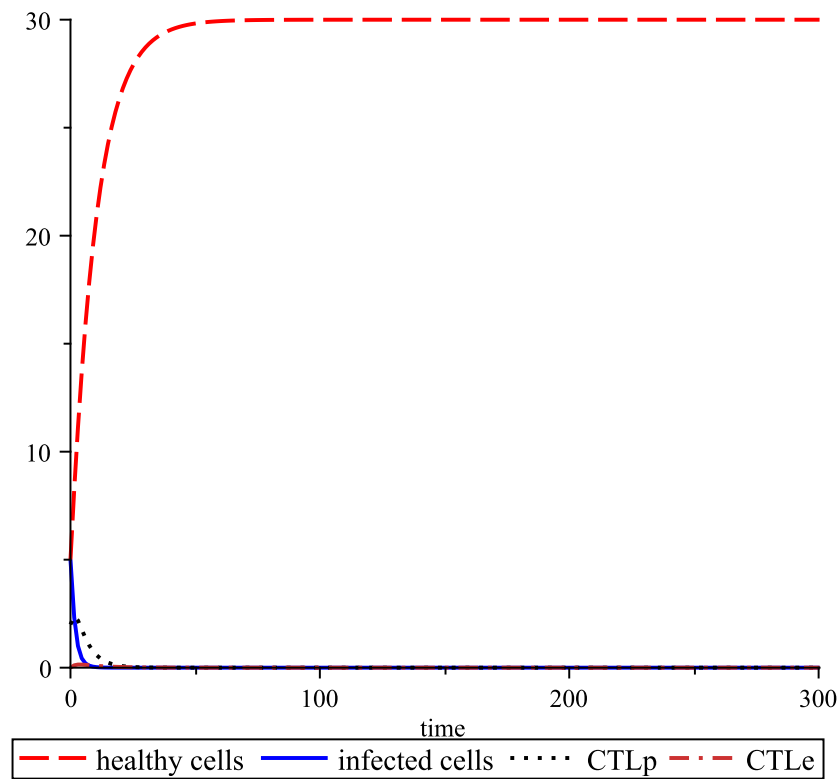


Figure 2.1: Simulations of system (2.3) at $\lambda = 3$.

2.5.2 Infectious equilibrium without CTL response E_1

Increasing λ further, R_0 passes one and E_0 loses stability to E_1 . According to Theorem 2.3.2, E_1 remains asymptotically stable when $1 \leq R_0 < R_1$, i.e. $\lambda_1^c = \frac{20}{3} \leq \lambda <$

$\frac{70}{9} \triangleq \lambda_2^c$. We choose $\lambda = 7.5$, so that the reproductive number is $R_0 = 1.125$.

Analytic equilibrium expression for E_1 is shown in (2.5) and as shown in Figure 2.2, the dynamics settle to the numerical values of $(x, y, w, z) = (66.6, 1.16, 0, 0)$. The

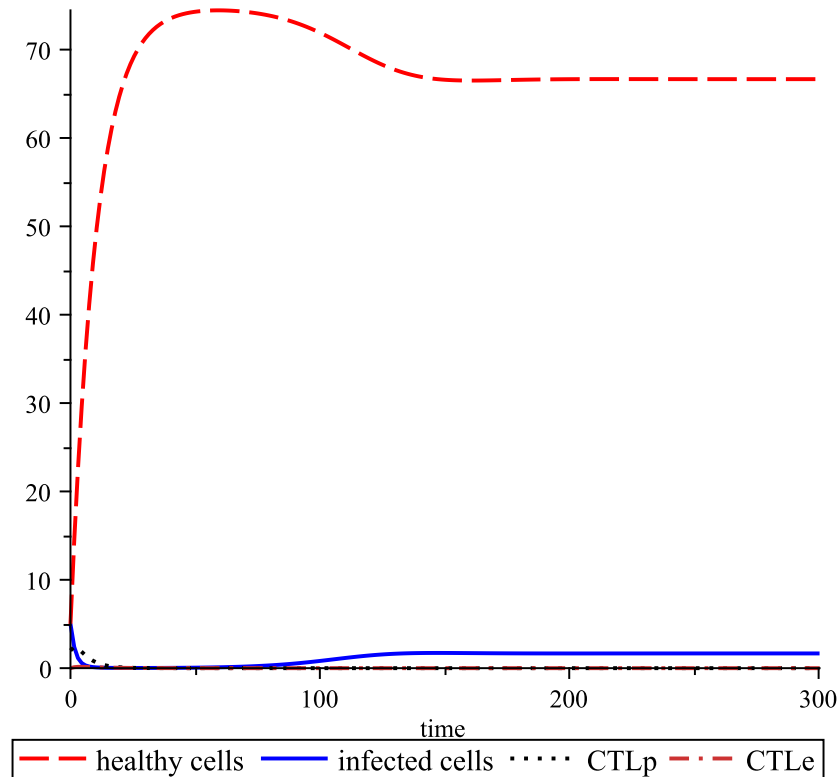


Figure 2.2: Simulations of system (2.3) at $\lambda = 7.5$.

healthy cell population decreased from the previous equilibrium and at the same time, the infected population increased. As expected from the analytic analysis, the simulation shows that there is no CTL response.

2.5.3 Infectious equilibrium with CTL response E_2

When R_0 increases and passes R_1 , E_1 loses its stability and the system is then stable at the third equilibrium E_2 . The reproductive number will be greater than R_1 when $\lambda > 70/9$. Local stability conditions for this equilibrium were shown in Theorem 2.4.2

using the Routh-Hurwitz stability theorem. Hence, we shall check the conditions for the theorem numerically. Using the selected parameters, the characteristic equation in terms of λ is

$$\Lambda_{E_2}(s) = s^4 + \frac{13}{60}s^3 + \left(\frac{3\lambda}{400} - \frac{23}{600}\right)s^2 + \left(\frac{3\lambda}{1400} - \frac{19}{1200}\right)s + \left(\frac{3\lambda}{20000} - \frac{7}{6000}\right).$$

From the characteristic polynomial, the relevant Hurwitz determinants are

$$\begin{aligned} \Delta_2(\lambda) &= -\frac{29}{56000}\lambda + \frac{271}{36000}, \\ \text{and } \Delta_3(\lambda) &= -\frac{87}{78400000}\lambda^2 + \frac{5809}{336000000}\lambda - \frac{2783}{43200000}. \end{aligned}$$

Solving for λ when $\Delta_3 = 0$, we find that the roots are

$$\lambda_1 = \frac{1610}{261} \approx 6.17 \quad \text{and} \quad \lambda_2 = \frac{847}{90} \approx 9.41. \quad (2.20)$$

Thus, E_2 is stable when $70/9 < \lambda < 847/90$. We choose $\lambda = 8$. Direct evaluations of Δ_2 and the coefficients of the characteristics polynomial at $\lambda = 8$ show that they are all positive. Hence, we have satisfied the local stability criteria from the Routh-Hurwitz theorem.

According to the formulas given in (2.16), we have

$$\begin{aligned} A_3 &= \frac{27}{9800} \left[\left(\lambda - \frac{3899}{540} \right)^2 + \frac{115199}{291600} \right] > 0, \\ B_3 &= \frac{27}{49000} \left[\left(\lambda - \frac{22561}{3240} \right)^2 + \frac{12175079}{10497600} \right] > 0, \\ C_3 &= \frac{1}{5600000} \lambda (30\lambda - 133) > 0 \quad \text{for } \lambda > \frac{70}{9}, \end{aligned}$$

which yields

$$\Delta = \frac{29}{38416000000}(18\lambda - 133)^2 \left[\left(\lambda - \frac{11935}{1566} \right)^2 - \frac{1250921}{613089} \right].$$

Hence, $\Delta = 0$ yields

$$\begin{aligned} \lambda &= \frac{11935 \pm 98\sqrt{521}}{1566}, \frac{133}{18}, \frac{133}{18} \\ &\approx 6.192917246, 7.388888889, 7.388888889, 9.049739204. \end{aligned}$$

Let $\lambda^* = \frac{11935+98\sqrt{521}}{1566} \approx 9.049739204$. Then, $\Delta < 0$ for $\frac{70}{9} < \lambda < \lambda^*$, $\Delta = 0$ for $\lambda = \lambda^*$, and $\Delta > 0$ for $\lambda > \lambda^*$. Therefore, E_2 is always stable for $\frac{70}{9} < \lambda < \lambda^*$. When $\lambda = \lambda^*$, we have $h^* = \frac{2839-25\sqrt{521}}{43080} \approx 0.05265469799 > 0$, so E_2 for this numerical example with the given value $h = \frac{1}{10} \neq h^*$ is stable. When $\lambda > \lambda^*$, we have two roots from the quadratic polynomial as

$$h_{1,2}^* = \frac{29160\lambda^2 - 436086\lambda + 1615775 \pm 5(18\lambda - 133)\sqrt{84564\lambda^2 - 1288980\lambda + 4739329}}{(540\lambda - 3899)^2 + 1151199}$$

It can be shown that both $h_{1,2}^* > 0$ for $\lambda > \lambda^*$. Thus, according to Theorem 2.4.4, we know that E_2 is stable for $(0, h_1^*) \cup (h_2^*, \infty)$. Suppose $\lambda = 9.2$, then $h_1^* = 0.03181658398$ and $h_2^* = 0.08247353652$. The given value $h = 0.10 > h_2^*$, implying that E_2 is stable. If take $\lambda = 10$, then we have $h_1^* = 0.01728507103$ and $h_2^* = 0.1270566231$, which indicates $h = 0.10 \in (h_1^*, h_2^*)$, and so E_2 is unstable.

Based on the analytic equilibrium expression of E_2 given by (2.6), there should be non-zero CTL responses at this equilibrium. In Figure 2.3, the response of each population settles to the expected equilibrium values of $(x, y, w, z) = (77.14, 2.22, 0.35, 0.8)$.

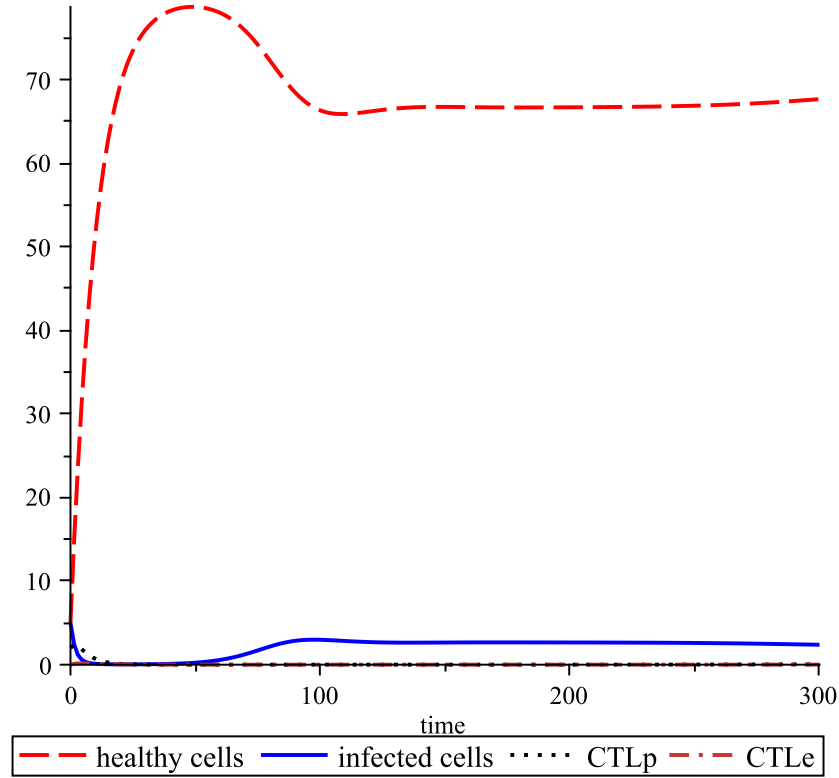


Figure 2.3: Simulations of system (2.3) at $\lambda = 8$.

2.5.4 Hopf bifurcation

As stated in Theorem 2.4.4, there will be a Hopf bifurcation for large enough R_0 . By calculations in (2.20), Δ_3 crosses zero and becomes negative when $\lambda = 847/90$. Hence, Hopf bifurcation occurs at $\lambda_H = 847/90$. Or in terms of reproductive number, we have $R_H = 847/600 \approx 1.4115$. Numerically, the Hurwitz determinants at $R_0 = R_H$ are

$$\Delta_2 = \frac{637}{240000}, \quad \text{and} \quad \Delta_3 = 0.$$

To show that Δ_3 crosses from the positive to the negative, we select $\lambda = 98/10 \approx 9.8$, at which

$$h_1^* = 0.01889876185, \quad h_2^* = 0.1198979582.$$

For the given value $h = 0.10$, E_2 is unstable and limit cycles bifurcating from the Hopf critical point $R_0 = R_H$. In fact, when $h = 0.10$, the relevant Hurwitz determinants become

$$\Delta_2 = \frac{883}{360000}, \quad \text{and} \quad \Delta_3 = -\frac{677}{432000000}.$$

Comparing the present numeric values to those evaluated earlier, we see that Δ_3 crosses from the positive into the negative non-degenerately. By Theorem 2.4.3, one pair of complex conjugate eigenvalues crosses from \mathbb{C}^- into \mathbb{C}^+ and Hopf bifurcation occurs. Numerical solutions of the system are plotted in Figure 2.4, showing oscillations for each variable. In Figure 2.5, a limit cycle among the healthy cells, infected cells and the CTLp populations is observed in the phase space .

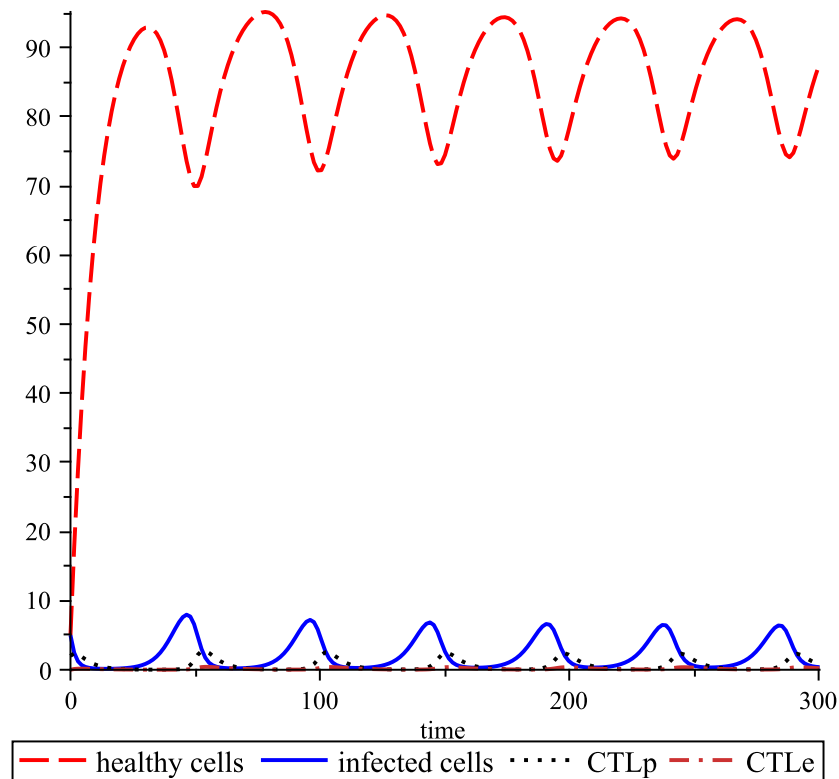


Figure 2.4: Simulations of system (2.3) with oscillations at $\lambda = 10$ ($\mu = 53/90$).

Stability conditions for the periodic solution can be obtained from method of nor-

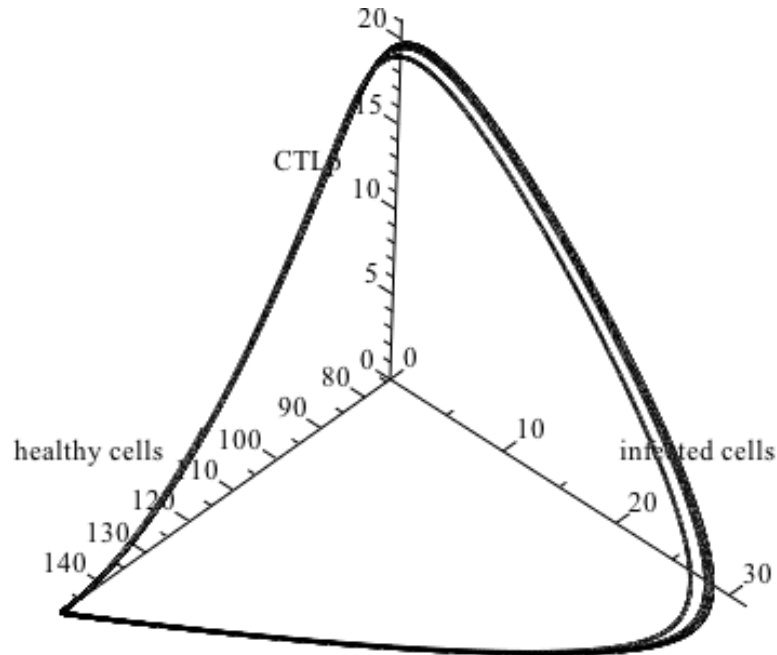


Figure 2.5: Limit cycles of system (2.3) at $\lambda = 10$ ($\mu = 53/90$).

mal form theory, Lyapunov-Schmidt reduction or Poincaré-Lindstedt expansion. While these methods proceed differently, they all require the explicit expressions for the eigenvalues and the eigenvectors from the Jacobian of the system for analytic calculations. As mentioned earlier, we were unable to obtain the necessary expressions for such analysis, so we turned to a numerical algorithm given by (Yu, 1998) to investigate the stability of the orbits. This algorithm employs the method of multiple time scale to expand the system in question at a critical Hopf bifurcation point. Solving the perturbed differential equations, one could determine the constants which uniquely determine the normal form of the system.

We use a Maple implementation of the aforementioned algorithm to determine the stability at critical point $R_H = 847/90$. In polar coordinates, the normal form for

Hopf bifurcations is described in (2.19). Applying to our present situation, we have $\mu = \lambda - \lambda_H = 10 - 847/90 = 53/90$. The form is uniquely determined by the constants $\nu_0, \nu_1, \omega_0, \tau_0$ and τ_1 . Imaginary component of the bifurcating eigenvalue pair is $\omega_0 = \sqrt{2}/10$. As shown in (Jiang *et al.*, 2009), the other constants are also determined by the Maple implementation from (Yu, 1998) and they are

$$\begin{aligned}\nu_0 &= \frac{8370}{1006943}, & \nu_1 &= -\frac{7159359703000}{25412370525507}, \\ \tau_0 &= \sqrt{2}\frac{23400}{1006943}, & \text{and } \tau_1 &= -\frac{724938191405000}{76237111576521}.\end{aligned}$$

Since $\nu_1 < 0$, the bifurcating limit cycles are stable. Other than stability, we can also find the amplitude and frequency of the periodic solutions. Based on the previously deduced parameters, we write the third-order normal form of (2.3) as

$$\begin{aligned}\dot{r} &= r \left(\frac{8370}{1006943}\mu - \frac{7159359703000}{25412370525507}r^2 \right), \\ \dot{\theta} &= \frac{\sqrt{2}}{10} + \sqrt{2}\frac{23400}{1006943}\mu - \frac{724938191405000}{76237111576521}r^2.\end{aligned}\tag{2.21}$$

By setting the first equation in (2.21) to zero, the roots are

$$r = 0 \quad \text{and} \quad r = \frac{171}{715935970300} \sqrt{5171871333929279\mu}.\tag{2.22}$$

The non-zero root in (2.22) corresponds to the amplitude of the bifurcation. Furthermore, the frequency of the said solution is given by

$$\omega = \sqrt{2}/10 + \left(\sqrt{2}\frac{23400}{1006943} - \frac{2022577554019950}{7209067137417929} \right) \mu.$$

2.6 Biological Implications

Wodarz *et al.* (2000) built a model to investigate the interactions between healthy and infected cells as well as primary and secondary CTL response cells. In terms of analytic investigation of the model, the authors only analyzed the structure of the equilibria and some specific cases. For a higher dimension system, equilibrium behaviour alone cannot fully describe the full dynamics of the system. Stability and bifurcation analysis are important for the full range of possibilities. In this work, we fully described the stability of the infection-free equilibrium E_0 , the infectious equilibrium without CTL response E_1 , and the infectious equilibrium with CTL response E_2 .

Analytically, we showed that when $0 < R_0 < 1$, the infection-free equilibrium is globally asymptotically stable; when $1 < R_0 < R_1$, the infection-free equilibrium becomes unstable and the infectious equilibrium without CTL response is globally asymptotically stable; when $R_1 < R_0 < R_H$, the infectious equilibrium with CTL response may be locally asymptotically stable; finally, given $\Delta > 0$, there exists a Hopf bifurcation from the infectious equilibrium with CTL response for an appropriate choice of the system's parameters. Given that R_0 , R_1 , R_H , and Δ are comprised of the parameters of the system, we have shown how the parameters effect the dynamics of the model.

From Section 2.1, we see that system (2.3) is formed by splitting the CTL class in system (2.2) into two different response classes. By a direct calculation, one can see that the basic productive number R_0 for systems (2.2) and (2.3) are the same. Hence, the parameters in the equations dealing with CTL responses have no effect on R_0 . In other words, the dynamics of the CTL responses do not affect the way system transition from infection-free equilibrium to the infectious equilibria. Given that the CTL cells have no role in preventing infections, this aspect of the model is consistent with biological situation.

Originally, the authors of (Wodarz *et al.*, 2000) only explored aspects of system (2.3)

numerically. In our analysis, we have identified periodic solutions of the model in a rigorous manner. These sustained oscillations stem from the infectious equilibrium with CTL response. For the immune system, this transition represents a change from homeostatic states to sustained fluctuations of the cell populations in the model. The sustained oscillations from the Hopf bifurcation imply that upon primary infection, the pathogen may not always be cleared entirely with the CTL responses. As one could see from Figure 2.4, the number of the infected cells may decrease, but over time, the population oscillates and cannot be completely eradicated. This phenomenon can be viewed as an individual having a chronic disease that may flare up from time to time.

Through the expressions obtained from the stability and bifurcation analysis, we are able to better understand the transition from a homeostatic state to oscillations triggered by a Hopf bifurcation. We showed that $\Delta > 0$ is a necessary condition for Hopf bifurcation in Theorem 2.4.4. This condition constraints that $h < b$ for sustained oscillations to occur. These two constants are the decaying rates of the two classes of immune cells. When effectors have longer life span than precursors ($h < b$), flare ups of the disease can occur. On the other hand, when the precursors have longer life span than the effectors ($h > b$), the immune system is able to prevent flare ups and control the system at a steady state. This result, based on expressions obtained from the bifurcation analysis, is in agreement with the analysis (Luzyanina *et al.*, 2001). Like system (2.3), this model of lymphocytic choriomeningitis virus has precursor and effector CTL classes and it also involves time-delay. These models both predict that the immune system is more efficient in controlling the disease when the precursors outlive the effectors.

Traditionally, immunologists have ignored the oscillatory behaviour of the immune system. They considered equilibrium states as the natural states of the immune system and any other behaviour, such as oscillations, were seen as transitional states between two equilibria. Studies of the immune system and pathogen interactions show that

equilibrium states may not be the only consistent behaviour in immune response (Stark *et al.*, 2007). To model the sustained oscillations in the aforementioned studies using differential equations, one must look to a model that could incorporate possible Hopf bifurcations. For in-host virus dynamics, models including intra-cellular delay (Culshaw *et al.*, 2003; Luzyanina *et al.*, 2001) and experimental treatment (Jiang *et al.*, 2009) have shown sustained oscillations. In this paper, we showed that, even without time-delay, the dynamics from the interactions of precursors and effectors added to the model of healthy and infected host cells could also produce a Hopf bifurcation. Thus, we have provided another theoretical reason to explain the periodic dynamics in future research.

Bibliography

- R. Anderson and R. May. *Infectious Diseases Of Humans: Dynamics And Control*. Oxford University Press, USA, 1991.
- C. Castillo-Chavez and H. Thieme. Asymptotically autonomous epidemic models. In *Mathematical Population Dynamics: Analysis of heterogeneity*, pages 33–50, 1995.
- R. Culshaw, S. Ruan, and G. Webb. A mathematical model of cell-to-cell spread of HIV-1 that includes a time delay. *Journal of Mathematical Biology*, 46(5):425–444, 2003. ISSN 0303-6812.
- R. De Boer and A. Perelson. Target cell limited and immune control models of HIV infection: a comparison. *Journal of Theoretical Biology*, 190(3):201–214, 1998.
- C. Egami. Bifurcation analysis of the Nowak-Bangham model in CTL dynamics. *Mathematical Biosciences*, 221(1):33–42, 2009.
- J. Guckenheimer and P. Holmes. *Nonlinear Oscillations, Dynamical Systems, and Bifurcations of Vector Fields*. Copernicus, 1990.
- W. Hirsch, H. Hanisch, and J. Gabriel. Differential equations models for some parasitic infections; methods for the study of asymptotic behavior. *Comm. Pure Appl. Math*, 38:733–753, 1985.

- X. Jiang, P. Yu, Z. Yuan, and X. Zou. Dynamics of an HIV-1 therapy model of fighting a virus with another virus. *Journal of Biological Dynamics*, 3(4):387–409, 2009.
- A. Korobeinikov. Global properties of basic virus dynamics models. *Bulletin of Mathematical Biology*, 66(4):879–883, 2004.
- T. Luzyanina, K. Engelborghs, S. Ehl, P. Klenerman, and G. Bocharov. Low level viral persistence after infection with LCMV: A quantitative insight through numerical bifurcation analysis. *Mathematical Biosciences*, 173(1):1–23, 2001.
- D. Male, J. Brostoff, D. Roth, and J. Roitt. *Immunology*. Elsevier, 2006.
- M. Nowak and C. Bangham. Population dynamics of immune responses to persistent viruses. *Science*, 272(5258):74, 1996.
- M. Nowak and R. May. *Virus Dynamics*. Oxford University Press, 2000.
- A. Pritchard. *Mathematical Systems Theory*. Springer, 2005.
- J. Stark, C. Chan, and A. George. Oscillations in the immune system. *Immunological Reviews*, 216(1):213–231, 2007. ISSN 1600-065X.
- H. R. Thieme. *Mathematics in Population Biology*. Princeton, 2003.
- Y. Wang, Y. Zhou, J. Wu, and J. Heffernan. Oscillatory viral dynamics in a delayed HIV pathogenesis model. *Mathematical Biosciences*, 219(2):104–112, 2009.
- D. Wodarz. *Killer Cell Dynamics: Mathematical and Computational Approaches To Immunology*. Springer Verlag, 2007.
- D. Wodarz, K. Page, R. Arnaout, A. Thomsen, J. Lifson, and M. Nowak. A new theory of cytotoxic T-lymphocyte memory: Implications for HIV treatment. *Philosophical Transactions of the Royal Society of London. Series B: Biological Sciences*, 355(1395):329, 2000.

- P. Yu. Computation of normal forms via a perturbation technique. *Journal of Sound and Vibration*, 211(1):19–38, 1998.
- P. Yu. Closed-form conditions of bifurcation points for general differential equations. *International Journal of Bifurcation and Chaos*, 15(4):1467–1483, 2005.
- P. Yu and K. Huseyin. A perturbation analysis of interactive static and dynamic bifurcations. *IEEE Transactions on Automatic Control*, 33(1):28–41, 1988.

Chapter 3

Synchrony-Breaking Hopf Bifurcation in a Model of Antigenic Variation

Antigenic variation is a successful strategy for pathogens to evade the immune system (Craig and Scherf, 2003). The exact process is not well-understood yet. We first give a summary of the currently accepted view on the subject here. Precursor cells of the immune system detect potential pathogens via specific chemical determinants, such as proteins and carbohydrates, on the surfaces of pathogens or infected cells. These chemical markers are called epitopes. Once detected, precursor cells may differentiate into effector cells and eliminate the potential threat. In the continual battle between pathogens and the immune system, some pathogens have evolved to have a wide variety and seemingly ever changing surface markers. Antigen specific precursors may fail to recognize them as harmful material immediately. This delay in recognition allows the pathogen population time to grow so that it can express another surface protein. By the time the effectors have cleared away one variant, another variant of the same pathogen would be growing. This strategy of presenting many different variants by the pathogens for the purpose of evading the immune system is called antigenic variation. Different variants can arise from point mutations of the pathogen, thus giving rise to new variants

with different genotypes. Alternatively, it can arise from programmed variation of the surface markers. In this case, the different surface markers are simply expression of the same genetic structures.

Plasmodium falciparum is a pathogen capable of antigenic variation and it causes malaria in humans. In this chapter, we will analyze the bifurcation dynamics of an ordinary differential equation model of this protozoan parasite, originally proposed by Recker *et al.* (2004). Research shows that the variants of *P. falciparum* presented inside the hosts are different phenotypes stemming from the *var* gene (Turner, 2002). On the surface of these different variants are various epitopes. This model assumes that there are major epitopes that are unique to each variant and minor epitopes that are shared across variants. It has been hypothesized that the major epitope from each variant elicits longterm CTL response that is variant specific. On the other hand, the minor epitopes that are shared by multiple variants elicit transient CTL response that will cross-react to any strains which share the minor epitope. The dynamics resulting from this feature of antigenic variation was the focus in (Recker *et al.*, 2004) and will be further examined analytically in this work.

Given that the interactions between *P. falciparum* and the immune system are not well understood, there are mathematical models in the literature studying the dynamics. Single variant model of the in-host dynamics have been considered by Saul (1998) and Gravenor and Lloyd (1998). Mutation dynamics of multi-strain pathogens have been studied in (De Leenheer and Pilyugin, 2008b). Furthermore, stochastic models of antigenic variation have been reviewed in (Frank and Barbour, 2006). For deterministic models, Recker *et al.* (2004) proposed a differential equation model, which describes the effects of antigenic variations on immune effectors and pathogens. This aforementioned model allows one to connect different sets of differential equations to examine the effects of immune cross-protection incited from shared epitopes between variants.

Specific cases from the aforementioned model have been further studied numerically and analytically in (Blyuss and Gupta, 2009). Mitchell and Carr (2010, 2011) considered the effects of time delay in the production of cross-reactive immune cells for the model in (Recker *et al.*, 2004) in their works.

In this chapter, we will add to the study of antigenic variation models by examining the bifurcation structure analytically for a general case described in (Blyuss and Gupta, 2009). In Section 3.1, we will describe the model on antigenic variation described in (Blyuss and Gupta, 2009). Next, we will show that the linear structure for this model can be studied using the techniques as described by Golubitsky and Lauterbach (2009) in Section 3.2. In Section 3.3, we use the simplified linear structure and techniques in (Yu, 2005) to analytically determine the Hopf bifurcation which occurs from the fully synchronous equilibrium. Numerical simulations showing the earlier analytic results are provided in Section 3.4. In Section 3.5, we discuss the biological implications based on insights gained from the mathematical analysis of the model.

3.1 The Model

In 2004, Recker *et al.* proposed their multi-variant within-host antigenic variation model of malaria, which was further studied in (Blyuss and Gupta, 2009) and its characteristics are described here. It is assumed that each variant of the pathogen, represented by y_i , shares minor epitopes with other variants. Each major variant is unique and we assume that the major epitope belonging to the variant elicits a long-lived immune response z_i . Similarly, the minor epitopes also bring forth immune responses from the host, but the responses caused by the minor epitopes w_i are assumed to be transient and cross-reactive. A particular variant i and its interactions with the immune system are

described by

$$\begin{aligned}
 \frac{dy_i}{dt} &= y_i(\phi - \alpha_1 z_i - \alpha_2 w_i), \\
 \frac{dz_i}{dt} &= \beta_1 y_i - \mu_1 z_i, \\
 \frac{dw_i}{dt} &= \beta_2 \left(y_i + \sum_{l \sim i} y_l \right) - \mu_2 w_i.
 \end{aligned} \tag{3.1}$$

In this model, specific variant i of the pathogen is produced at the constant rate ϕ , and this pathogen population is eliminated by the long-lived and transient immune responses at rates α_1 and α_2 , respectively. The host immune system produces the long-lived response at rate β_1 when it is stimulated by y_i and it has a natural decaying rate of μ_1 . We use $l \sim i$ to denote the set of all variants that share a minor epitope with variant i . Given that the transient response is triggered by any variants of the pathogen that shares a particular minor epitope, the growth rate of the transient response is proportional to $y_i + \sum_{l \sim i} y_l$ at rate β_2 and it has a natural decaying rate of μ_2 .

As shown in (Recker *et al.*, 2004), this model can be extended to study the effects of many major variants with numerous minor epitopes. The general case can be difficult to analyze with analytic methods due to large number of variables. Potentially, there can be many different configurations based on biological conditions. Mathematically, these configurations correspond to different coupling structures consisting of system (3.1). In this chapter, we will study the case proposed in (Blyuss and Gupta, 2009) when each variant can have two minor epitopes and there are finite number of minor epitope variants.

3.2 Antigenic Variation Model as a Product Network

To study the effects of cross-reactivity, one would describe the dynamics of each variant of *P. falciparum* with the set of differential equations in system (3.1) and couple these systems based on shared epitopes amongst variants. As stated in (Blyuss and Gupta, 2009), the simplest nontrivial case is when each variant of the pathogen has two different minor epitopes. Even with such few variants and couplings, it is still difficult to analyze the dynamics of the system analytically. In this section, we will show that when each variant of the *P. falciparum* has only two minor epitopes, the model can be described as the product network of two all-to-all networks as described in (Golubitsky and Lauterbach, 2009). By recasting the model in a connected network, we can utilize the methods of coupled cell systems (Golubitsky *et al.*, 2005) to analyze stability and bifurcation of equilibria and their dynamics are studied in Section 3.3.

To carry out the analysis, we first describe the theory necessary. In the terminology employed by Golubitsky and Stewart (2006) and the references therein, a *cell*, or *node*, of the directed graph, represents a system of ordinary differential equations and a *coupled cell system* is a network of nodes coupled with each other. Couplings between the differential equation systems are graphically represented using a digraph. The shape, or label, of a node is used to indicate a particular system of differential equations. Let \mathcal{C} denote the set of nodes and $\sim_{\mathcal{C}}$ denote an equivalence relation of nodes on \mathcal{C} . Similarly, the shape of the *arrow*, or a *directed edge*, indicates the type of coupling between two nodes. Let \mathcal{E} denote the set of edges and $\sim_{\mathcal{E}}$ denote an equivalence relation of edges on \mathcal{E} . For each $e \in \mathcal{E}$, the functions $\mathcal{H} : \mathcal{E} \rightarrow \mathcal{C}$ and $\mathcal{T} : \mathcal{E} \rightarrow \mathcal{C}$ denotes the node at the *head* and *tail* of e , respectively. Two arrows are equivalent if they have equivalent tails and heads (i.e. for $e_1, e_2 \in \mathcal{E}$, $e_1 \sim_{\mathcal{E}} e_2 \Rightarrow \mathcal{H}(e_1) \sim_{\mathcal{C}} \mathcal{H}(e_2)$ and $\mathcal{T}(e_1) \sim_{\mathcal{C}} \mathcal{T}(e_2)$).

In general, the framework of coupled cell systems allows for different types of nodes and couplings mixed together in one system. A system that has only one type

of node is called *homogenous* and similarly, a system with only one type of arrow is called *regular*. In other words, a regular homogenous n -node network is composed of identical systems of differential equations which are coupled together with identical coupling terms.

Using the method described in (Golubitsky and Lauterbach, 2009), any two coupled cell systems can be formed as a product network. Suppose that N_1 and N_2 are two regular homogenous coupled cell networks with node sets $\mathcal{C} = \{c_1, \dots, c_{n_1}\}$ and $\mathcal{D} = \{d_1, \dots, d_{n_2}\}$, respectively. We form a product network $N = N_1 \boxtimes N_2$ by replacing each node c_i in N_1 by a copy of N_2 . Let p_{ij} represent the node in N that is from the j th node in the copy of N_2 which replaces the i th node in N_1 . There is a coupling from node p_{ij} to p_{lj} if and only if there is a coupling from c_i to c_l in N_1 . Furthermore, there is a coupling from p_{ij} to p_{il} if and only if there is a coupling from d_j to d_l . This convention for forming a product network allows for the nodes as well as the couplings from N_1 and N_2 to be distinct from each network.

Applying the aforementioned theory in the context of the antigenic variation models (Recker *et al.*, 2004; Blyuss and Gupta, 2009), each node represents the differential equations in system (3.1), which in turn describes the dynamics for a particular variant i of the pathogen. As mentioned earlier, when two major variants share a variant of the minor epitope, they are coupled with each other. Based on the third equation in system (3.1), the coupling between any variants must be the same. Since there is only one set of differential equations and one kind of couplings, any coupled cell network formed by coupling copies of system (3.1) together would be a regular homogenous coupled cell network. For the case when there are two minor epitopes, we suppose that there are n_1 classes with the first minor epitope and n_2 classes with the second minor epitope.

In the next theorem, we will show that the model of antigenic variation can be

constructed through the product networks of two all-to-all connected networks. Given that the digraphs for the networks constructed using the following theorem lack the self-couplings on each node that are present in the digraphs of the networks shown in (Blyuss and Gupta, 2009), we will show in Theorem 3.2.2 that the networks are ODE-equivalent as described in (Dias and Stewart, 2005).

Theorem 3.2.1. *Suppose there are two minor epitopes for each variant of the pathogen and there are n_1 and n_2 classes for each minor epitope, respectively. Let N_1 be an n_1 -node all-to-all connected network and similarly let N_2 be an n_2 -node all-to-all connected network. Let nodes in N_1 and N_2 be represented by system (3.1). Then, the product network $N = N_1 \boxtimes N_2$ satisfies the biological requirement as set out in (Blyuss and Gupta, 2009). That is, each variant which shares a minor epitope must be coupled.*

Proof. We label the nodes of N_1 as c_1, \dots, c_{n_1} and those of N_2 as d_1, \dots, d_{n_2} . To construct $N = N_1 \boxtimes N_2$, we replace the i th node in N_1 with a copy of N_2 . There are $n_1 n_2$ nodes in N and we denote these new nodes as p_{ij} , with index i corresponding to the i th node in N_1 that has been replaced with N_2 . The index j refers to the j th node in N_2 which replaces the i th node in N_1 .

The rule in creating a product network dictates that there is a coupling from p_{ij} to p_{il} if and only if there is a coupling from d_j to d_l . This rule implies that all nodes with the same index i must have a coupling between them. Since nodes having the same index i must share the same variant of a minor epitope, this rule and the fact that N_2 is an all-to-all connected network ensure that all nodes sharing a variant of the minor epitope belonging to N_2 are coupled. With the rules regarding the second index, there is a coupling from node p_{ij} to p_{lj} if and only if there is a coupling from c_i to c_l in N_1 . Again, this rule and the fact that N_1 is also an all-to-all connected network ensure that all nodes sharing the variant of minor epitope in N_1 must be coupled. Hence, we have shown that all nodes that share a variant minor epitope would share a coupling as

described in (Blyuss and Gupta, 2009). \square

We provide an example of applying Theorem 3.2.1 in Figure 3.1. Two 2-node all-to-

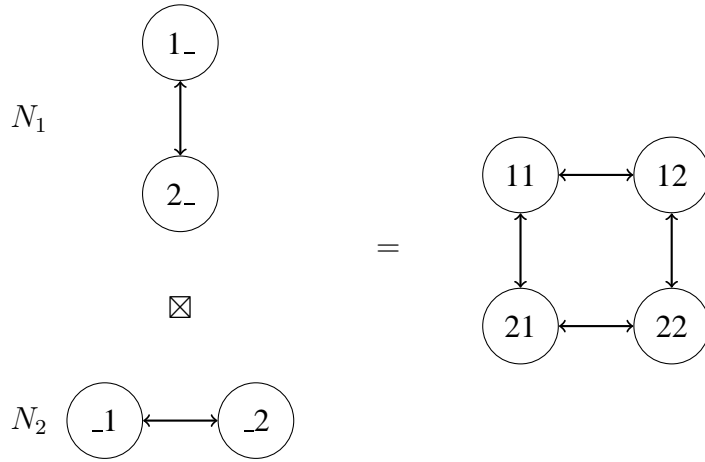


Figure 3.1: An example of forming a new network with two other networks based on Theorem 3.2.1: N_1 and N_2 are both 2-node all-to-all connected networks; and the resulting network has four nodes in the network.

all connected networks are combined to represent the dynamics with four variants and each having two minor epitopes. The same dynamics are described by a different example in (Blyuss and Gupta, 2009), but the digraph shown in that paper has self-couplings for each node that are not present in our work. While the representing digraphs differ, we will show that these two representations are equivalent.

As mentioned by Golubitsky *et al.* (2005), two different digraphs representing coupled cell systems can have the same admissible vector fields and such networks are called *ODE-equivalent*. Let $\mathbf{x} \in \mathbb{R}^3$, then the admissible vector fields for the representation shown in (Blyuss and Gupta, 2009) have the form

$$H(\mathbf{x}_1, \mathbf{x}_2, \mathbf{x}_3, \mathbf{x}_4) = (h(\mathbf{x}_1, \mathbf{x}_1, \mathbf{x}_2, \mathbf{x}_4), h(\mathbf{x}_2, \mathbf{x}_2, \mathbf{x}_1, \mathbf{x}_2), h(\mathbf{x}_3, \mathbf{x}_3, \mathbf{x}_2, \mathbf{x}_4), h(\mathbf{x}_4, \mathbf{x}_4, \mathbf{x}_3, \mathbf{x}_1)),$$

where $h : (\mathbb{R}^3)^4 \rightarrow \mathbb{R}^3$ is a smooth function. For the system shown in Figure 3.1, the

admissible vector fields take the form

$$F(\mathbf{x}_1, \mathbf{x}_2, \mathbf{x}_3, \mathbf{x}_4) = (f(\mathbf{x}_1, \mathbf{x}_2, \mathbf{x}_4), f(\mathbf{x}_2, \mathbf{x}_1, \mathbf{x}_2), f(\mathbf{x}_3, \mathbf{x}_2, \mathbf{x}_4), f(\mathbf{x}_4, \mathbf{x}_3, \mathbf{x}_1)),$$

where $f : (\mathbb{R}^3)^4 \rightarrow \mathbb{R}^3$ is a smooth function. One can see that the set $\{H\}$ of all H is the same as the set of $\{F\}$ of all F . For any given f , we can set $h(\mathbf{x}_i, \mathbf{x}_i, \mathbf{x}_j, \mathbf{x}_k) = f(\mathbf{x}_i, \mathbf{x}_j, \mathbf{x}_k)$, so clearly $\{H\} \subseteq \{F\}$. Conversely, for any given h we can set $f(\mathbf{x}_i, \mathbf{x}_j, \mathbf{x}_k) = h(\mathbf{x}_i, \mathbf{x}_i, \mathbf{x}_j, \mathbf{x}_k)$, so that $\{F\} \subseteq \{H\}$. Hence we have shown that $\{F\} = \{H\}$ and thus shown that the two formulations of the networks are ODE-equivalent in the sense of Dias and Stewart (2005). In general, we can summarize the equivalence between the systems formed in Theorem 3.2.1 and the networks formed in (Blyuss and Gupta, 2009) in the next theorem.

Theorem 3.2.2. *Suppose N_1 and N_2 are all-to-all connected networks and each has n_1 and n_2 nodes, respectively. Then, any network $N = N_1 \boxtimes N_2$ formed using Theorem 3.2.1 describes the same $S_{n_1} \times S_{n_2}$ model of antigenic variation as described in (Blyuss and Gupta, 2009).*

Proof. A direct comparison of the digraph representing N and the one representing the one in $S_{n_1} \times S_{n_2}$ system will show that they only differ by the lack self-couplings in the digraph representing N . We can repeat our earlier argument for ODE-equivalence between the examples in Figure 3.1 and the same as the example shown in (Blyuss and Gupta, 2009) for networks of any size. With ODE-equivalence and each node in the networks representing the same system (3.1), the system trivially describes the same model of antigenic variation as needed. \square

In studying this antigenic variation model, N_1 and N_2 have the same type of nodes and coupling structures, so $N_1 \boxtimes N_2$ is the same as $N_2 \boxtimes N_1$. For the sake of clarity and convenience, we introduce new index notations for systems formed under Theo-

rem 3.2.1. Suppose $N = N_1 \boxtimes N_2$, then we form the system as

$$\begin{aligned}\frac{dy_{ij}}{dt} &= y_{ij}(\phi - \alpha_1 z_{ij} - \alpha_2 w_{ij}), \\ \frac{dz_{ij}}{dt} &= \beta_1 y_{ij} - \mu_1 z_{ij}, \\ \frac{dw_{ij}}{dt} &= \beta_2 \left(y_{ij} + \sum_{l \in I_i} y_{lj} + \sum_{l \in J_j} y_{il} \right) - \mu_2 w_{ij},\end{aligned}\tag{3.2}$$

where $i \in \{1, \dots, n_1\}$ and $j \in \{1, \dots, n_2\}$. Let $\mathbf{x}_{ij} = (y_{ij}, z_{ij}, w_{ij})^T$ and let I_i and J_j represent index sets consisting of the indices which are connected to node ij via the first position and the second position, respectively. We define the function $F : \mathbb{R}^3 \rightarrow \mathbb{R}^3$ such that the vector differential equation

$$\frac{d\mathbf{x}_{ij}}{dt} = \mathbf{F}(\mathbf{x}_{ij}, \mathbf{x}_{I_i, j}, \mathbf{x}_{i, J_j})\tag{3.3}$$

represents the general network formed in Theorem 3.2.1.

3.3 Stability and Bifurcation Analysis

The system formed based on Theorem 3.2.1 has $2^{n_1 n_2}$ equilibria (Blyuss and Gupta, 2009). Of all these equilibria, there are two fully synchronous equilibria, given by

$$\begin{aligned}\mathbf{x}_1^* &= (y_1^*, z_1^*, w_1^*)^T = (0, 0, 0)^T, \text{ and} \\ \mathbf{x}_2^* &= (y_2^*, z_2^*, w_2^*)^T = \left(\frac{\phi \mu_1 \mu_2}{\alpha_1 \beta_1 \mu_2 + n_c \alpha_2 \beta_2}, \frac{\beta_1 \phi \mu_2}{\alpha_1 \beta_1 \mu_2 + n_c \alpha_2 \beta_2}, \frac{\beta_2 \phi \mu_1}{\alpha_1 \beta_1 \mu_2 + n_c \alpha_2 \beta_2} \right)^T,\end{aligned}$$

where \mathbf{x}_i^* represents the equilibrium expression for each node and $n_c = n_1 + n_2 - 2$ denotes the number of connection per node. Clearly, \mathbf{x}_1^* corresponds to trivial dynamics for a biological model. We will investigate the stability at these equilibria as well as possible bifurcations from these equilibria. Stability of the synchronous equilibria will

be analyzed using the product network structure and bifurcations will be analyzed based on balanced colouring and quotient networks.

3.3.1 Local stability near x_1^*

To understand the stability of the two synchronous equilibria, we describe the Jacobian structure of a system formed using product networks. Suppose N_1 and N_2 are two coupled cells systems with A_1 and A_2 as the respective adjacency matrix. Based on the adjacency matrices, linearized internal and coupling dynamics, we can directly find the expression of the Jacobian at any fully synchronous equilibria (Golubitsky and Lauterbach, 2009). If N_1 has n_1 nodes and N_2 has n_2 nodes, then the Jacobian matrix for $N = N_1 \boxtimes N_2$ can be written as

$$J = \eta \otimes \mathbf{I}_{r_1} \otimes \mathbf{I}_{r_2} + \gamma_1 \otimes A_1 \otimes \mathbf{I}_{r_2} + \gamma_2 \otimes \mathbf{I}_{r_1} \otimes A_2,$$

where \otimes denotes tensor products between two matrices, $\eta \in \mathbb{R}^{k \times k}$ is linearized internal dynamics of N_2 and $\gamma_1, \gamma_2 \in \mathbb{R}^{k \times k}$ are the linearized coupling dynamics in networks N_1 and N_2 , respectively. Furthermore, the eigenvalues of J are the same as the eigenvalues of

$$M_{u,v} = \eta + u\gamma_1 + v\gamma_2, \tag{3.4}$$

where $u \in \text{spec}(A_1)$ and $v \in \text{spec}(A_2)$. In other words, one knows the entire eigenvalue structure of a product network system by only knowing the linearized internal dynamics, linearized coupling dynamics, and the eigenvalues of the adjacency matrices of N_1 and N_2 .

In application to antigenic variation model, we shall now find the linearized internal dynamics, linearized coupling dynamics, and the eigenvalues of the adjacency matrices of N_1 and N_2 . Through a direct calculation, the linearized internal dynamics of each

node is

$$\eta = (d\mathbf{F})_{\mathbf{x}_{ij}} = \begin{pmatrix} \phi - \alpha_1 z - \alpha_2 w & -\alpha_1 y & -\alpha_2 y \\ \beta_1 & -\mu_1 & 0 \\ \beta_2 & 0 & -\mu_2 \end{pmatrix}$$

and the linearized coupling dynamics is

$$\gamma = (d\mathbf{F})_{\mathbf{x}_{I_i,j}} = (d\mathbf{F})_{\mathbf{x}_{i,J_j}} = \begin{pmatrix} 0 & 0 & 0 \\ 0 & 0 & 0 \\ \beta_2 & 0 & 0 \end{pmatrix}.$$

As for the eigenvalues of the adjacency matrices, we established in Theorem 3.2.1 that N_1 and N_2 must be all-to-all connected networks for the antigenic variation model. An n -node all-to-all network adjacency matrix has the form

$$A_n = \begin{pmatrix} 0 & 1 & 1 & \dots & 1 \\ 1 & 0 & 1 & \dots & 1 \\ \vdots & & \ddots & & \vdots \\ 1 & \dots & & 0 & 1 \\ 1 & \dots & & 1 & 0 \end{pmatrix} \in \mathbb{R}^{n \times n}.$$

We now describe the eigenvalues of A_n in the following lemma.

Lemma 3.3.1. *The eigenvalues for the adjacency matrix of an n -node all-to-all coupled are $n - 1$ and -1 . The eigenvalues $n - 1$ and -1 have multiplicities 1 and $n - 1$, respectively.*

Proof. Since the row sum for each row in A_n is $n - 1$, $n - 1$ is going to be an eigenvalue with $(1, 1, \dots, 1)^T$ as its eigenvector. Furthermore, a direct calculation shows that -1

is also an eigenvalue and its associated $n - 1$ eigenvectors are

$$\begin{pmatrix} -1 \\ 1 \\ 0 \\ 0 \\ \vdots \\ 0 \end{pmatrix}, \begin{pmatrix} -1 \\ 0 \\ 1 \\ 0 \\ \vdots \\ 0 \end{pmatrix}, \dots, \begin{pmatrix} -1 \\ 0 \\ 0 \\ 0 \\ \vdots \\ 1 \end{pmatrix}.$$

Therefore, the eigenvalue $n - 1$ has multiplicity of 1 and the eigenvalue -1 has multiplicity of $n - 1$. \square

Since the linearized coupling for N_1 and N_2 are the same, we can simplify equation (3.4) to

$$M_{u,v} = \eta + (u + v)\gamma.$$

In general, each $M_{u,v}$ block has the form

$$M_{u,v} = \begin{pmatrix} \phi - \alpha_1 z - \alpha_2 w & -\alpha_1 y & -\alpha_2 y \\ \beta_1 & -\mu_1 & 0 \\ (1 + u + v)\beta_2 & 0 & -\mu_2 \end{pmatrix}. \quad (3.5)$$

Given that $\text{spec}(A_{n_1}) = \{n_1 - 1, -1\}$ and $\text{spec}(A_{n_2}) = \{n_2 - 1, -1\}$, we only need to analyze the eigenvalues of M_{n_1-1, n_2-1} , $M_{n_1-1, -1}$, $M_{n_2-1, -1}$, and $M_{-1, -1}$ to know all the eigenvalues for J at each synchronous equilibrium. Instead of analyzing the eigenvalues of an $n_1 n_2 \times n_1 n_2$ matrix, we have reduced the analysis to only four 3×3 matrices at a synchronous equilibrium.

Theorem 3.3.2. *The trivial equilibrium \mathbf{x}_1^* is always unstable.*

Proof. At \mathbf{x}_1^* , the general $M_{u,v}$ block for our system becomes

$$M_{u,v}(\mathbf{x}_1^*) = \begin{pmatrix} \phi & 0 & 0 \\ \beta_1 & -\mu_1 & 0 \\ (1+u+v)\beta_2 & 0 & -\mu_2 \end{pmatrix}.$$

Each $M_{u,v}$ block is lower triangular, so ϕ , $-\mu_1$ and $-\mu_2$ are the roots of the corresponding characteristic polynomial regardless of the value of u and v . Given that these constants are positive for a biologically realistic model, there is always an unstable root ϕ . Hence, the system is always unstable at \mathbf{x}_1^* . \square

3.3.2 Local stability near \mathbf{x}_2^*

We have shown in Theorem 3.3.2 that the trivial equilibrium \mathbf{x}_1^* is always unstable. More importantly, we showed that the real part of any eigenvalues cannot be zero at this equilibrium for biologically realistic conditions (i.e. positive parameters). Hence, there would be no bifurcation from this equilibrium. In this section, we show in Theorem 3.3.3 that \mathbf{x}_2^* can be asymptotically stable.

Theorem 3.3.3. *The nontrivial equilibrium \mathbf{x}_2^* is locally asymptotically stable for appropriately small values of $\alpha_2\beta_2$.*

Proof. At \mathbf{x}_2^* , the $M_{u,v}$ block becomes

$$M_{u,v}(\mathbf{x}_2^*) = \begin{pmatrix} 0 & -\alpha_1 y_2^* & -\alpha_2 y_2^* \\ \beta_1 & -\mu_1 & 0 \\ (1+u+v)\beta_2 & 0 & -\mu_2 \end{pmatrix},$$

and the corresponding characteristic polynomial is

$$\lambda^3 + a_1\lambda^2 + a_2\lambda + a_3 = 0,$$

where

$$a_1 = \mu_1 + \mu_2,$$

$$a_2 = \alpha_1\beta_1y_2^* + \alpha_2\beta_2y_2^*(1 + u + v) + \mu_1\mu_2,$$

$$a_3 = \alpha_1\beta_1\mu_2y_2^* + \alpha_2\beta_2\mu_1y_2^*(1 + u + v).$$

By the Routh-Hurwitz criterion, the equilibrium \mathbf{x}_2^* is asymptotically stable at \mathbf{x}_2^* if $a_1 > 0$, $a_3 > 0$, and $a_1a_2 - a_3 > 0$. Through a direct calculation, the expression $a_1a_2 - a_3$ is simplified to

$$a_1a_2 - a_3 = (\alpha_1\beta_1\mu_1 + (1 + u + v)\alpha_2\beta_2\mu_2)y_2^* + \mu_1\mu_2(\mu_1 + \mu_2).$$

Clearly, the expressions for a_1 , a_3 , and $a_1a_2 - a_3$ are all positive for $u, v, |u + v + 1| > 0$. We know from Lemma 3.3.1 that $u \in \text{spec}(A_{n_1}) = \{n - 1, -1\}$ and $v \in \text{spec}(A_{n_2}) = \{m - 1, -1\}$. For any nontrivial case of the system, M_{n_1-1, n_2-1} , $M_{u, -1}$, and $M_{-1, v}$ will always produce eigenvalues with negative real part.

Given that the eigenvalues from the other three blocks must all have negative real part, we focus on $M_{-1, -1}$. When $u, v = -1$, a_3 and $a_1a_2 - a_3$ become

$$a_3 = (\alpha_1\beta_1\mu_2 - \alpha_2\beta_2\mu_1)y_2^*$$

and

$$a_1a_2 - a_3 = (\alpha_1\beta_1\mu_1 - \alpha_2\beta_2\mu_2)y_2^* + \mu_1\mu_2(\mu_1 + \mu_2).$$

It is easy to see that for small enough combinations of $\alpha_2\beta_2\mu_2$, the stability condition from Routh-Hurwitz criterion are satisfied. Therefore, \mathbf{x}_2^* can be locally asymptotically stable for small values of $\alpha_2\beta_2\mu_2$. \square

3.3.3 Bifurcation analysis

To analyze the bifurcations from the synchronous nontrivial equilibrium \mathbf{x}_2^* , we introduce the concepts of balanced colouring and quotient network from Golubitsky *et al.* (2005) to aid the process. The notion of balanced colouring is related to the inputs of each node and finding patterns of synchrony for the nodes in a coupled cell system. To start, we need to define the set of inputs for each node in the network.

Definition 3.3.4. For $c \in \mathcal{C}$, the input set of c is

$$I(c) = \{e \in \mathcal{E} : \mathcal{H}(e) = c\}.$$

An element of $I(c)$ is called an input edge or input arrow of c .

Definition 3.3.5. The relation \sim_I of input equivalence on \mathcal{C} is defined by $c \sim_I d$ if and only if there exists an arrow type preserving bijection

$$\beta : I(c) \rightarrow I(d).$$

That is, for every input arrow $i \in I(c)$

$$i \sim_{\mathcal{E}} \beta(i).$$

Any such bijection β is called an input isomorphism from node c to node d .

At a synchronous equilibrium, all the nodes have the same states. When subsets of nodes are synchronized with each other, these nodes may be equilibria, periodic or

even chaotic states, forming a pattern of synchrony or a *polysynchronous subspace*. For a given polysynchronous subspace, we can define an equivalence relation \bowtie such that the subspace is defined as

$$\Delta_{\bowtie} = \{\mathbf{x} \in P : c \bowtie d \Leftrightarrow \mathbf{x}_c = \mathbf{x}_d\},$$

where P denotes the appropriate phase space for \mathbf{x} . This equivalence relation partitions the nodes in synchrony into equivalence classes and it forms the polysynchronous subspace. We can define a specific type of equivalence relations based on the inputs received by each node (Golubitsky *et al.*, 2005):

Definition 3.3.6. *Suppose a coupled cell system is associated with digraph \mathcal{G} . Let the node set \mathcal{C} denote the set of nodes of \mathcal{G} and let \mathcal{E} denote the set of edges of \mathcal{G} . An equivalence relation \bowtie on the node set \mathcal{C} is balanced if for every $c, d \in \mathcal{C}$ with $c \bowtie d$, there exists an input isomorphism β such that $\mathcal{T}(i) \bowtie \mathcal{T}(\beta(i))$ for $i \in \mathcal{I}(c)$, where $\mathcal{T}(i)$ is a function denoting the node at the end of edge i and \mathcal{I} denotes the input set for c .*

There can be many different equivalence relations for a given network. Based on a given balanced equivalence relation, one could associate a colour for each class of nodes. Hence, a balanced relation \bowtie with k classes is equivalent to a balanced k -colouring of a digraph.

The notion of balanced equivalence is important in simplifying a coupled cell system. Based on a balanced equivalence relation \bowtie on a network N , we can always reduce the system to a *quotient network* N_{\bowtie} . The dynamics of the reduced network can be *lifted* to the original network (Golubitsky *et al.*, 2005). In other words, finding a balanced colouring allows one to analyze a reduced quotient system and any dynamics of the simpler system must also be in the original system. Suppose the network N has the node set $\mathcal{C} = \{c_1, \dots, c_n\}$ and \bowtie is a balanced equivalence relation on N with m

classes. We outline the steps to construct the quotient network N_{\bowtie} from N :

1. Let \bar{c} denote the \bowtie -equivalence class of $c \in \mathcal{C}$. The nodes in \mathcal{C}_{\bowtie} are the \bowtie -equivalence classes in \mathcal{C} ; that is,

$$\mathcal{C}_{\bowtie} = \{c : c \in \mathcal{C}\}.$$

Thus we obtain \mathcal{C}_{\bowtie} by forming the quotient of \mathcal{C} by \bowtie , that is, $\mathcal{C}_{\bowtie} = \mathcal{C} / \bowtie$.

2. Define

$$\bar{c} \sim_{\mathcal{C}_{\bowtie}} \bar{d} \Leftrightarrow c \sim_{\mathcal{C}} d.$$

The relation $\sim_{\mathcal{C}_{\bowtie}}$ is well defined since \bowtie refines $\sim_{\mathcal{C}}$.

3. Let $\mathcal{S} \subset \mathcal{C}$ be a set of nodes consisting of precisely one node c from each \bowtie -equivalence class. The input arrows for a quotient node \bar{c} are identified with the input arrows in node c , where $c \in \mathcal{S}$, that is, $I(\bar{c}) = I(c)$.

When viewing the arrow $i \in I(c)$ as an arrow in $I(\bar{c})$, we denote that arrow by \bar{i} . Thus, the arrows in the quotient network are the projection of arrows in the original network formed by the disjoint union

$$\mathcal{E}_{\bowtie} = \bigcup_{c \in \mathcal{S}} I(c).$$

The definition of the quotient network structure is independent of the choice of the representative nodes $c \in \mathcal{S}$.

4. Two quotient arrows are equivalent when the original arrows are equivalent. That is,

$$\bar{i}_1 \sim_{\mathcal{E}_{\bowtie}} \bar{i}_2 \Leftrightarrow i_1 \sim_{\mathcal{E}} i_2,$$

where $i_1 \in I(c_1)$, $i_2 \in I(c_2)$, and $c_1, c_2 \in \mathcal{S}$.

5. Define the heads and tails of quotient arrows by

$$\mathcal{H}(i) = \mathcal{H}(i) \quad \text{and} \quad \mathcal{T}(i) = \mathcal{T}(i).$$

6. For $e_1, e_2 \in \mathcal{E}_{\bowtie}$, it is easy to verify that the quotient network satisfies that $e_1 \sim_{\mathcal{E}_{\bowtie}} e_2 \Rightarrow \mathcal{H}(e_1) \sim_{\mathcal{C}} \mathcal{H}(e_2)$ and $\mathcal{T}(e_1) \sim_{\mathcal{C}} \mathcal{T}(e_2)$. The quotient network is independent of the choice of nodes in \mathcal{S} because \bowtie is balanced.

In the above procedure, one node is chosen from each equivalence class in determining the arrow structure. Since all nodes in the same class of a balanced relation have isomorphic input sets, the choice of the nodes in each class of N does not matter. Mathematical details of constructing a quotient network from a coupled cell system can be found in (Golubitsky *et al.*, 2005).

For a given network, there can be many different k -colourings. For example, the network in Figure 3.1 can have two different 2-colouring patterns and these patterns are illustrated in Figure 3.2. In general, a network that has been reduced to its 2-colouring

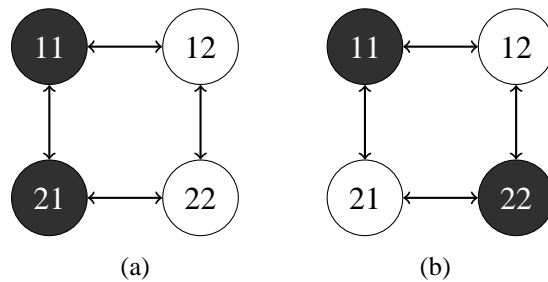


Figure 3.2: Two different 2-colouring possible for the $S_2 \times S_2$ formulation of the system where each node represents system (3.2).

quotient network has the form in Figure 3.3. Given that dynamics of the quotient network lifts to the original network, we will analyze the general 2-colour quotient network with each node representing system (3.2). We will show that synchrony-breaking Hopf

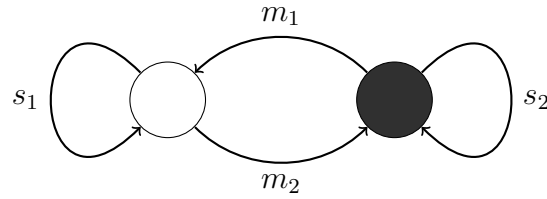


Figure 3.3: Minimizing the number of arrows used in the Figure 3.2 with s_i representing the number of self-connections and m_i the number of external connections.

bifurcation occurs in the antigenic variation model. Each node of network in Figure 3.3 represents

$$\begin{aligned}
 \frac{dy_i}{dt} &= y_i(\phi - \alpha_1 z_i - \alpha_2 w_i), \\
 \frac{dz_i}{dt} &= \beta_1 y_i - \mu_1 z_i, \\
 \frac{dw_i}{dt} &= \beta_2 ((s_i + 1)y_i + m_i y_j) - \mu_2 w_i,
 \end{aligned} \tag{3.6}$$

where i denotes the index for one node and j denotes the index for the other node in Figure 3.3. Suppose \mathbf{x}_i^\boxtimes represents the equilibrium expression for each node of the quotient network. The point $\mathbf{x}_1^\boxtimes = (0, 0, 0)^T$ is the synchronous trivial equilibrium and the synchronous nontrivial equilibrium point \mathbf{x}_2^\boxtimes is given by

$$\mathbf{x}_2^\boxtimes = \begin{pmatrix} y_2^\boxtimes \\ z_2^\boxtimes \\ w_2^\boxtimes \end{pmatrix} = \begin{pmatrix} \phi \mu_1 \mu_2 h \\ \phi \beta_1 \mu_2 h \\ \phi \beta_2 \mu_1 k \end{pmatrix},$$

where

$$h = \frac{\alpha_1 \beta_1 \mu_2 + \alpha_2 \beta_2 \mu_1 (s_1 + s_2 - n_c + 1)}{\alpha_1^2 \beta_1^2 \mu_2^2 + \alpha_1 \beta_1 \mu_2 \alpha_2 \beta_2 \mu_1 (s_1 + s_2 + 2) + \alpha_2^2 \beta_2^2 \mu_1^2 ((s_1 + 1)(s_2 + 1) - m_1 m_2)},$$

and

$$k = \frac{\alpha_1\beta_1\mu_2n_c + \alpha_2\beta_2\mu_1((s_1 + 1)(s_2 + 1) - m_1m_2)}{\alpha_1^2\beta_1^2\mu_2^2 + \alpha_1\beta_1\mu_2\alpha_2\beta_2\mu_1(s_1 + s_2 + 2) + \alpha_2^2\beta_2^2\mu_1^2((s_1 + 1)(s_2 + 1) - m_1m_2)},$$

are constants in terms of the parameters of the system. These terms are results of the configuration of the 2-colour quotient network.

The nontrivial equilibrium is always positive for the system formed according to Theorem 3.2.1 because of its configuration, but this property does not hold for all 2-colour quotient networks for the system. With certain combination of the parameters, the nontrivial equilibrium for the reduced system can have negative components due to the terms $(s_1 + s_2 - n_c + 2)$ and $((s_1 + 1)(s_2 + 1) - m_1m_2)$ in the expressions for h and k . Different configuration of systems formed using system (3.2) resulting in possible negative values for the nontrivial equilibrium is consistent with the results in (De Leenheer and Pilyugin, 2008a). To keep our analysis biologically realistic, we assume that the combination of parameters and the number of arrows for the system produce a positive nontrivial equilibrium. In other words, we now assume that the choice of parameters and configuration always give positive h and k .

Based on the aforementioned assumption, we will analyze possible bifurcations for system (3.6). Conditions for Hopf bifurcation are stated in the following theorem.

Theorem 3.3.7. *For system (3.6), 2-colour synchrony-preserving bifurcations cannot occur from \mathbf{x}_2^{\boxtimes} . If*

$$\frac{\alpha_1\beta_1\mu_2}{\alpha_2\beta_2\mu_1} > n_c - (1 + s_1 + s_2) > \frac{\alpha_1\beta_1\mu_1}{\alpha_2\beta_2\mu_2}, \quad (3.7)$$

then synchrony-breaking Hopf bifurcation occurs from \mathbf{x}_2^{\boxtimes} when

$$\phi = \frac{\mu_1 + \mu_2}{h(\alpha_2\beta_2\mu_2(n_c - (1 + s_1 + s_2)) - \alpha_1\beta_1\mu_1)}.$$

Proof. The Jacobian for the 2-colour quotient system is

$$J = \begin{pmatrix} \eta + s_1\gamma & m_1\gamma \\ m_2\gamma & \eta + s_2\gamma \end{pmatrix},$$

where $\eta(\mathbf{x}_i^{\boxtimes}, \phi)$ is the matrix of linearized internal dynamics and $\gamma(\mathbf{x}_i^{\boxtimes}, \phi)$ is the matrix of the linearized coupling dynamics. This Jacobian matrix has the same structure as the case studied in (Golubitsky *et al.*, 2005). We see that $n_c = s_1 + m_1 = s_2 + m_2$. Let $\mathbf{v} \in \mathbb{R}^3$, then

$$J \begin{pmatrix} \mathbf{v} \\ \mathbf{v} \end{pmatrix} = \begin{pmatrix} (\eta + n_c\gamma)\mathbf{v} \\ (\eta + n_c\gamma)\mathbf{v} \end{pmatrix}$$

and

$$J \begin{pmatrix} m_1\mathbf{v} \\ -m_2\mathbf{v} \end{pmatrix} = \begin{pmatrix} (\eta + (s_1 + s_2 - n_c)\gamma)m_1\mathbf{v} \\ -(\eta + (s_1 + s_2 - n_c)\gamma)m_2\mathbf{v} \end{pmatrix}.$$

Hence, the combined eigenvalues of $\eta + n_c\gamma$ and $\eta + (s_1 + s_2 - n_c)\gamma$ are the eigenvalues of J .

Given that $n_c, s_1 + s_2 - n_c \in \mathbb{Z}$, we shall study the eigenvalues for the general matrix $\eta + n\gamma$ for any $n \in \mathbb{Z}$. The corresponding characteristic polynomial for $\eta + n\gamma$ block is

$$\lambda^3 + a_1\lambda^2 + a_2\lambda + a_3 = 0,$$

where

$$a_1 = \mu_1 + \mu_2,$$

$$a_2 = \phi\mu_1\mu_2h(\alpha_1\beta_1 + \alpha_2\beta_2(1 + n)) + \mu_1\mu_2,$$

$$a_3 = \phi\mu_1\mu_2h(\alpha_1\beta_1\mu_2 + \alpha_2\beta_2\mu_1(1 + n)).$$

By the Routh-Hurwitz criterion, the \mathbf{x}_2^{\boxtimes} is asymptotically stable if $a_1 > 0$, $a_3 > 0$, and

$a_1 a_2 - a_3 > 0$. Through a direct calculation, the expression $a_1 a_2 - a_3$ simplifies to

$$a_1 a_2 - a_3 = \phi \mu_1 \mu_2 h(\alpha_1 \beta_1 \mu_1 + (1 + n) \alpha_2 \beta_2 \mu_2) + \mu_1 \mu_2 (\mu_1 + \mu_2). \quad (3.8)$$

Clearly, the expressions for a_1 , a_3 , and $a_1 a_2 - a_3$ are all positive for $n > 0$. For any formulation of the system, all the eigenvalues of the block $\eta + n_c \gamma$ always have negative real part. Given that $(\mathbf{v}, \mathbf{v})^T \in \Delta = \{(\mathbf{x}, \mathbf{x})^T \in (\mathbb{R}^3)^2\}$ is the eigenvector associated with the $\eta + n_c \gamma$ block, we will not have any synchrony preserving bifurcation from \mathbf{x}_2^{\boxtimes} .

We now focus our attention on the $\eta + (s_1 + s_2 - n_c) \gamma$ block to find possible Hopf bifurcation. A Hopf bifurcation occurs if the conditions $a_1 > 0$ and $a_3 > 0$ hold true while $a_1 a_2 - a_3$ crosses from the positive to the negative as a parameter of the system varies (Yu, 2005). For all parameter values, a_1 is always positive and a_3 is positive by the assumption in the first inequality of (3.7). Hence, the Hurwitz conditions for local stability are satisfied.

For the bifurcation analysis, we choose ϕ as the bifurcation parameter. We see that for small enough ϕ , $a_1 a_2 - a_3$ is necessarily positive. For bifurcation to occur, the expression

$$\phi \mu_1 \mu_2 h(\alpha_1 \beta_1 \mu_1 + (1 + s_1 + s_2 - n_c) \alpha_2 \beta_2 \mu_2) + \mu_1 \mu_2 (\mu_1 + \mu_2)$$

must cross from positive to negative. Given that all the parameters of the system are positive, the previous expression can only be negative if

$$\frac{\alpha_1 \beta_1 \mu_1}{\alpha_2 \beta_2 \mu_2} < n_c - (1 + s_1 + s_2).$$

Hence, we require the second inequality of Equation (3.7). As ϕ increases, the system

reaches the critical point when $a_1 a_2 - a_3 = 0$. Given that ϕ is linear in $a_1 a_2 - a_3$, we can isolate ϕ in $a_1 a_2 - a_3 = 0$ to obtain the bifurcation condition. Because the eigenvector associated with $\eta + (s_1 + s_2 - n_c)\gamma$ is $(m_1 \mathbf{v}, -m_2 \mathbf{v})^T$ and it is obviously not part of the synchrony subspace. Therefore, there can only be synchrony-breaking bifurcation from \mathbf{x}_2^{\boxtimes} . \square

For the 2-colouring shown in Figure 3.2(a), $n_c = 2$, $s_i = 1$ and $m_i = 1$. A direct calculation shows that $2 - (1 + 1 + 1) = -1$. Since all the parameters are positive constants, the necessary condition in (3.7) cannot be satisfied and this pattern does not occur via Hopf bifurcation. On the other hand, the 2-colouring shown in Figure 3.2(b), $n_c = 2$, $s_i = 0$ and $m_i = 2$ and the necessary condition can be satisfied based on the selection of parameters. The synchrony-breaking Hopf bifurcation from \mathbf{x}_2^{\boxtimes} to this pattern will be considered numerically in the next section.

3.4 Numerical Simulations

In this section, we use numerical tools to demonstrate the analytic results obtained in earlier sections. For any system formed by Theorem 3.2.1, we have shown in Theorem 3.3.7 that there exists a 2-colour pattern associated with a synchrony-breaking Hopf bifurcation from the nontrivial synchronous equilibrium. To show these analytical results, we fix the parameters at $\alpha_1 = 10^{-3}$, $\alpha_2 = 10^{-3}$, $\beta_1 = 10^{-4}$, $\beta_2 = 10^{-4}$, $\mu_1 = 1/100$ and $\mu_2 = 1/50$ (Blyuss and Gupta, 2009) and use ϕ as the bifurcation parameter as shown in Theorem 3.3.7.

3.4.1 System with four strains

In Figure 3.4, we see that for $\phi = 0.5$ the system in Figure 3.2 is at the nontrivial equilibrium. As we increase the bifurcation value to $\phi = 1.5$, we see that oscillations

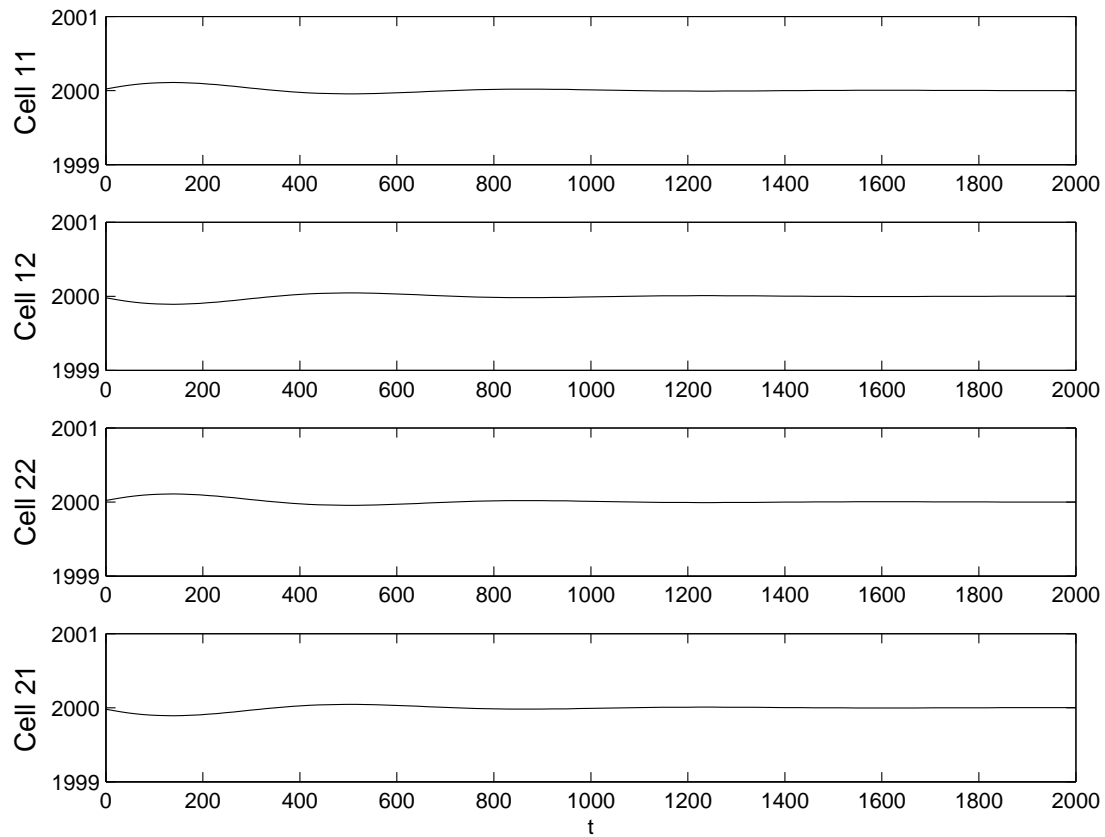


Figure 3.4: Simulated pathogen populations (y_{ij}) of the system shown in Figure 3.1 for $\phi = 0.5$: A nontrivial synchronous equilibrium.

from synchrony-breaking bifurcation occur as shown in Figure 3.5. Clearly, nodes 11 and 22 are synchronized and nodes 12 and 21 are also synchronized. Based on this configuration, the inequality in (3.7) is satisfied with our selection of parameters. We also see that these two sets of nodes are out of phase by $T/2$, where T is the period of the periodic solution. These results agree with the synchrony-breaking subspace being supported by $(m_1 \mathbf{v}, -m_2 \mathbf{v})^T$. Given that $m_1 = m_2 = 2$ in this case, the amplitudes of the oscillations for the nodes are also in agreement of the earlier theoretical results.

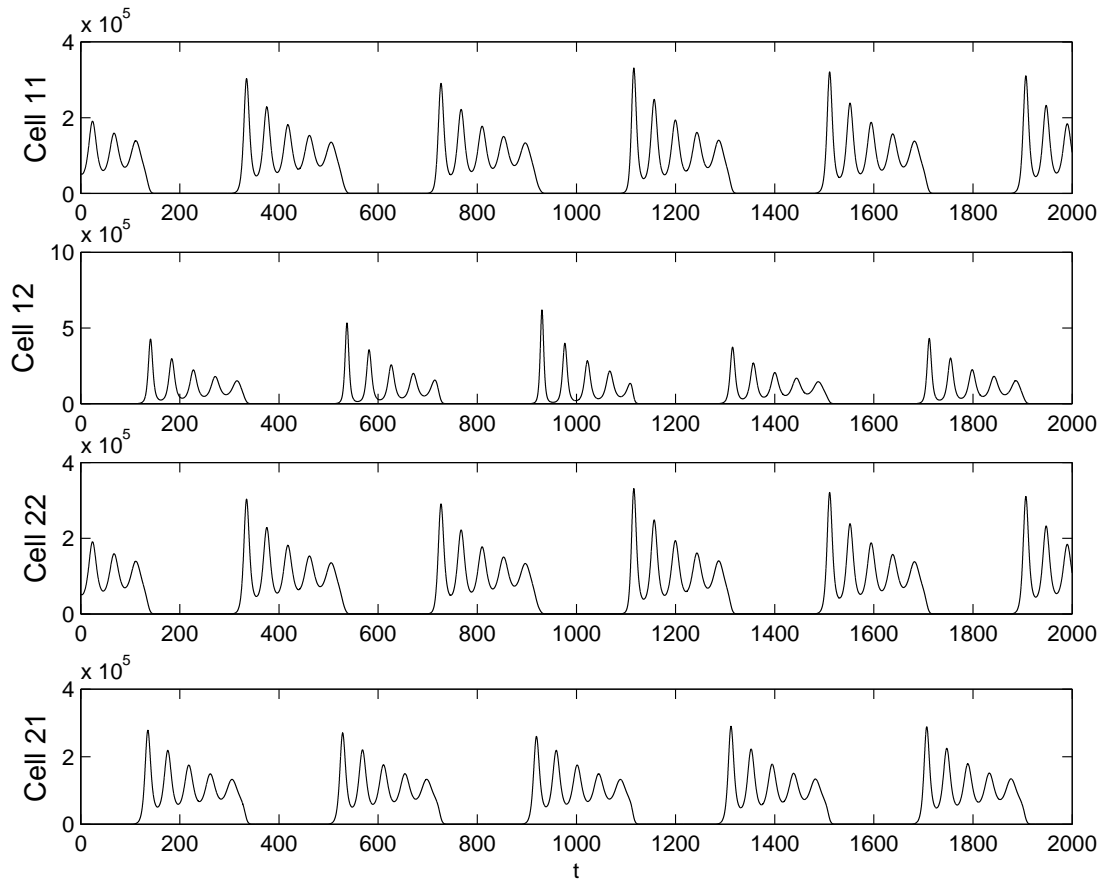


Figure 3.5: Simulated pathogen populations (y_{ij}) of the system shown in Figure 3.1 for $\phi = 1.5$: Hopf bifurcation.

3.4.2 System with eight strains

To show that the method presented in this chapter works for larger systems, we form a system with $n_1 = 2$ and $n_2 = 4$. This configuration is depicted in Figure 3.6. Numerical

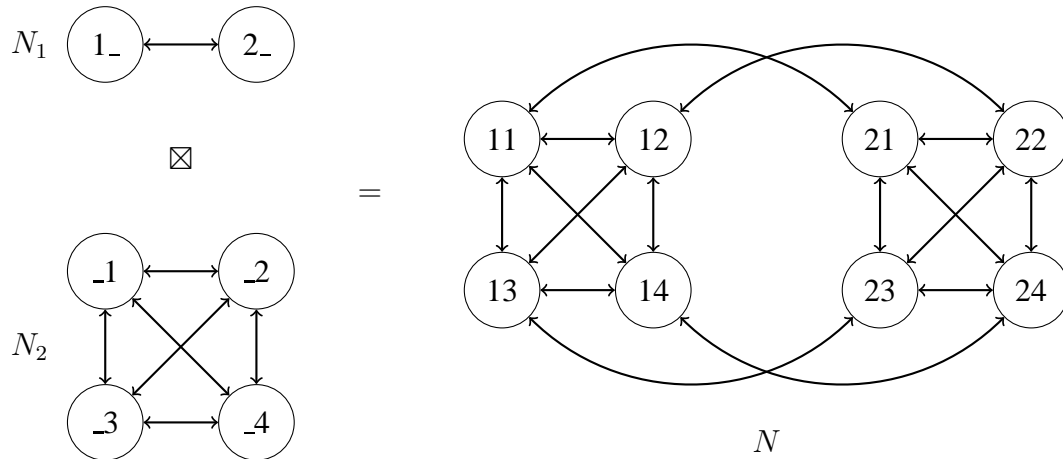


Figure 3.6: A network modelling the eight strains formed by two networks with $n_1 = 2$ and $n_2 = 4$.

simulations of this configuration are shown in Figures 3.7 and 3.8. The solutions shown in these figures are in periodic synchrony that is in accordance to the configurations in Figure 3.9(a) and 3.9(b), respectively. The two different colour patterns in Figure 3.9 are produced using different initial conditions.

The two patterns in Figure 3.9 both have the quotient parameters $s_1 = s_2 = 1$. Hence, the number of white nodes coupled to a white node is the same number of black nodes coupled to a black node for all the aforementioned patterns. In the numerical simulations of these cases (Figures 3.9(a) and 3.9(b)), the solutions for the two classes are out of phase by half the period. The phase shifted solutions here agree with the results for the 4-strain system as well as the work by Golubitsky *et al.* (2005, Corollary 9.3).

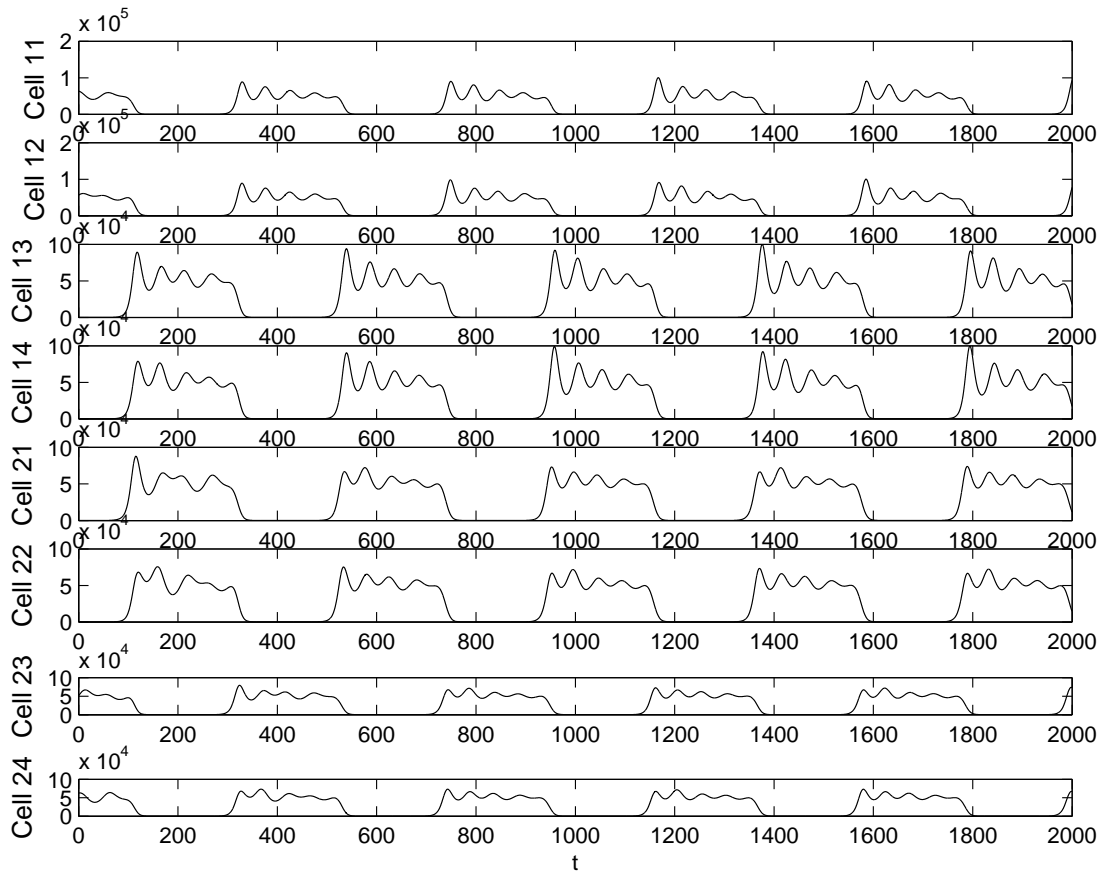


Figure 3.7: Simulated pathogen populations (y_{ij}) of the system shown in Figure 3.6 for $\phi = 1$: 2-colour pattern, in agreement with Figure 3.9(a).

3.5 Conclusions and Discussions

In our mathematical analysis, we have shown in Theorem 3.2.1 that the general system described in (Blyuss and Gupta, 2009) can be formulated using the product network method discussed in (Golubitsky and Lauterbach, 2009). The digraphs used in this chapter to represent the networks are different from those used by Blyuss and Gupta (2009), but they represent the same system because these systems are equivalent in the sense of (Dias and Stewart, 2005). The formulation of the model as two all-to-all networks allows us to analyze the linear stability at any fully synchronous equilibrium. Instead of directly dealing with an $n_1 n_2 \times n_1 n_2$ matrix, we have reduced the analysis

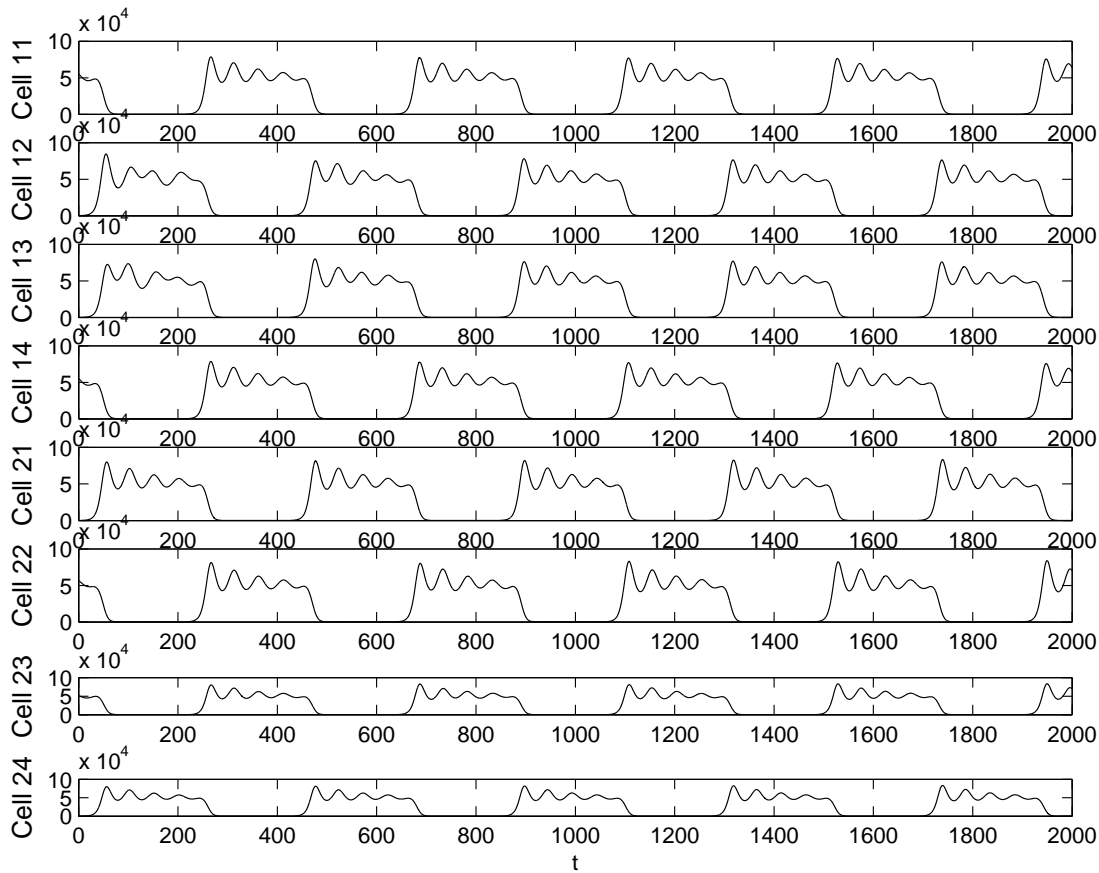


Figure 3.8: Simulated pathogen populations (y_{ij}) of the system shown in Figure 3.6 for $\phi = 1$: 2-colour pattern, in agreement with Figure 3.9(b).

to four 3×3 matrices. Analytically, it is difficult to determine the eigenvalues for large matrices. Our reduction allows one to directly analyze the stability at the trivial equilibrium. As stated in Theorem 3.3.2, the trivial synchronous equilibrium is always unstable. This result is important because we have shown that any possible dynamics from a fully synchronous equilibrium must arise from the nontrivial equilibrium.

We have also obtained the necessary condition in (3.7) for the nontrivial equilibrium to be stable and that for Hopf bifurcation to occur in Theorem 3.3.7. In the proof, we have shown that any type of synchrony-preserving dynamics cannot arise from the nontrivial synchronous equilibrium through bifurcation. Mathematically, we have ruled out the possible dynamics. By ruling out synchrony-preserving bifurcation

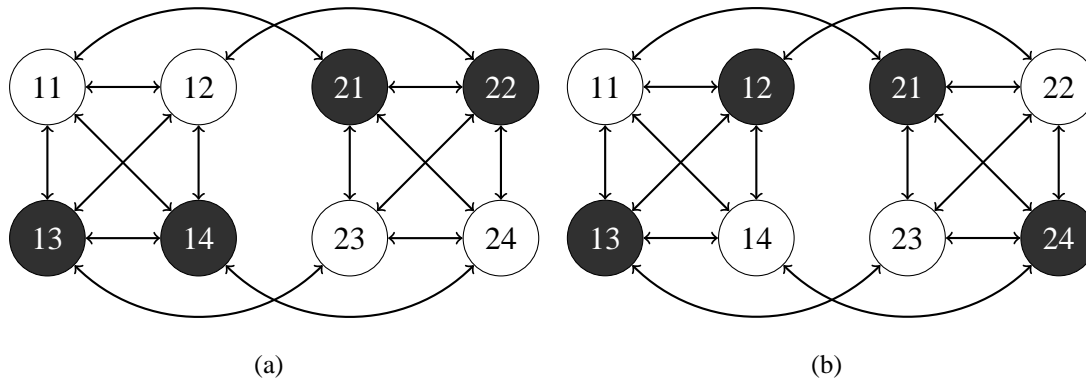


Figure 3.9: These are two synchrony patterns consistent with the results found analytically found in Theorem 3.3.7 and numerical results in Figure 3.7 and 3.8. These patterns correspond to $s_1 = s_2 = 1$ and $m_1 = m_2 = 3$ for the 2-colour quotient network.

in this model, we have shown that the bifurcation dynamics is consistent with this biological behaviour for antigenic variation. As stated in (Craig and Scherf, 2003), it is important that variants are not expressed at the same time for antigenic variation to be a successful strategy for the pathogen. Our results imply that any synchrony pattern arising from bifurcation would be consistent with this biological requirement for antigenic variation.

Other than ruling out synchrony-preserving bifurcation, Theorem 3.3.7 also shows that synchrony-breaking Hopf bifurcation can arise from this nontrivial equilibrium. In (Recker *et al.*, 2004), the authors showed numerically that in some parameter ranges oscillations occur for the model (3.3) and these oscillations described hierarchies of the sequential appearance of variants. In this chapter, we have showed that the numerical pattern which corresponds to the hierarchy of sequential immunodominant is a result of bifurcations and it corresponds to 2-colour patterns of synchrony.

Furthermore, for antigenic variation to be a successful immune escape strategy, it is essential that the pathogen must have the ability for some variants to be expressed while others stay relatively dormant (Craig and Scherf, 2003). It must also be able to switch

from the actively expressed variants to the dormant variants. Analytically, we have shown that the increase in growth rate will eventually cause the system to go from the nontrivial synchronous equilibrium to a synchrony-breaking Hopf bifurcation and the switching mechanism is the Hopf bifurcation. The peaks and valleys in the oscillations may correspond to the active and dormant requirement of antigenic variation.

The condition in equation (3.7) shows that not all variants can necessarily be synchronized and synchronization patterns must be based on the same condition. This condition is based on the parameters of the system and the number of self-connections in the 2-colour quotient system. We can rule out some patterns directly. For example, the pattern shown in Figure 3.2(a) corresponds to $s_1 = s_2 = 1$ and $m_1 = m_2 = 1$ in the 2-colour quotient network. We can see that the inequality in (3.7) cannot be satisfied for any biologically meaningful parameter values.

As shown by Blyuss and Gupta (2009), the strain space investigated in this work has $S_{n_1} \times S_{n_2}$ symmetry. Other authors of intra-host multi-strain models, such as Dawes and Gog (2002) and Gog and Swinton (2002), have also purposed strain spaces that have symmetry in them. This symmetry in the strain space is based on the assumption that all combination of epitopes are viable. However, only certain combinations of the epitopes on the pathogens may work for their target cells (Craig and Scherf, 2003). Thus, the strain space for a given pathogen may not necessarily be symmetric. The general coupled cell method used here does not require any specific symmetry, so our approach might be more suitable to investigate more specific biological scenarios.

Biologically, these 2-colour patterns correspond to all variants being synchronized in two separate groupings. These separate groups are out of phase by half of the period of the oscillations. The 2-colour synchrony-breaking Hopf bifurcation fits requirement for antigenic variation to occur of expressing variants and at different time as well as other synchronized variants stay relatively dormant over time oscillating. Given that

multiple variants are expressed at the same time in a 2-colour pattern, it reduces the potential effectiveness of immune escape. The limitation of two groupings barely fits the minimum of two variants needed for features of antigenic variation as outlined in (Turner, 2002). The framework set out by Golubitsky *et al.* (2005) can be used to analyze k -colouring and therefore it is possible to study finite number of variants in synchrony-breaking patterns in future works.

For future work, we can expand the analysis in this chapter by specifically analyzing patterns that may be more biologically relevant. As the number of the major variants in the model gets higher, there are many more patterns, making it impossible to enumerate all these patterns. One can certainly take advantage of the framework of k -colourings provided in (Golubitsky *et al.*, 2005). We believe that the extension of our work from 2-colour bifurcations to k -colour bifurcation would provide a more realistic analysis for the model.

One can also further the research by modifying assumptions made in this chapter. In simplifying the calculations, we have assumed that all strains have identical parameters. Our analysis can be extended to incorporate different parameters for different strains by altering the coupled cell representation. Instead of having only one type of nodes in the digraph, different shapes of nodes can be used to denote strains with different parameters.

Aside from the identical parameters assumption, we have also restricted the analysis to only 2-colourings of the systems. Again, we made this assumption to simplify the calculations. Since each colour in a colouring pattern corresponds to one cluster, our analysis can only produce patterns with two different groups of synchrony. A more general analysis for larger number of colours in the colourings can generate more possible patterns.

Bibliography

- K. Blyuss and S. Gupta. Stability and bifurcations in a model of antigenic variation in malaria. *Journal of Mathematical Biology*, 58(6):923–937, 2009. ISSN 0303-6812.
- A. Craig and A. Scherf. *Antigenic Variation*. Academic Pr, 2003.
- J. Dawes and J. Gog. The onset of oscillatory dynamics in models of multiple disease strains. *Journal of Mathematical Biology*, 45(6):471–510, 2002.
- P. De Leenheer and S. Pilyugin. Immune response to a malaria infection: properties of a mathematical model. *Journal of Biological Dynamics*, 2(2):102–120, 2008a.
- P. De Leenheer and S. Pilyugin. Multistrain virus dynamics with mutations: A global analysis. *Mathematical Medicine and Biology*, 25(4):285, 2008b. ISSN 1477-8599.
- A. Dias and I. Stewart. Linear equivalence and ODE-equivalence for coupled cell networks. *Nonlinearity*, 18:1003, 2005.
- S. Frank and A. Barbour. Within-host dynamics of antigenic variation. *Infection, Genetics and Evolution*, 6(2):141–146, 2006. ISSN 1567-1348.
- J. Gog and J. Swinton. A status-based approach to multiple strain dynamics. *Journal of Mathematical Biology*, 44(2):169–184, 2002.
- M. Golubitsky and R. Lauterbach. Bifurcations from synchrony in homogeneous networks: Linear theory. *SIAM Journal on Applied Dynamical Systems*, 8:40, 2009.

- M. Golubitsky and I. Stewart. Nonlinear dynamics of networks: The groupoid formalism. *Bulletin of the American Mathematical Society*, 43(3):305, 2006. ISSN 0273-0979.
- M. Golubitsky, I. Stewart, and A. Török. Patterns of synchrony in coupled cell networks with multiple arrows. *SIAM J. Appl. Dynam. Sys*, 4(1):78–100, 2005.
- M. Gravenor and A. Lloyd. Reply to: Models for the in-host dynamics of malaria revisited: errors in some basic models lead to large over-estimates of growth rates. *Parasitology*, 117(5):409–410, 1998. ISSN 0031-1820.
- J. Mitchell and T. Carr. Oscillations in an intra-host model of *Plasmodium falciparum* malaria due to cross-reactive immune response. *Bulletin of Mathematical Biology*, 72(3):590–610, 2010.
- J. Mitchell and T. Carr. Synchronous versus asynchronous oscillations for antigenically varying *Plasmodium falciparum* with host immune response. *Journal of Biological Dynamics*, 2011.
- M. Recker, S. Nee, P. Bull, S. Kinyanjui, K. Marsh, C. Newbold, and S. Gupta. Transient cross-reactive immune responses can orchestrate antigenic variation in malaria. *Nature*, 429(6991):555–558, 2004. ISSN 0028-0836.
- A. Saul. Models for the in-host dynamics of malaria revisited: errors in some basic models lead to large over-estimates of growth rates. *Parasitology*, 117(05):405–407, 1998. ISSN 1469-8161.
- C. Turner. A perspective on clonal phenotypic (antigenic) variation in protozoan parasites. *Parasitology*, 125:17–24, 2002.
- P. Yu. Closed-form conditions of bifurcation points for general differential equations. *International Journal of Bifurcation and Chaos*, 15(4):1467–1483, 2005.

Chapter 4

Bifurcation, Stability, and Cluster Formation of Multi-Strain Infection Models

4.1 Introduction

Pathogens, such as viruses and parasites, are detected by the immune system via chemicals on their surface. Based on the chemical detected, the immune system sends specific antibodies to clear away the pathogen (Coico and Sunshine, 2009). Some pathogens can present themselves as many different variants in order to avoid detection, prolong infection, and infect another host. Many diseases, such as AIDS (Nowak *et al.*, 1995a), malaria (Recker *et al.*, 2004), dengue fever (Recker *et al.*, 2009), and the common flu (Omori *et al.*, 2010) are caused by pathogens that present themselves with many subtypes.

Each strain or subtype of the pathogen elicits specific immune response from the immune system. Some of these strains share epitopes, so they can also incite immune

responses that will target multiple subtypes. Immune responses that target multiple types of such responses are called *cross-protective* or *cross-reactive*. If the host is infected by one particular subtype, it may be partially protected against another variant. Scientists have devised various within-host (Nowak *et al.*, 1995a,b; Gjini *et al.*, 2010) and epidemiological models (Gog and Grenfell, 2002; Dawes and Gog, 2002; Omori *et al.*, 2010) to better understand the underlying dynamics of the multi-strain infections.

Separating different strains into subsystems of differential equations is one approach to modelling pathogens with multiple variations. Gupta *et al.* (1996) developed a model that incorporates multiple strain types with shared allele to understand the discrete strain structures found experimentally. There are two compartments in this model. For each strain i , there is a proportion of the population (z_i) which is immune and there is another portion which is infectious (y_i). In this model, the dynamics particular to each strain are described by

$$\begin{aligned}\dot{z}_i &= \lambda_i(1 - z_i) - \mu z_i, \\ \dot{y}_i &= \lambda_i(1 - z_i)[1 - \gamma(1 - \phi_i)] - \sigma y_i,\end{aligned}\tag{4.1}$$

where $\phi_i = \prod_{j \sim i} (1 - z_j)$ and $\lambda_i = \beta f(y_i, y_j)$. Parameters $1/\mu$ and $1/\sigma$ are respectively the average life expectancy of the host and the average duration of the infections. Strains that shared allele are denoted in the ϕ_i term, where $j \sim i$ indicates strains j and i share alleles. The strength of cross-protection as a result of the share allele is measured by the parameter γ . Transmission parameter, β , along with a suitable recombination function, $f(y_i, y_j)$, describe the force of infection, λ_i .

Gupta *et al.* (1998) expanded upon model (4.1) to incorporate another compartment: a portion of the population (w_i) which is immune to any strain j that shares allele with strain i . With variables z_i and y_i similarly defined as in system 4.1, this model has the

form

$$\begin{aligned}
\dot{z}_i &= \lambda_i(1 - z_i) - \mu z_i, \\
\dot{w}_i &= (1 - w_i) \sum_{j \sim i} \lambda_j - \mu w_i, \\
\dot{y}_i &= \lambda_i((1 - w_i) + (1 - \gamma)(w_i - z_i)) - \sigma y_i,
\end{aligned} \tag{4.2}$$

where $\lambda_i = \beta y_i$ and j is indexed over strains which share any allele with strain i , including i itself. As noted in (Gupta *et al.*, 1998), the behaviour of the model is largely unaffected by the exact functional form of the force of infection term λ_i , so we choose the same form used by Recker and Gupta (2005).

To study the effects of the number of variants shared on immune mediated cross-protection and strain-structure, Recker and Gupta (2005) added another compartment to model (4.2). With z_i , w_i , and y_i similarly defined as in model (4.2), the new class, v_i , denotes the portion of the population that are immune to strains that share more than one allele with strain i . For this model, the system describing the dynamics of each strain i has the form

$$\begin{aligned}
\dot{z}_i &= \lambda_i(1 - z_i) - \mu z_i, \\
\dot{w}_i &= \sum_{j \sim i} \lambda_j(1 - w_i) - \mu w_i, \\
\dot{v}_i &= \sum_{k \sim i} \lambda_k(1 - v_i) - \mu v_i, \\
\dot{y}_i &= \lambda_i((1 - w_i) + (1 - \gamma_1)(w_i - z_i) + (1 - \gamma_2)(v_i - z_i)) - \sigma y_i,
\end{aligned} \tag{4.3}$$

where $\lambda_i = \beta_i y_i$ is the force of infection, $j \sim i$ indicates the strains which share alleles with strain i , and $k \sim i$ indicates the strains which share more than one allele with strain i .

As noticed by Calvez *et al.* (2005), the solutions of these models and other related

models (Gupta *et al.*, 1996; Gupta and Galvani, 1999) seem to self-organized into clusters. In this chapter, we will show that the clustering behaviour found in the model by Gupta *et al.* (1998) as well as the model by Recker and Gupta (2005) can be analytically explained by semi-simple double zero bifurcation of their 2-colour quotient networks. For each of the models, we assume the subsystems describing the dynamics of the strains have the same parameter values.

The paper is organized as follows. In Section 4.2, we outline the general approach in finding and understanding the related bifurcation and clustering patterns resulting from the bifurcation. Specific calculations related to each model are illustrated in Section 4.3. In Section 4.4, we numerically demonstrate the analytic results found in Section 4.3. Finally, conclusions and discussions are given in Section 4.5.

4.2 General Approach

As mentioned in Section 4.1, we will show analytically that the clustering solutions of some multi-strain infection models are the results of semi-simple double zero bifurcations of their 2-colour quotient networks. Given that the general approach to both models is the same, we provide our approach to the problem in this section and leave the specific details to each model in Section 4.3.

4.2.1 Coupled cell network representation

The first step in this analysis is to represent the models of Gupta *et al.* (1998) and Recker and Gupta (2005) as coupled cell networks by the formalism introduced by Stewart *et al.* (2003) and refined by Golubitsky *et al.* (2005). This method is a systemic way to represent systems of coupled differential equations using directed graphs and analyze synchronization patterns resulting from bifurcations. Each node in the directed graph

represents a specific set of differential equations. Shapes of the nodes denote specific set of differential equations, so identical sets of differential equations are represented in the graph with nodes of the same shape. In the two models, the dynamics related to each strain is described by system (4.2) or (4.3). In each model, all strains have the same parameter values, so all the nodes in the graph have the same shape.

Similarly, each directed edge, or arrow, in the graph represents the coupling between different sets of differential equations. In our cases, two sets of differential equations are coupled if they share alleles. Based on the model by Gupta *et al.* (1998), there is only one type of coupling terms, so there would be one type of arrow. As for the model by Recker and Gupta (2005), there are different types of couplings based on the number of shared alleles between strains. In this case, two different types of edges represent different couplings.

Having defined the sets of nodes and edges for each of the model, we now represent these models as coupled cell networks. For example, if we let each node in Figure 4.1 represent the differential equations of system (4.2), then this directed graph gives a coupled cell representation of the 2 locus-2 allele form of the model by Gupta *et al.* (1998). As mentioned before, each strain has identical parameters, so all of them are

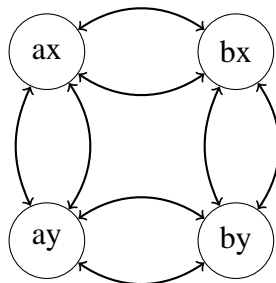


Figure 4.1: The directed graph representing the coupled cell network of the 2 locus-2 allele form of the model by Gupta *et al.* (1998): Each node represents the differential equations set in system (4.2) and each arrow represents the coupling between strains that shares allele; alleles $\{a, b\}$ are used at the first locus and alleles $\{x, y\}$ are used at the second locus.

represented with a circle in the digraph. Given that only one type of coupling is present

in the system, there is only one type of arrow. For another example, the 3 locus-2 allele form of the model from Recker and Gupta (2005) is shown in Figure 4.2. Again, based

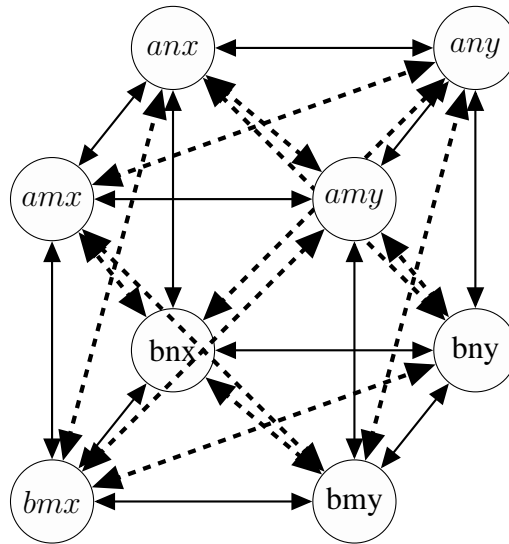


Figure 4.2: The three-dimensional directed graph representing the coupled cell network of the 3 locus-2 allele form of the model by Recker and Gupta (2005): Each node represents the set of differential equations in system (4.3); similarly, dashed arrow represents the coupling between two strains when they only share one allele and solid arrow represents the coupling between two strains when they share more than one allele; allele sets $\{a, b\}$, $\{m, n\}$, and $\{x, y\}$ are used respectively at the first, second, and third locus; double headed arrows, minimizing the number of arrow drawn, are used to indicate that there is an arrow originating from each node of the pair.

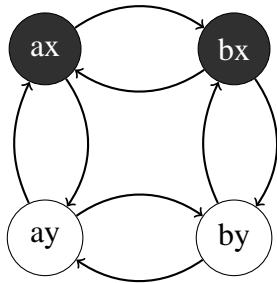
on the identical parameter assumption, we only have one type of nodes in this figure. As we can see from system (4.3), there are two types of couplings in this model, so correspondingly, we have two different types of edges in its coupled cell network.

4.2.2 Possible 2-colouring patterns

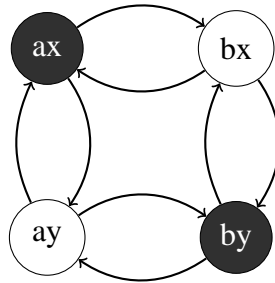
To study the possible clustering formations after bifurcation, the concept of balanced colouring in a coupled cell networks is needed (Golubitsky *et al.*, 2005). We need a way to indicate patterns of synchrony and this can be achieved rigorously using equivalence relations to partition the nodes of the system. We can partition the nodes in the directed

graph according to some equivalence relation \approx . Conversely, any partition of the nodes will also form an equivalence relation. If all the nodes of the same class receive the same input sets, then such colouring is *balanced*.

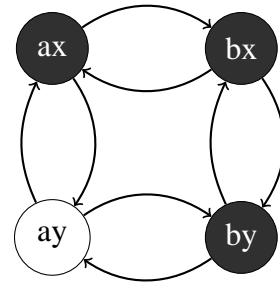
We can graphically check whether a particular equivalence relation, \approx , is balanced. In the directed graph, nodes are of the same colour if they are in the same \approx -equivalence class. Then, we colour the tails the nodes of these nodes using the same colour as well. An equivalence relation, \approx , is balanced if and only if the inputs of the nodes in the same class have isomorphic inputs, i.e. same number of edges that have the same colour. A colouring pattern with k colours is a k -colouring of the system. To illustrate balanced colouring, we have provided a few different 2-colourings of the aforementioned 2 locus-2 allele example in Figure 4.3. We can see that the networks in Figures 4.3(a) and 4.3(b)



(a) In this case, each black node receives one input from a white node and one input from a black node. Similarly, each white node receives one input from a white node and one input from a black node.



(b) In this case, each black node receives two inputs from white nodes and no input from a black node. Similarly, each white node receives two inputs from black nodes and no input from a white node.



(c) In this case, there are three black nodes. Node bx receives inputs only from other black nodes. Nodes ax and by receive inputs from black and white nodes.

Figure 4.3: Three different possible colouring patterns for the 2 locus-2 allele form of the model by Gupta *et al.* (1998), where black and white represent the two possible classes in each of the coupled cell network.

are balanced while the network in Figure 4.3(c) is not.

The models by Gupta *et al.* (1998) and Recker and Gupta (2005) can accommodate finite number of strains of pathogens in the system. Since each node represents the dynamics generated by one strain of the pathogen, there would be the same number of

nodes in the coupled cell network. As such, it will not be feasible to study all balanced k -colourings for all the possible m locus- n allele forms of the multi-strain models. Instead of studying all possible k -colourings, we restrict the scope of this study to only the possible balanced 2-colourings.

4.2.3 Quotient networks

For the general m locus- n allele form of the multi-strain model, there would be m^n strains. Suppose k is the number of differential equations in the system required to describe the dynamics of each strain. To analyze the possible bifurcation of the model, we would have to deal with a kn^m -dimensional system. Instead of directly dealing with the potentially high-dimensional system, we can use the balanced colourings of the coupled cell network to reduce the system to its quotient network and analyze a less complicated network (Golubitsky *et al.*, 2005). Given that we are only interested in 2-colourings of the system, we only need to study a $2k$ -dimensional system after the quotient reduction.

From any balanced 2-colourings, we can always reduce the systems based on models to the quotient networks shown in Figures 4.4 and 4.5. Each balanced colouring induces a canonical quotient network. The nodes of the quotient network represent the equivalence classes in a balanced \bowtie -equivalence relation. Because we are interested in the 2-colourings, there would be two nodes in the quotient network. From the balanced colouring, we pick one node from each colour class to define the parameters of the quotient network. Given that the nodes of the same equivalence class receive isomorphic inputs, the choice of node for each class does not change the resulting quotient network. For each equivalence class, we define inputs received by the node representing this class in the quotient network to be identical to the inputs received by the node we selected in the original network.

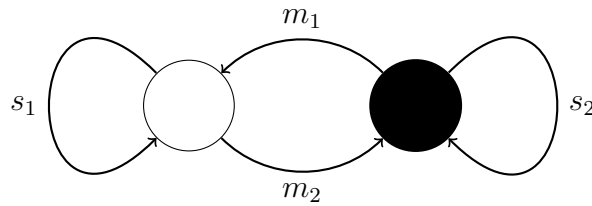


Figure 4.4: The directed graph representing the general quotient network for all balanced 2-colourings of the model by Gupta *et al.* (1998): The topological parameters, s_i , indicating the number of self-connections for each class, and similarly, the topological parameters, m_i , indicating the number of connections received from the other class.

To reduce the complexity of the digraph of the quotient network, we denote the number of inputs on the digraph of the quotient network with their topological parameters shown in the figures. Details for constructing quotient networks from balanced k -colourings can be found in (Golubitsky *et al.*, 2005; Golubitsky and Stewart, 2006). For example, the colouring pattern in Figure 4.3(a) corresponds to quotient parameters $m_i = 1$ and $s_i = 1$; similarly, the colouring pattern in Figure 4.3(b) corresponds to quotient parameters $m_i = 2$ and $s_i = 0$.

4.2.4 The semi-simple double zero bifurcation

After forming the coupled cell networks and quotient reductions, we can now begin the dynamic analysis. For each of these models, we show that a semi-simple double zero bifurcation occurs from the trivial equilibrium of the quotient network. At a locally stable equilibrium, a bifurcation occurs when some of the eigenvalues with negative real part cross smoothly from the left side of the complex plane into the right side due to changes in the system parameters. Hence, we must understand the eigenvalue structure of the Jacobian in order to understand the type of bifurcation occurring.

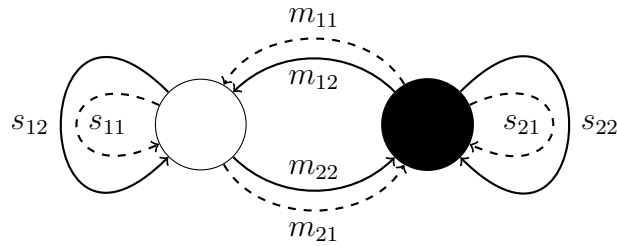


Figure 4.5: The directed graph representing the general quotient network for all balanced 2-colourings of the model by Recker and Gupta (2005): The parameters, s_{i1} and s_{i2} , indicating respectively the number of dashed and solid self-connections received for each class, and similarly, the parameter, m_{i1} and m_{i2} indicating respectively the number of dashed and solid connections received from the other class.

Suppose $\text{spec}(J) = \{\sigma_1, \dots, \sigma_n\}$, then σ_i is a repeated eigenvalue for J if there is a j , such that $\sigma_i = \sigma_j$ and $i \neq j$. Let κ_i , the *algebraic multiplicity*, be the number of times σ_i is repeated and let η_i , the *geometric multiplicity*, be the number of linearly independent eigenvectors associated with σ_i . By the definition of eigenvalues, we must have $\kappa_i \geq \eta_i$. An eigenvalue is called *semi-simple* when $\kappa_i = \eta_i$. Thus, a *semi-simple double zero bifurcation* refers to the bifurcation of a twice repeated zero eigenvalue associated with two linearly independent eigenvectors.

4.2.5 Jordan canonical form and center manifold reduction

With a semi-simple double zero bifurcation, we can further simplify the system by transferring it to its Jordan canonical form. To start, we perform a linear change of coordinates so that the bifurcation occurs at $(\mathbf{x}, \tilde{\beta})^T = (\mathbf{0}, 0)^T \in \mathbb{R}^{2k+1}$, where \mathbf{x} is the generalized coordinates of the system and $\tilde{\beta}$ is the bifurcation parameter.

Let n_c and n_s respectively be the numbers of eigenvalues with zero real-part and negative real-part of the Jacobian. For this type of bifurcation, there would be two eigenvalues with zero real part and $2k - 2$ eigenvalues with negative real part. Using

the eigenvectors of J to form a transformation matrix, the system can be rewritten in block matrix form as

$$\begin{aligned}\dot{\mathbf{x}}_c &= A\mathbf{x}_c + \mathbf{f}(\mathbf{x}_c, \mathbf{x}_s) \\ \dot{\mathbf{x}}_s &= B\mathbf{x}_s + \mathbf{g}(\mathbf{x}_c, \mathbf{x}_s)\end{aligned}\quad (\mathbf{x}_c, \mathbf{x}_s) \in \mathbb{R}^2 \times \mathbb{R}^{2k-2}, \quad (4.4)$$

where $A \in \mathbb{R}^{2 \times 2}$ and $B \in \mathbb{R}^{(2k-2) \times (2k-2)}$. With the eigenvalues having zero real-part, the Centre Manifold Theorem guarantees that there exists a smooth manifold $W_c = \{(\mathbf{x}_c, \mathbf{x}_s) | \mathbf{x}_s = \mathbf{h}(\mathbf{x}_c)\}$ near the equilibrium point such that the local behaviour in the centre direction of the system is qualitatively the same as that on the manifold (Wiggins, 2003). The $2k - 2$ nonessential generalized coordinates are represented on the centre manifold as

$$x_{i+2} = h_i = a_i x_1^2 + b_i x_2^2 + c_i \tilde{\beta}^2 + d_i x_1 x_2 + e_i x_1 \tilde{\beta} + f_i x_2 \tilde{\beta} + \dots,$$

where $i \in \{1, \dots, 2k - 2\}$.

By differentiating $\mathbf{x}_s = \mathbf{h}(\mathbf{x}_c)$, we get $\dot{\mathbf{x}}_s = D\mathbf{h}(\mathbf{x}_c)\dot{\mathbf{x}}_c$. Substituting the equations in (4.4) into the previous identity and rearranging the equation, we get

$$D\mathbf{h}(\mathbf{x}_c)[A\mathbf{x}_c + \mathbf{f}(\mathbf{x}_c, \mathbf{h}(\mathbf{x}_c))] - B\mathbf{h}(\mathbf{x}_c) - \mathbf{g}(\mathbf{x}_c, \mathbf{h}(\mathbf{x}_c)) = 0. \quad (4.5)$$

Coefficients of the expansions h_i can be explicitly calculated by solving equation (4.5). Using these coefficients, we can express the dynamics on the centre manifold as

$$\dot{\mathbf{x}}_c = A\mathbf{x}_c + \mathbf{f}(\mathbf{x}_c, \mathbf{h}(\mathbf{x}_c), \tilde{\beta}). \quad (4.6)$$

4.2.6 Stability of semi-simple double zero bifurcation

Following the centre manifold reduction, essential dynamics of the model have been reduced to

$$\begin{aligned}\dot{x}_1 &= f_1(x_1, x_2, \tilde{\beta}) \\ \dot{x}_2 &= f_2(x_1, x_2, \tilde{\beta}),\end{aligned}\tag{4.7}$$

where $i \in \{1, 2\}$ and f_i 's are scalar nonlinear functions representing the same dynamics in equation (4.6). Given that a semi-simple double zero bifurcation occurs, we now explicitly calculate the stability conditions under which the clusterings occur for a given model (Iooss and Joseph, 1990, Chapter V.8). To proceed, we define a convenient set of coordinates and their corresponding equations as

$$\hat{x}_i = \frac{x_i}{\tilde{\beta}} \quad \text{and} \quad \hat{f}_i = \frac{f_i(x_1, x_2, \tilde{\beta})}{\tilde{\beta}^2} = 0.\tag{4.8}$$

At the bifurcation value of $\tilde{\beta} = 0$, the equations $\hat{f}_{i0} = \hat{f}_i(\hat{x}_1, \hat{x}_2, 0)$ are conic sections and the points of intersections of these two conics are the possible bifurcation solutions. These conics can have two, three or four intersection points. The trivial solution $(0, 0)$ is always one of the intersection points. To find the stability of bifurcation solutions, let

$$J_0(\hat{x}_1, \hat{x}_2) = \begin{bmatrix} \frac{\partial \hat{f}_{10}(\hat{x}_1, \hat{x}_2, 0)}{\partial \hat{x}_1} & \frac{\partial \hat{f}_{10}(\hat{x}_1, \hat{x}_2, 0)}{\partial \hat{x}_2} \\ \frac{\partial \hat{f}_{20}(\hat{x}_1, \hat{x}_2, 0)}{\partial \hat{x}_1} & \frac{\partial \hat{f}_{20}(\hat{x}_1, \hat{x}_2, 0)}{\partial \hat{x}_2} \end{bmatrix}\tag{4.9}$$

and σ_{i0} be the eigenvalues of J_0 . Similarly, let J be the Jacobian for system (4.7) and σ_i be its eigenvalues. Because of the parametrization chosen in equation (4.8), a direct calculation shows that $J(\tilde{\beta}) = \tilde{\beta}J_0 + \mathcal{O}(\tilde{\beta}^2)$. The determinants and the eigenvalues of J and J_0 are related as

$$\det J = \tilde{\beta}^2 \det J_0 + \mathcal{O}(|\tilde{\beta}^3|)$$

and

$$\sigma_i = \tilde{\beta}\sigma_{i0} + \mathcal{O}(|\tilde{\beta}^2|).$$

For small values of $\tilde{\beta}$, the determinants and the eigenvalues of J and J_0 have the same sign. If $\det J_0 = \sigma_{10}\sigma_{20} < 0$, one of σ_{10} or σ_{20} must be positive and the bifurcation must be unstable. When $\det J_0 > 0$, the real parts of σ_{10} and σ_{20} must have the same sign. Hence, the bifurcating solution is stable when $\det J_0 > 0$ and both of its eigenvalues have negative real part. In each of the multi-strain models, we have found that there are four intersection points for the respective conics. Details pertaining the stability of each model are presented in Section 4.3

4.3 Stability and Bifurcation Analysis

In the previous section, we outlined the necessary steps to understand the clustering patterns of the multi-strain models. Specific details on the calculations are presented here.

4.3.1 The model by Gupta, Ferguson, and Anderson (1998)

For the general m locus- n allele form of the model by Gupta *et al.* (1998), the dynamics of each strain is described by system (4.2). To understand the possible strain partitions, we analyze the quotient network obtained from any 2-colour pattern.

Let each node in Figure 4.4 represent system (4.2). Combining the topological parameters, each node in the 2-colour quotient model represents

$$\dot{z}_i = \lambda_i(1 - z_i) - \mu z_i,$$

$$\dot{w}_i = ((1 + s_i)\lambda_i + m_i\lambda_j)(1 - w_i) - \mu w_i,$$

$$\dot{y}_i = \lambda_i((1 - w_i) + (1 - \gamma)(w_i - z_i)) - \sigma y_i,$$

where $\lambda_i = \beta y_i$ and i denotes the index for one of the nodes and j denotes the index for the other node in Figure 4.4. Equilibrium points of the system are

$$\begin{aligned} \mathbf{p}_1 &= (0, 0, \dots, 0)^T, \\ \mathbf{p}_2 &= (z_1^*, w_1^*, y_1^*, 0, w_2^*, 0)^T, \\ \mathbf{p}_3 &= (0, w_2^*, 0, z_1^*, w_1^*, y_1^*)^T, \\ \text{and } \mathbf{p}_4 &= (z_3^*, w_3^*, y_3^*, z_3^*, w_3^*, y_3^*)^T, \end{aligned}$$

where $z_1^*, w_1^*, y_1^*, w_2^*, z_3^*, w_3^*, y_3^*$ are implicit equilibrium expressions.

After transferring the system to its Jordan canonical form at the trivial equilibrium, the Jacobian at this point is

$$J = \begin{bmatrix} \beta - \sigma & 0 & 0 & 0 & 0 & 0 \\ 0 & \beta - \sigma & 0 & 0 & 0 & 0 \\ 0 & 0 & -\mu & 0 & 0 & 0 \\ 0 & 0 & 0 & -\mu & 0 & 0 \\ 0 & 0 & 0 & 0 & -\mu & 0 \\ 0 & 0 & 0 & 0 & 0 & -\mu \end{bmatrix}.$$

Given that the parameters of the system are always positive, the system is locally stable at the equilibrium for $\beta - \sigma < 0$. To simplify the computation, we substitute the parameter β with $\tilde{\beta} \triangleq \beta - \sigma$. Hence, the newly transformed system undergoes a semi-simple double zero bifurcation at $\tilde{\beta} = 0$ and the system can be written as

$$\begin{aligned} \dot{\mathbf{x}}_c &= A\mathbf{x}_c + \mathbf{f}(\mathbf{x}_c, \mathbf{x}_s) \\ \dot{\mathbf{x}}_s &= B\mathbf{x}_s + \mathbf{g}(\mathbf{x}_c, \mathbf{x}_s) \end{aligned} \quad (\mathbf{x}_c, \mathbf{x}_s) \in \mathbb{R}^2 \times \mathbb{R}^4, \quad (4.10)$$

where

$$A = \begin{bmatrix} 0 & 0 \\ 0 & 0 \end{bmatrix},$$

$$B = \begin{bmatrix} -\mu & 0 & 0 & 0 \\ 0 & -\mu & 0 & 0 \\ 0 & 0 & -\mu & 0 \\ 0 & 0 & 0 & -\mu \end{bmatrix},$$

and \mathbf{f} as well as \mathbf{g} are nonlinear functions of the system after the transformation.

As described in Section 4.2.5, we can now reduce the system to the centre manifold.

For $i = 1, \dots, 4$, let

$$x_{i+2} = h_i = a_i x_1^2 + b_i x_2^2 + c_i \tilde{\beta}^2 + d_i x_1 x_2 + e_i x_1 \tilde{\beta} + f_i x_2 \tilde{\beta} + \dots \quad (4.11)$$

Then,

$$D\mathbf{h} = \begin{bmatrix} 2a_1 x_1 + d_1 x_2 + e_1 \tilde{\beta} & 2b_1 x_2 + d_1 x_1 + f_1 \tilde{\beta} \\ 2a_2 x_1 + d_2 x_2 + e_2 \tilde{\beta} & 2b_2 x_2 + d_2 x_1 + f_2 \tilde{\beta} \\ 2a_3 x_1 + d_3 x_2 + e_3 \tilde{\beta} & 2b_3 x_2 + d_3 x_1 + f_3 \tilde{\beta} \\ 2a_4 x_1 + d_4 x_2 + e_4 \tilde{\beta} & 2b_4 x_2 + d_4 x_1 + f_4 \tilde{\beta} \end{bmatrix}. \quad (4.12)$$

By substituting equations (4.10), (4.11) and (4.12) into equation (4.5), we obtain the necessary equations to determine the twenty-four coefficients for the expansions and thus, the centre manifold as well.

After the centre manifold reduction, we find that the two conics necessary to study

the stability of the possible solutions are

$$\begin{aligned}\hat{f}_{10}(\hat{x}_1, \hat{x}_2) &= -\frac{\sigma(s_1\gamma + 1)}{m_2}\hat{x}_1^2 + \hat{x}_1 - \frac{\sigma^2(\gamma m_1 m_2 + (m_2\gamma - 2 - 2s_1\gamma))}{\mu m_2}\hat{x}_1\hat{x}_2 \\ &\quad + \frac{(m_1 m_2(1 + s_2\gamma) + m_2(s_2 + 1)(\gamma - 1) - (s_2 + 1)^2(1 + s_1\gamma))}{m_2\mu^2}\hat{x}_2^2 \\ \hat{f}_{20}(\hat{x}_1, \hat{x}_2) &= -\gamma\sigma\hat{x}_1\hat{x}_2 + \hat{x}_2 + \frac{\sigma^2(\gamma - 1)}{\mu}\hat{x}_2^2.\end{aligned}$$

In this case, the four intersections of the two conics are

$$\begin{aligned}\hat{\mathbf{x}}_1^* &= (0, 0), \\ \hat{\mathbf{x}}_2^* &= \left(\frac{m_2}{\sigma(1 + s_1\gamma)}, 0\right), \\ \hat{\mathbf{x}}_3^* &= \left(\frac{1 + s_2}{\sigma(1 + s_2\gamma)}, \frac{\mu}{\sigma^2(1 + s_2\gamma)}\right), \\ \text{and } \hat{\mathbf{x}}_4^* &= \left(\frac{\mu(\gamma(m_2 - s_1) - 1)}{\sigma^2\gamma(\gamma(m_1 m_2 - s_1 s_2) - (s_1 + s_2) - 1)}, \frac{\gamma(m_2(m_1 + 1) - s_1(s_2 + 1)) - m_2 - s_2 - 1}{\sigma^2\gamma(\gamma(m_1 m_2 - s_1 s_2) - (s_1 + s_2) - 1)}\right).\end{aligned}$$

Performing the necessary inverse operations, we find that each $\hat{\mathbf{x}}_i^*$ corresponds to equilibrium points \mathbf{p}_i of the quotient system. To check the stability at each point, we must calculate the determinant found in equation (4.9) and the corresponding eigenvalues at each point. A direct calculation shows that the determinants are

$$\begin{aligned}D_1 &= 1, \\ D_2 &= \frac{\gamma(m_2 - s_1) - 1}{1 + s_1\gamma},\end{aligned}\tag{4.13}$$

$$D_3 = \frac{\gamma(m_1 - s_2) - 1}{1 + s_2\gamma},\tag{4.14}$$

$$\text{and } D_4 = \frac{[1 + \gamma(s_2 - m_1)][1 + \gamma(s_1 - m_2)]}{\gamma^2(s_1 s_2 - m_1 m_2) + \gamma(s_1 + s_2) + 1}.$$

The corresponding sets of eigenvalues of J_0 at each intersection of the conics are

$$E_1 = \{1, 1\},$$

$$E_2 = \{-1, D_2\},$$

$$E_3 = \{-1, D_3\},$$

and $E_4 = \{-1, D_4\}.$

As mentioned in Section 4.2.6, the eigenvalues must both be negative while the determinant remain positive, so we see that the trivial equilibrium is always unstable while the other three solutions can be stable depending on the topological parameters of particular balanced 2-colouring and the strain parameters.

4.3.2 The model by Recker and Gupta (2005)

As mentioned in Section 4.1, the model from Recker and Gupta (2005) is an extension of the model in Gupta *et al.* (1998). The authors incorporated a new compartment for individuals being non-susceptible to pathogens strains sharing more than one allele with a particular strain i . This new compartment introduces a new type of coupling and thus there will be two types of arrows in the coupled cell network representation of the system. Instead of reducing the system to the quotient network shown in Figure 4.4, any balanced 2-colourings of the system can be reduced to the quotient network shown in Figure 4.5.

Based on the equations in (4.3), each node in Figure 4.5 has the form

$$\dot{z}_i = \lambda_i(1 - z_i) - \mu z_i,$$

$$\dot{w}_i = ((1 + s_{i1} + s_{i2})\lambda_i + (m_{i1} + m_{i2})\lambda_j)(1 - w_i) - \mu w_i,$$

$$\dot{v}_i = ((1 + s_{i2})\lambda_i + m_{i2}\lambda_j)(1 - v_i) - \mu v_i,$$

$$\dot{y}_i = \lambda_i((1 - w_i) + (1 - \gamma_1)(w_i - z_i) + (1 - \gamma_2)(v_i - z_i)) - \sigma y_i,$$

where $\lambda_i = \beta y_i$ and i denotes the index for one node and j denotes the index for the other node in Figure 4.5. The equilibrium points of the system are

$$\mathbf{p}_1 = (0, 0, \dots, 0)^T,$$

$$\mathbf{p}_2 = (z_1^*, w_1^*, v_1^*, y_1^*, 0, w_2^*, v_2^*, 0)^T,$$

$$\mathbf{p}_3 = (0, w_2^*, v_2^*, 0, z_1^*, w_1^*, v_1^*, y_1^*)^T,$$

$$\text{and } \mathbf{p}_4 = (z_3^*, w_3^*, v_3^*, y_3^*, z_3^*, w_3^*, v_3^*, y_3^*)^T,$$

where $z_1^*, w_1^*, v_1^*, y_1^*, w_2^*, v_2^*, z_3^*, w_3^*, v_3^*, y_3^*$ are implicit equilibrium expressions.

Subsequent to transforming the system to its Jordan canonical form at the trivial equilibrium, the Jacobian at this point is

$$J = \begin{bmatrix} \beta - \sigma & 0 & 0 & 0 & 0 & 0 & 0 & 0 \\ 0 & \beta - \sigma & 0 & 0 & 0 & 0 & 0 & 0 \\ 0 & 0 & -\mu & 0 & 0 & 0 & 0 & 0 \\ 0 & 0 & 0 & -\mu & 0 & 0 & 0 & 0 \\ 0 & 0 & 0 & 0 & -\mu & 0 & 0 & 0 \\ 0 & 0 & 0 & 0 & 0 & -\mu & 0 & 0 \\ 0 & 0 & 0 & 0 & 0 & 0 & -\mu & 0 \\ 0 & 0 & 0 & 0 & 0 & 0 & 0 & -\mu \end{bmatrix}.$$

We perform similar simplification as before and transform the parameter β with $\tilde{\beta} \triangleq \beta - \sigma$. With $\tilde{\beta}$ as the bifurcation parameter, this system also undergoes a semi-simple double zero bifurcation at $\tilde{\beta} = 0$ and this system can be written as

$$\begin{aligned} \dot{\mathbf{x}}_c &= A\mathbf{x}_c + \mathbf{f}(\mathbf{x}_c, \mathbf{x}_s) \\ \dot{\mathbf{x}}_s &= B\mathbf{x}_s + \mathbf{g}(\mathbf{x}_c, \mathbf{x}_s) \end{aligned} \quad (\mathbf{x}_c, \mathbf{x}_s) \in \mathbb{R}^2 \times \mathbb{R}^6, \quad (4.15)$$

where

$$A = \begin{bmatrix} 0 & 0 \\ 0 & 0 \end{bmatrix},$$

$$B = \begin{bmatrix} -\mu & 0 & 0 & 0 & 0 & 0 \\ 0 & -\mu & 0 & 0 & 0 & 0 \\ 0 & 0 & -\mu & 0 & 0 & 0 \\ 0 & 0 & 0 & -\mu & 0 & 0 \\ 0 & 0 & 0 & 0 & -\mu & 0 \\ 0 & 0 & 0 & 0 & 0 & -\mu \end{bmatrix},$$

and \mathbf{f} as well as \mathbf{g} are nonlinear functions of the system after the transformation.

We again follow the method in Section 4.2.5 and reduce the system to its centre manifold. For $i = 1, \dots, 6$, let

$$x_{i+2} = h_i = a_i x_1^2 + b_i x_2^2 + c_i \tilde{\beta}^2 + d_i x_1 x_2 + e_i x_1 \tilde{\beta} + f_i x_2 \tilde{\beta} + \dots \quad (4.16)$$

Then,

$$Dh = \begin{bmatrix} 2a_1x_1 + d_1x_2 + e_1\tilde{\beta} & 2b_1x_2 + d_1x_1 + f_1\tilde{\beta} \\ 2a_2x_1 + d_2x_2 + e_2\tilde{\beta} & 2b_2x_2 + d_2x_1 + f_2\tilde{\beta} \\ 2a_3x_1 + d_3x_2 + e_3\tilde{\beta} & 2b_3x_2 + d_3x_1 + f_3\tilde{\beta} \\ 2a_4x_1 + d_4x_2 + e_4\tilde{\beta} & 2b_4x_2 + d_4x_1 + f_4\tilde{\beta} \\ 2a_5x_1 + d_5x_2 + e_5\tilde{\beta} & 2b_5x_2 + d_5x_1 + f_5\tilde{\beta} \\ 2a_6x_1 + d_6x_2 + e_6\tilde{\beta} & 2b_6x_2 + d_6x_1 + f_6\tilde{\beta} \end{bmatrix}. \quad (4.17)$$

By substituting equations (4.15), (4.16) and (4.17) into equation (4.5), we obtain the necessary equations to determine the thirty-six coefficients for the expansions and thus, the centre manifold as well.

In this case, we find that the conics for stability calculations are

$$\begin{aligned} \hat{f}_{10}(\hat{x}_1, \hat{x}_2) &= -\frac{\sigma^2(m_{21}\gamma_1s_{22} + \gamma_2m_{22} - \gamma_1m_{22}s_{21} - m_{22} + m_{21}\gamma_1)}{m_{22}\mu}\hat{x}_1^2 + \hat{x}_1 \\ &\quad - \frac{\sigma(\gamma_1m_{21} + \gamma_2m_{22})}{m_{22}}\hat{x}_1\hat{x}_2, \\ \hat{f}_{20}(\hat{x}_1, \hat{x}_2) &= -\frac{\sigma^3((1 + s_{22})(1 + s_{22} + m_{22}) +)}{m_{22}\mu^2}\hat{x}_2^2 \\ &\quad - \frac{\sigma^2}{m_{22}\mu}\hat{x}_1\hat{x}_2 + \hat{x}_2 - \frac{\sigma(1 + s_{11}\gamma_1 + s_{12}\gamma_2)}{m_{22}}\hat{x}_2^2, \end{aligned}$$

and intersections of these two conics are

$$\begin{aligned} \hat{\mathbf{x}}_1^* &= (0, 0), \\ \hat{\mathbf{x}}_2^* &= \left(0, \frac{m_{22}}{\sigma(1 + \gamma_1s_{11} + \gamma_2s_{12})}\right), \\ \hat{\mathbf{x}}_3^* &= \left(\frac{\mu}{\sigma^2(1 + \gamma_1s_{21} + \gamma_2s_{22})}, \frac{m_{22}}{\sigma(1 + \gamma_1s_{21} + \gamma_2s_{22})}\right), \\ \text{and } \hat{\mathbf{x}}_4^* &= \left(\frac{\mu[(m_{21} - s_{11})\gamma_1 + (m_{22} - s_{12})\gamma_2 - 1]}{\sigma^2[B_1\gamma_1^2 + B_2\gamma_1 + B_3\gamma_1\gamma_2 + B_4\gamma_2 + B_5\gamma_2^2 + 1]}, \right. \\ &\quad \left. \frac{A_1\gamma_1 + A_2\gamma_2 + m_{22} + s_{22} + 1}{\sigma[B_1\gamma_1^2 + B_2\gamma_1 + B_3\gamma_2 + B_4\gamma_1\gamma_2 + B_5\gamma_2^2 + 1]}\right), \end{aligned}$$

where

$$A_1 = (s_{11} - m_{21})(1 + s_{22}) + m_{22}(s_{21} - m_{11}),$$

$$A_2 = s_{12} - m_{22} - m_{12}m_{22} + s_{12}s_{22},$$

$$B_1 = s_{11}s_{21} - m_{11}m_{21},$$

$$B_2 = s_{11} + s_{21},$$

$$B_3 = s_{12} + s_{22},$$

$$B_4 = s_{12}s_{21} - m_{12}m_{21} - m_{11}m_{22} + s_{22}s_{11},$$

and $B_5 = s_{12}s_{22} - m_{12}m_{22}.$

Performing the necessary inverse operations, we find that each $\hat{\mathbf{x}}_i^*$ corresponds to equilibrium points \mathbf{p}_i of the quotient system. The relevant determinants corresponding to the four equilibria are

$$D_1 = 1,$$

$$D_2 = \frac{\gamma_1(m_{21} - s_{11}) + \gamma_2(m_{22} - s_{12}) - 1}{1 + \gamma_1s_{11} + \gamma_2s_{12}}, \quad (4.18)$$

$$D_3 = \frac{\gamma_1(m_{11} - s_{21}) + \gamma_2(m_{12} - s_{22}) - 1}{1 + \gamma_1s_{21} + \gamma_2s_{22}}, \quad (4.19)$$

and $D_4 = \frac{C_1\gamma_1^2 + C_2\gamma_1 + C_3\gamma_1\gamma_2 + C_4\gamma_2 + C_5\gamma_2^2}{\sigma[B_1\gamma_1^2 + B_2\gamma_1 + B_3\gamma_2 + B_4\gamma_1\gamma_2 + B_5\gamma_2^2 + 1]},$

where

$$C_1 = m_{11}m_{21} + s_{11}s_{21} - s_{21}m_{21} - m_{11}s_{11},$$

$$C_2 = s_{11} - m_{21} + s_{21} - m_{11},$$

$$C_3 = (m_{21} - s_{11})(m_{12} - s_{22}) + m_{22}(m_{11} - m_{21})$$

$$C_4 = s_{12} - m_{22} + s_{22} - m_{12},$$

$$\text{and } C_5 = m_{12}m_{22} + s_{12}s_{22} - s_{22}m_{22} - m_{12}s_{12}.$$

The corresponding eigenvalues of J_0 at each intersection of the conics are

$$E_1 = \{1, 1\},$$

$$E_2 = \{-1, D_2\},$$

$$E_3 = \{-1, D_3\},$$

$$\text{and } E_4 = \{-1, D_4\}.$$

Like the previous model, the trivial intersection point \hat{x}_1 is unstable because both the eigenvalues are always positive. We can see that for suitable choices of parameters, the constants D_i can be negative.

4.4 Numerical Results

In this section, we numerically demonstrate some possible clustering patterns.

4.4.1 Numerical results of the model by Gupta *et al.* (1998)

There are three possible 2-colour patterns for the 2 locus-2 allele version of the model from Gupta *et al.* (1998) and they are shown in Figure 4.3. Already mentioned in Section 4.2.2, the pattern shown in Figure 4.3(c) is not a balanced colouring, so it does not occur numerically. The pattern in Figure 4.3(a) is balanced and in its 2-colour quotient form, the parameters are $s_i = 1$ and $m_i = 1$. Similarly, the pattern in Figure 4.3(b) is also balanced and in its 2-colour quotient form, the parameters are $s_i = 0$ and $m_i = 2$. Analytically, we calculate from equations (4.13) and (4.14) that for the clustering to be stable, we must have

$$m_i - s_j > \frac{1}{\gamma}. \quad (4.20)$$

Given that γ is a positive parameter, a direct calculation shows that the pattern in Figure 4.3(a) cannot occur and the pattern in Figure 4.3(b) will occur for appropriate choice of γ . The numerical results in Figure 4.6 agree with the analytic predictions. The two patterns shown are symmetrical to each other and they are induced by choosing different initial conditions.

Extending the 2 locus-2 allele form, numerical results and the corresponding 2-colour patterns of the 3 locus-2 allele model are shown in Figures 4.7 and 4.8. Clusters of numerical solutions found in Figures 4.7(a) and 4.8(a) correspond to the colouring patterns shown in Figures 4.7(b) and 4.8(b), respectively. We can derive the corresponding parameters for the 2-colour quotient network from the balanced colouring. Combining the topological parameters as well as the system parameters, a direct calculation shows that the stability condition in equation (4.20) is satisfied.

Based on the stability expressions shown and the numerical results found in Figures 4.7 and 4.8, we see that different patterns can emerge under identical parameter conditions. Calvez *et al.* (2005) noticed the appearance of a particular pattern which is dependent on initial conditions. The simulation results shown in Figures 4.7 and 4.8

are simulated with identical parameter values but different initial conditions. This phenomenon is possible because both patterns satisfy the stability condition found for balanced 2-colourings.

On the other hand, we can change the system parameter values such that the clustering no longer occurs. In Figure 4.9, we have decreased the value of γ so that, along with the topological parameters corresponding to the network in Figure 4.8(b), the inequality in equation (4.20) is no longer satisfied. Given that the other three solutions from the semi-simple double zero bifurcation are unstable, the system converges to the fourth and fully synchronized solution.

4.4.2 Numerical results of the model by Recker and Gupta (2005)

For the model by Recker and Gupta (2005), the stability criterion obtained from equations (4.18) and (4.19) is

$$\gamma_1(m_{i1} - s_{j1}) + \gamma_2(m_{i2} - s_{j2}) > 1. \quad (4.21)$$

For this model, the numerical results and the corresponding balanced 2-colouring of the 3 locus-2 allele form of the system are shown in Figures 4.10 and 4.11. Applying equation (4.21) to the topological parameters of the quotient networks in Figures 4.10(b) and 4.11(b), we see that these patterns are clearly stable.

Like the previous model, we can choose the system parameter values such that the clustering patterns become unstable. In Figure 4.12, we decrease γ_1 and γ_2 so that the clustering disappears and all the strains are synchronized.

4.4.3 Periodic and chaotic motions

As shown numerically by authors of Gupta *et al.* (1998) and Recker and Gupta (2005), the two models discussed in this work may have cyclical and chaotic solutions for some parameter values. In this section, we will investigate these two types of solutions numerically.

For the model by Recker and Gupta (2005), we can see from Figures 4.13 and 4.14 that periodic solutions of the system correspond to balanced colourings of the networks in Figure 4.10(b) and 4.11(b). Like our previous results on semi-simple double zero bifurcations, these different patterns of synchrony can be induced using different initial conditions.

While keeping the parameter values same as the periodic solutions, we see from Figure 4.15(a) that chaotic motions may occur under different initial conditions. Like the other solutions of the system, the different strains also synchronize with each other chaotically. The synchrony pattern of the synchronized chaos correspond to the balanced colouring shown in Figure 4.15(b). The corresponding quotient network for this balanced colouring is shown in Figure 4.15(c). While the numerical solutions in Figures 4.13, 4.14, and 4.15(a) are all produced using the same parameter values, their respective balanced colourings do not have the same number of equivalence classes. This result suggests that, for any given set of parameter values, the basin of attraction of the system may contain multiple stable regions corresponding to multiple patterns of balanced colourings.

4.5 Concluding Remarks

As noticed by Calvez *et al.* (2005), clusters of solutions can be found in multi-strain infection models, such as those by Gupta *et al.* (1998) and Recker and Gupta (2005).

Through the calculations in Section 4.3, the phenomenon can be explained through bifurcation and stability analysis of the 2-colour quotient networks of the models. For each of these models, we calculated specific stability criteria for the semi-simple double zero bifurcation. From the expressions in equations (4.20) and (4.21), we see that the criteria involve strain specific parameters from systems (4.2) and (4.3) as well as topological parameters of the quotient networks as shown in Figures 4.4 and 4.5. Hence, the clustering behaviour of these systems is a result of both strain specific dynamics and the strength of coupling.

In an earlier paper, Calvez *et al.* (2005) concluded that the clustering phenomenon “is intrinsic feature of the strain system itself.” In our analysis, the dynamics corresponding to each strain is treated as a separate subsystem in the coupled cell network and the effects of cross-immunity are treated as coupling terms. Given that casting the model as a coupled cell system relies on the strains being separate subsystems, we must agree that the clustering is a result of the strain system.

After understanding the mathematical mechanisms of the clustering phenomenon, we investigate the possible patterns of clustering. To find them, it is necessary to first translate cross-immunity and other biological considerations into a digraph and find balanced colourings of these graphs. These multi-strain models are designed to accommodate the analysis of any number of strains. The complexities of the coupled cell network and the number of balanced colourings grow as the number of strains increase. Thus, it is not feasible to analyze every possible pattern. Rather than an exhaustive approach, the stability criteria provide a direct method to analyze a given pattern of interest. More importantly, we have used these criteria in Section 4.4 to show that not all possible balanced colourings can occur for a given version of the model.

Calvez *et al.* (2005) also postulated that clustering is independent of the model used, but we have shown that this is not entirely true. While clustering is a result of

modelling the dynamics of various strains as coupled subsystems, the related stability criteria are dependent on the model parameters. As we mentioned already, expressions for stable 2-colour patterns depend upon both parameters from the topology of the system as well as model specific parameters. Different coupling terms and system parameters will produce different patterns in different situations. The authors of Calvez *et al.* (2005) also noticed that the patterns are stable once formed and our results agree. The expression related pattern forming is a direct result of calculating the stability of the related bifurcation.

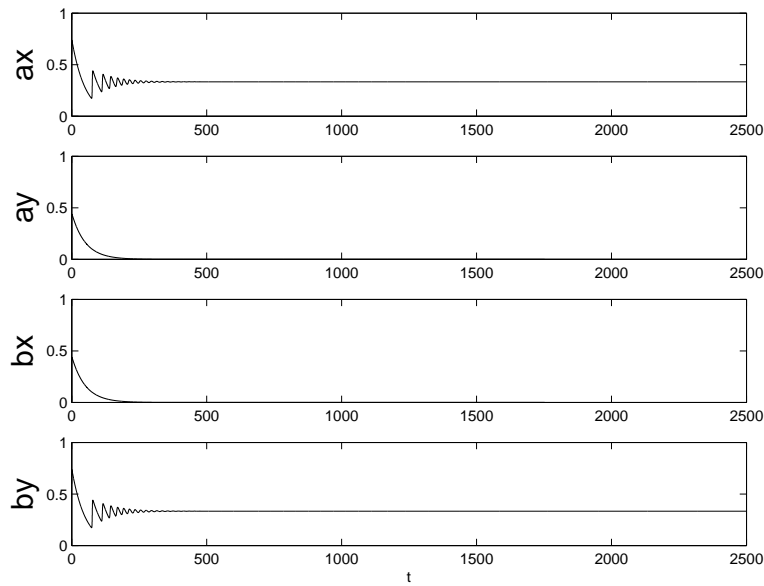
The transition from one pattern to another can be observed from the differences between Figures 4.7 and 4.9. As we decrease the system parameter, γ , the stable discrete strain structure in Figure 4.7(a) is destabilized and the strain structure disappeared. Based on this observation, we may conclude that strain structure found in the model by Gupta *et al.* (1998) is related to the effectiveness of cross-immunity. The more effective the cross-protection, the more likely the discrete strain structure appears. This observation is consistent with the idea that discrete strain structure is a result of immune selection. In a similar fashion, we can destabilize the discrete strain structure found in the model by Recker and Gupta (2005) by decreasing the parameters, γ_1 and γ_2 . For this model, the transition from discrete strain structure to no structure can be observed in Figures 4.10 and 4.12.

As one can see from the Figures 4.1 and 4.2, the topologies of the digraphs in the coupled cell networks have symmetries. These symmetries are present because we have assumed that all possible strains of the m locus- n allele model are present in the system and the effects of cross-immunity exist identically and perfectly between strains that share alleles. Without these assumptions, there may be no symmetry in the topology. In such situation, our method still applies because the coupled cell formalism does not require symmetry. In this method, synchronization of strains as clusters may still be

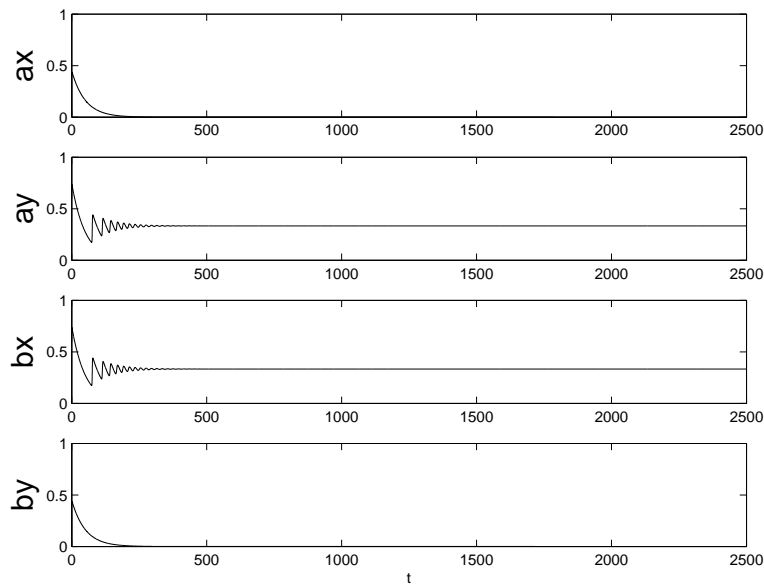
possible as long as there are suitable balanced colourings of the strain space.

In the future, one can further the research by expanding on assumptions made here. In simplifying the calculations, we have assumed that all strains have identical parameters. Our analysis here can be extended to incorporate different parameters for different strains by altering the coupled cell representation. Instead of having only one type of nodes in the digraph, different shapes of nodes can be used to denote strains with different parameters.

Aside from the identical parameters assumption, we have also restricted the analysis to only 2-colourings of the systems. Again, we made this assumption to simplify the calculations. Since each colour in a colouring pattern corresponds to one cluster, our analysis can only produce patterns with two different groups of synchrony. A more general analysis of higher number of colours in the colourings can generate more possible patterns.

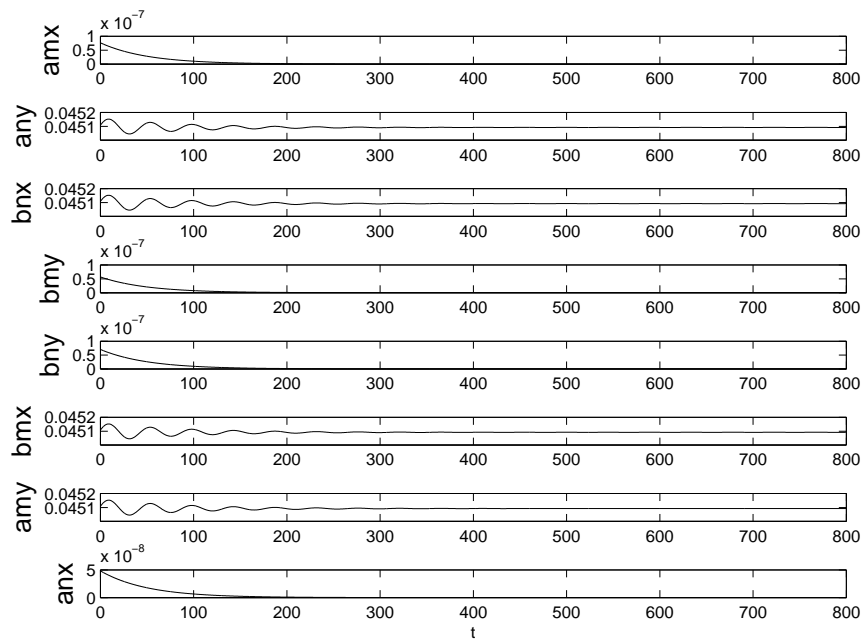


(a)

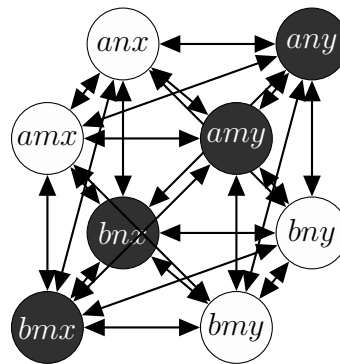


(b)

Figure 4.6: Simulation results of the 2 locus-2 allele form of system (4.2) for $\sigma = 10$, $\gamma = 0.85$, $\mu = 0.02$, $\beta = 15$, showing the clustering patterns of z_i for each strain. The patterns in these 4.6(a) and 4.6(b) can be obtained by using different initial conditions.

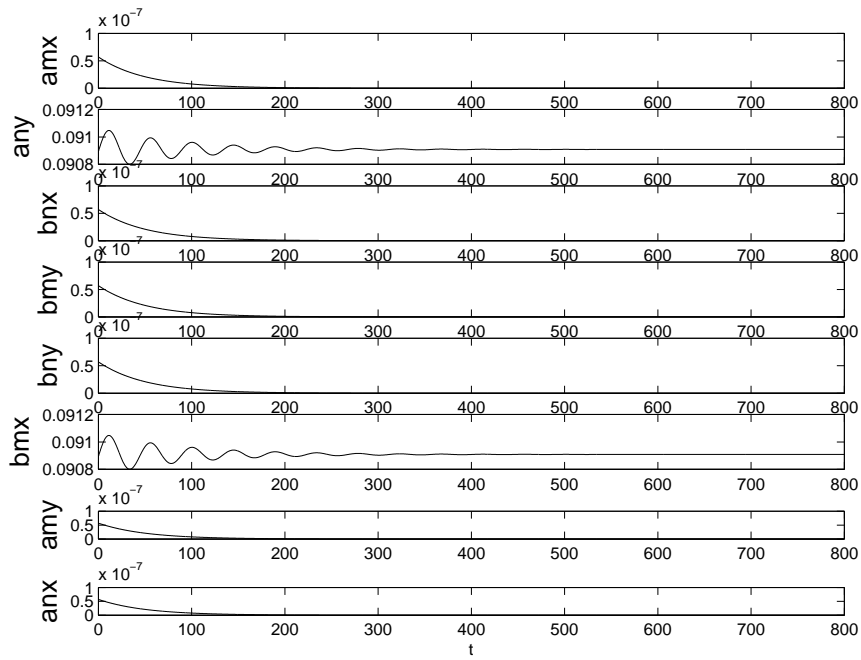


(a)

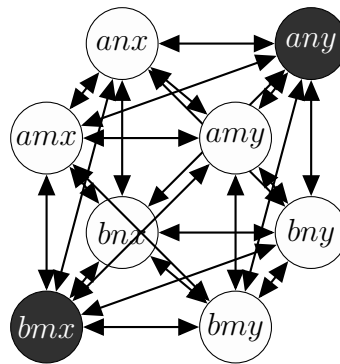


(b)

Figure 4.7: Results for the 3 locus-2 allele version of the model from Gupta *et al.* (1998): (a) Simulated time history of z_i for $\sigma = 10$, $R_0 = 1.1$, $\gamma = 0.58$, $\mu = 0.02$ with identical initial conditions for strains any , bnx , bm_x and amy ; and (b) The balanced 2-colour pattern corresponding to the numerical results, with each dark node receiving four inputs from white nodes and two from the other dark nodes; similarly, each white node receiving four inputs from dark nodes and two from the other white nodes, and the corresponding 2-colour quotient network having the parameter values $m_i = 4$ and $s_i = 2$.

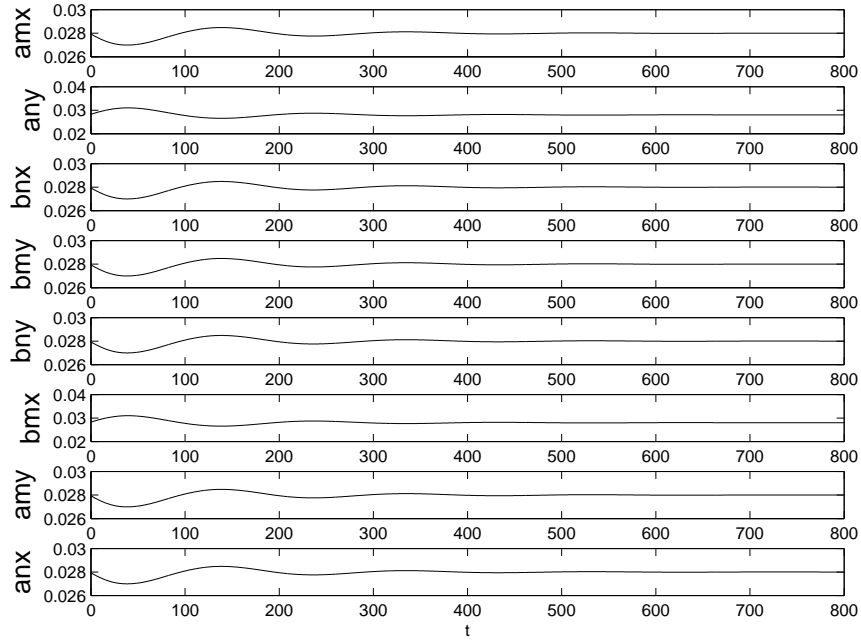


(a)

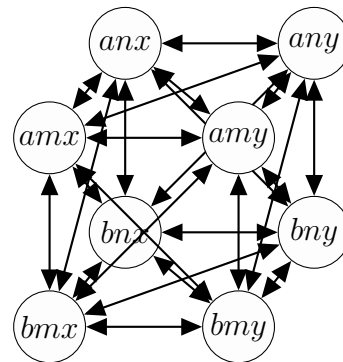


(b)

Figure 4.8: Results for the 3 locus-2 allele version of the model from Gupta *et al.* (1998): (a) Simulated time history of z_i for $\sigma = 10$, $R_0 = 1.1$, $\gamma = 0.58$, and $\mu = 0.02$ with identical initial conditions for strains any and bm_x ; and (b) The balanced 2-colour pattern corresponding to the numerical results and with each dark node receiving six inputs from white nodes and none from the other dark node; similarly, each white node receiving one input from dark nodes and five from the other white nodes, and the corresponding 2-colour quotient network having the parameter values $m_1 = 2$, $s_1 = 4$, $m_2 = 6$ and $s_2 = 0$.

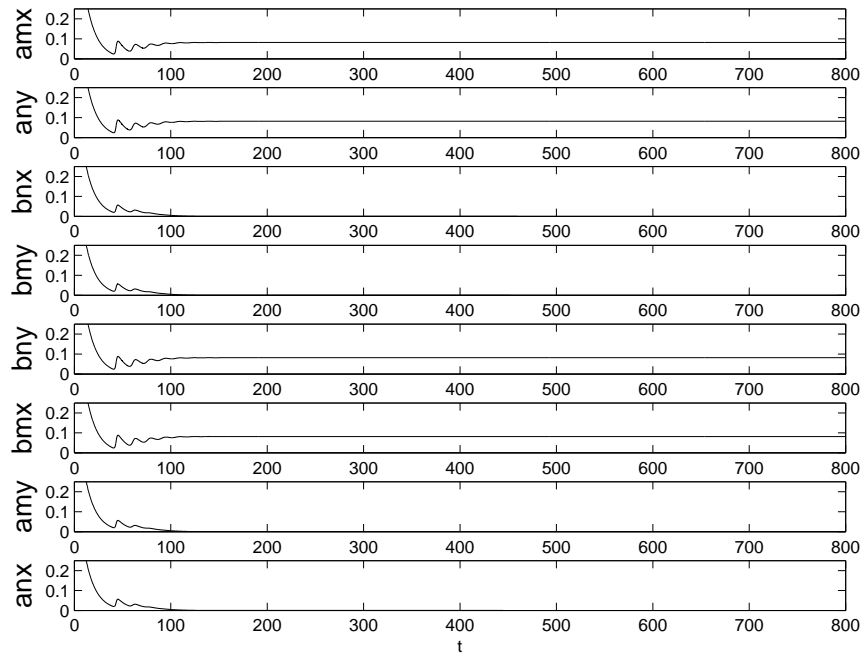


(a)

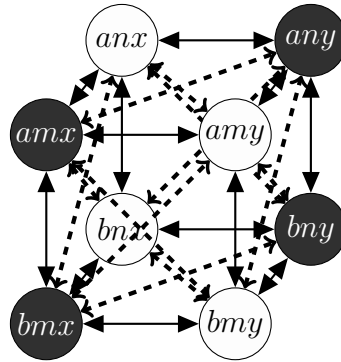


(b)

Figure 4.9: Results for 3 locus-2 allele version of the model from Gupta *et al.* (1998): (a) Simulated time history of z_i for $\sigma = 10$, $R_0 = 1.1$, $\gamma = 0.45$, $\mu = 0.02$ with mixed initial conditions are used. (b) The corresponding coupled cell system showing that all strains being synchronized in identical steady-state.

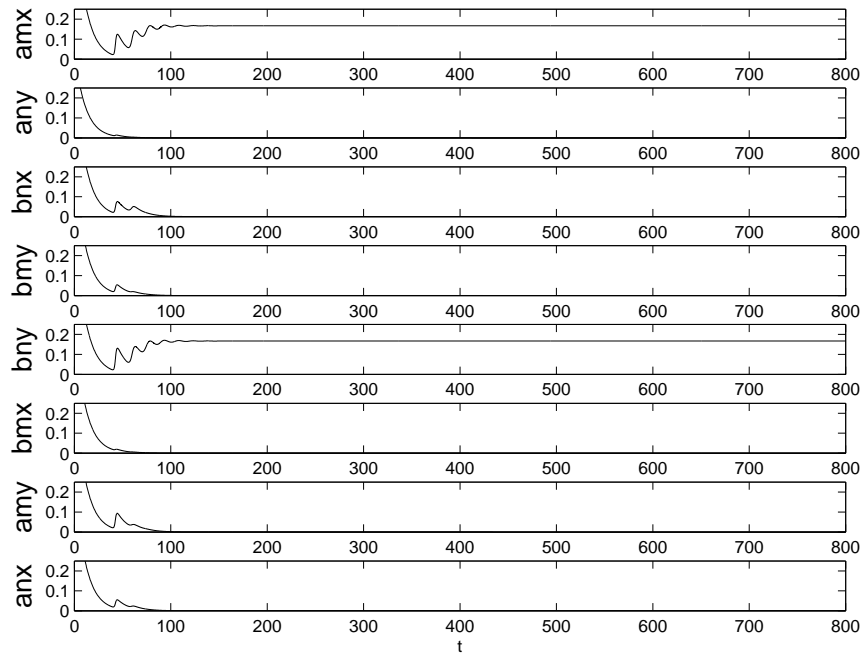


(a)

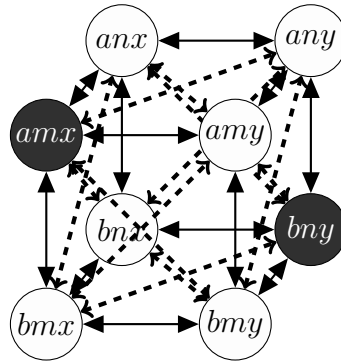


(b)

Figure 4.10: Results for the 3 locus-2 allele version of the model from Recker and Gupta (2005): (a) Simulated time history of z_i for $\sigma = 10, R_0 = 1.2, \gamma_1 = 0.5, \gamma_2 = 0.8, \mu = 0.09$ with identical initial conditions for strains $amx, any, bny,$ and $bm x$; and (b) The balanced 2-colour pattern corresponding to the numerical results, and the corresponding 2-colour quotient network having the parameter values $m_{ij} = 2$ and $s_{ij} = 1$, for $i, j \in \{1, 2\}$.

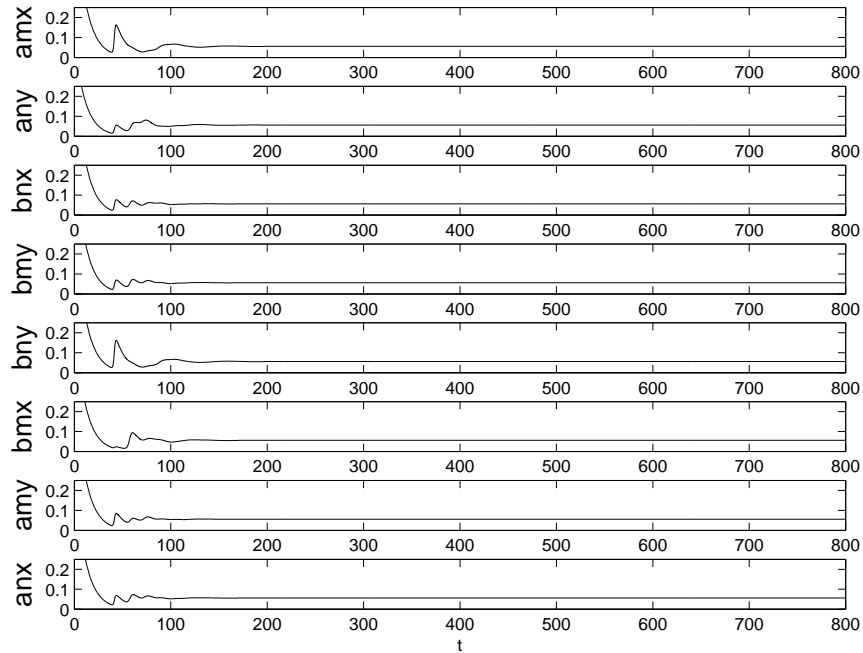


(a)

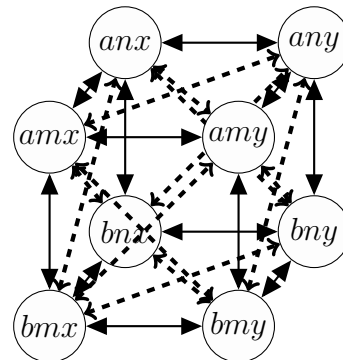


(b)

Figure 4.11: Results for the 3 locus-2 allele version of the model from Recker and Gupta (2005): (a) Simulated time history of z_i for $\sigma = 10, R_0 = 1.2, \gamma_1 = 0.5, \gamma_2 = 0.8, \mu = 0.09$ with identical initial conditions for strains amx and bny ; and (b) The balanced 2-colour pattern corresponding to the numerical results and the corresponding 2-colour quotient network having the parameter values $m_{1i} = 1, m_{2i} = 3, s_{1i} = 2$ and $s_{2i} = 0$, for $i \in \{1, 2\}$.



(a)



(b)

Figure 4.12: Results for the 3 locus-2 allele version of the model from Recker and Gupta (2005): (a) Simulated time history of z_i for $\sigma = 10$, $R_0 = 1.2$, $\gamma_1 = 0.45$, $\gamma_2 = 0.48$, $\mu = 0.09$; and (b) The corresponding coupled cell system showing that all strains being synchronized in identical steady-state.

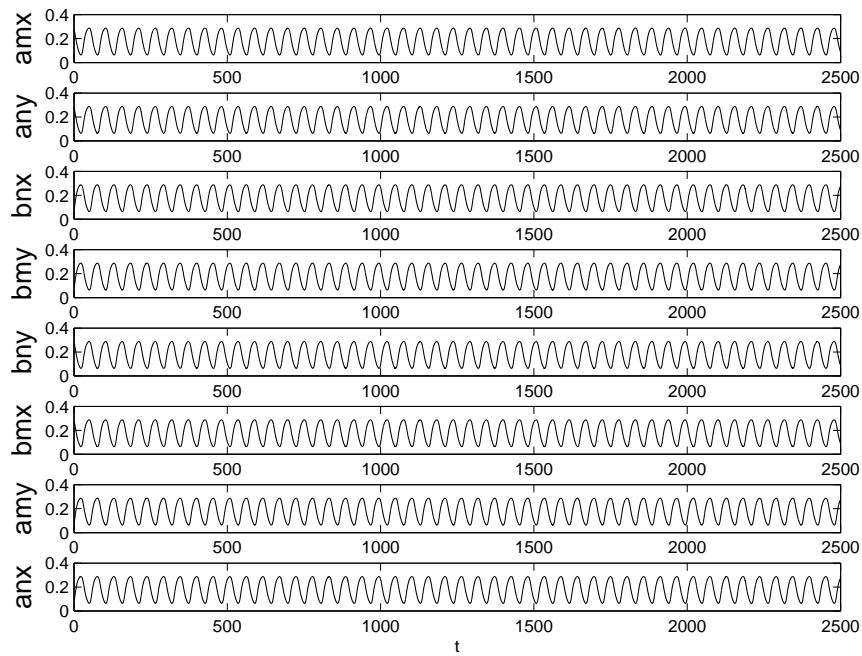


Figure 4.13: Simulated time history of z_i for $\sigma = 10, R_0 = 2, \gamma_1 = 0.65, \gamma_2 = 0.76, \mu = 0.09$ with identical initial conditions for strains $amx, any, bny,$ and $bm x,$ converging to two classes ($amx, any, bny,$ and $bm x; bnx, bmy, amy,$ and anx) of periodic solutions with the same amplitude but a phase difference of half-period.

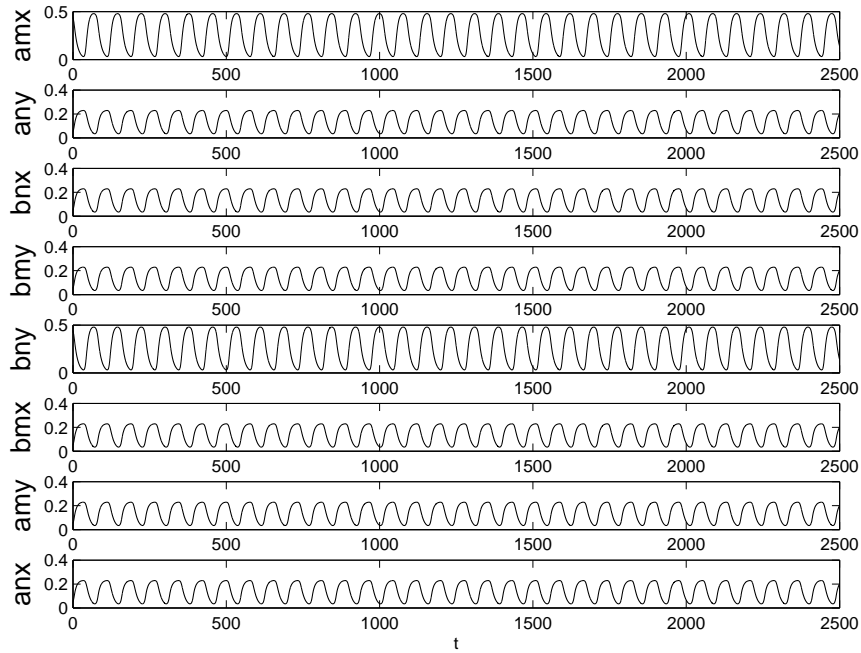
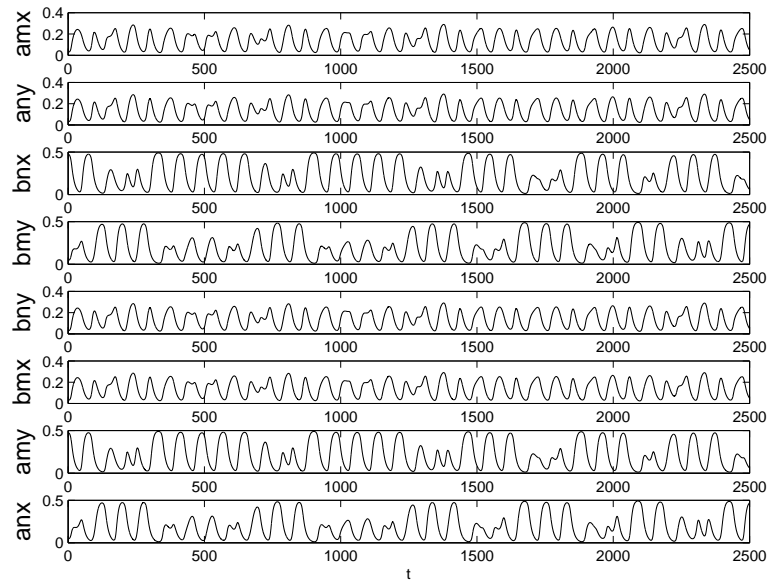
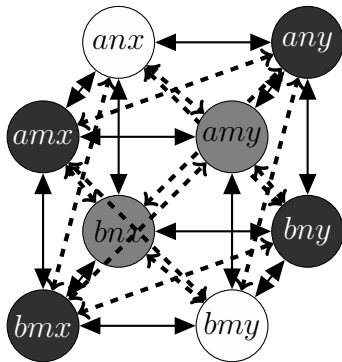


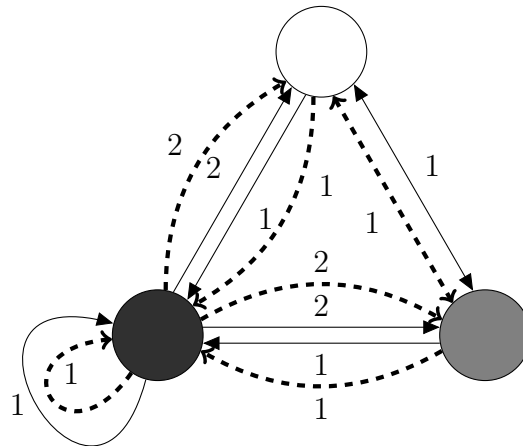
Figure 4.14: Simulated time history of z_i for $\sigma = 10, R_0 = 2, \gamma_1 = 0.65, \gamma_2 = 0.76, \mu = 0.09$ with identical initial conditions for strains amx and bny , converging to two classes (amx and bny ; $any, bnx, bmy, bmx, amy,$ and anx) of periodic solutions with different amplitudes and phase difference of half-period.



(a)



(b)



(c)

Figure 4.15: Results for the 3 locus-2 allele version of the model from Recker and Gupta (2005): (a) Simulated time history of z_i for $\sigma = 10$, $R_0 = 2$, $\gamma_1 = 0.65$, $\gamma_2 = 0.76$, $\mu = 0.09$ with mixed initial conditions, showing three classes (anx and bmy ; amy and bnx ; any , amx , bny , and $bm x$) of chaotically synchronized motions; (b) The corresponding coupled cell system with a balanced 3-colouring pattern; and (c) Quotient network of the 3-colouring pattern.

Bibliography

- V. Calvez, A. Korobeinikov, and P. Maini. Cluster formation for multi-strain infections with cross-immunity. *Journal of Theoretical Biology*, 233(1):75–83, 2005.
- R. Coico and G. Sunshine. *Immunology: A Short Course*. Blackwell Pub, 2009.
- J. Dawes and J. Gog. The onset of oscillatory dynamics in models of multiple disease strains. *Journal of Mathematical Biology*, 45(6):471–510, 2002.
- E. Gjini, D. Haydon, J. Barry, and C. Cobbold. Critical interplay between parasite differentiation, host immunity, and antigenic variation in Trypanosome infections. *The American Naturalist*, 176(4):424–439, 2010.
- J. Gog and B. Grenfell. Dynamics and selection of many-strain pathogens. *Proceedings of the National Academy of Sciences*, 99(26):17209, 2002.
- M. Golubitsky and I. Stewart. Nonlinear dynamics of networks: The groupoid formalism. *Bulletin of the American Mathematical Society*, 43(3):305, 2006. ISSN 0273-0979.
- M. Golubitsky, I. Stewart, and A. Török. Patterns of synchrony in coupled cell networks with multiple arrows. *SIAM J. Appl. Dynam. Sys*, 4(1):78–100, 2005.
- S. Gupta and A. Galvani. The effects of host heterogeneity on pathogen population

- structure. *Philosophical Transactions of the Royal Society of London. Series B: Biological Sciences*, 354(1384):711, 1999.
- S. Gupta, M. Maiden, I. Feavers, S. Nee, R. May, and R. Anderson. The maintenance of strain structure in populations of recombining infectious agents. *Nature Medicine*, 2(4):437–442, 1996.
- S. Gupta, N. Ferguson, and R. Anderson. Chaos, persistence, and evolution of strain structure in antigenically diverse infectious agents. *Science*, 280(5365):912, 1998.
- G. Iooss and D. Joseph. *Elementary Stability and Bifurcation Theory*. Springer, 1990.
- M. Nowak, R. May, R. Phillips, S. Rowland-Jones, D. Lalloo, S. McAdam, P. Klenerman, B. Köppe, K. Sigmund, C. Bangham, *et al.* Antigenic oscillations and shifting immunodominance in HIV-1 infections. *Nature*, 1995a.
- M. Nowak, R. May, and K. Sigmund. Immune responses against multiple epitopes. *Journal of Theoretical Biology*, 175(3):325–353, 1995b.
- R. Omori, B. Adams, and A. Sasaki. Coexistence conditions for strains of influenza with immune cross-reaction. *Journal of Theoretical Biology*, 262(1):48–57, 2010.
- M. Recker and S. Gupta. A model for pathogen population structure with cross-protection depending on the extent of overlap in antigenic variant repertoires. *Journal of Theoretical Biology*, 232(3):363–373, 2005.
- M. Recker, S. Nee, P. Bull, S. Kinyanjui, K. Marsh, C. Newbold, and S. Gupta. Transient cross-reactive immune responses can orchestrate antigenic variation in malaria. *Nature*, 429(6991):555–558, 2004. ISSN 0028-0836.
- M. Recker, K. Blyuss, C. Simmons, T. Hien, B. Wills, J. Farrar, and S. Gupta. Immunological serotype interactions and their effect on the epidemiological pattern of

- dengue. *Proceedings of the Royal Society B: Biological Sciences*, 276(1667):2541, 2009.
- I. Stewart, M. Golubitsky, and M. Pivato. Symmetry groupoids and patterns of synchrony in coupled cell networks. *SIAM J. Appl. Dynam. Sys*, 2(4):609–646, 2003.
- S. Wiggins. *Introduction to Applied Nonlinear Dynamical Systems and Chaos*. Springer Verlag, 2003.

Chapter 5

Conclusions and Future Works

5.1 Conclusions

Dynamics of infectious diseases have been studied by countless researchers from within-host to the epidemiological level. Some fundamental questions about the mechanisms at work are still unanswered. The precise role of effectors and memory cells in short and long term immune defence is not yet known. For the pathogens, mechanisms of antigenic variation, such as switching rate and hierarchy, are not well understood. In terms of interactions between hosts and pathogens, the influence of cross-protective immunity on pathogen survival and evolution is actively researched. Results from this work show some intriguing properties of models of infectious diseases further the research of the aforementioned topics.

Even for a single strain model, the interplay between virus and the host immune system is a complicated process, which involves cell production, viral attachment, viral replication and pathogen clearance. Corresponding to homeostasis states, we have shown that some infectious can be asymptotically stable under appropriate conditions. While we have shown that oscillatory patterns can be obtained for a wide range of parameters in a model, not all of these patterns are necessarily biologically realistic.

Experimental works to confirm such behaviour are necessary and essential.

Building upon our work in a single-strain model, we have provided several mathematical results for the model of multi-strain pathogen of antigenic variation. We have shown that synchrony-breaking Hopf bifurcation may occur in such a model and this dynamical process provides the mechanism for switching in antigenic variation in a deterministic system. We have also shown that the different synchrony patterns can occur in the model with large number of variants. These patterns correspond to the hierarchical structure of antigenic variation that is present in some *Plasmodium* species. We have also illustrated these findings through specific examples and numerical simulations.

Expanding on the work of multi-strain within-host models, we demonstrated the mathematical details of the cluster formations in two multi-strain transmission models. These patterns are induced from semi-simple double zero bifurcation of the quotient coupled cell network representations. Many 2-colour patterns are possible for a given configuration of the network, but not all of them may occur under biologically realistic conditions. We showed that parameters of the 2-colour patterns must fulfill the bifurcation and stability conditions.

5.2 Future Work

For future works, we may include different therapeutic options into the models to understand their effects on different types of CTLs and more importantly, the overall health of the individual. One may also introduce the delay effects of viral gestation in latently infected cells to provide a more realistic model. These added dynamics will be sure to make the mathematical model more challenging to analyze.

Instead of limiting the mathematical analysis to patterns of synchrony of only two colours, we may relax this requirement and analyze the general k -colour case. Furthermore, we have assumed that strains in multi-strain systems have identical parameter

values. Given that the fitness of different strains may vary, the parameter values to describe their properties will likely not be identical. We may use different classes of nodes and edges to more realistically describe these differences.

The self-organized clustering behaviour for multi-strain models can be found in models in different areas of study, such as neuroscience (Rubin and Terman, 2000a,b) and multi-agents systems (Hu and Hong, 2007; Zhang *et al.*, 2011). Our analysis may be modified or extended to study those models with suitable mathematical structure.

Bibliography

- J. Hu and Y. Hong. Leader-following coordination of multi-agent systems with coupling time delays. *Physica A: Statistical Mechanics and its Applications*, 374(2): 853–863, 2007.
- J. Rubin and D. Terman. Analysis of clustered firing patterns in synaptically coupled networks of oscillators. *Journal of Mathematical Biology*, 41(6):513–545, 2000a.
- J. Rubin and D. Terman. Geometric analysis of population rhythms in synaptically coupled neuronal networks. *Neural Computation*, 12(3):597–645, 2000b.
- H. Zhang, C. Zhai, and Z. Chen. A general alignment repulsion algorithm for flocking of multi-agent systems. *Automatic Control, IEEE Transactions on*, 56(2):430–435, 2011.

Curriculum Vitae

Name:	Bernard Shang Li Chan		
Post-Secondary Education and Degrees:	Queen's University	Kingston, Ontario, Canada	2007
	M.Sc. (Mathematics)		
	Queen's University	Kingston, Ontario, Canada	2006
	M.Eng. (Mechanical Engineering)		
	Queen's University	Kingston, Ontario, Canada	2005
	B.Sc. (Eng.) (Mathematics and Engineering)		
Honours and Awards:	Faculty of Science Learning Development Fellowship	The University of Western Ontario	2010-2011
	OGSST	The University of Western Ontario	2009-2010
	NSERC URSA	Royal Military College	2005
	Albert H. Ruddell Award	Queen's University	2001-2004
Related Work Experience:	Lecturer	The University of Western Ontario	2012
	Teaching Assistant	The University of Western Ontario	2007-2011
	Teaching Assistant	Queen's University	2003-2007

Publications: Chan, B. S. and Yu, P. (2012) Bifurcation analysis in a model of cytotoxic T-lymphocyte response to viral infections. *Nonlinear Analysis: Real World Applications*. 13: 64-77.

Chan, B. S. and Yu, P. Synchrony-Breaking Bifurcation of a Model of Antigenic Variation. *International Journal of Bifurcation and Chaos*. (accepted for publication).

Chan, B. S. and Yu, P. Bifurcation, Stability, and Clustering Formation of Multi-strain Infection Models. *J. Mathematical Biology*. (submitted for publication).

Chan, B. S. and Wahl, L. M. The scholarship of teaching and learning in Canadian post-secondary mathematics: 2000-2010. (submitted for publication)